

**A NOVEL DOPAMINE DEPLETION PARADIGM: INVESTIGATION OF  
PROGRESSIVE CIRCUIT DYSFUNCTION IN PARKINSON'S DISEASE**

by

**Amanda Marie Willard**

Bachelor of Science in Biology, Seton Hill University, 2012

A dissertation submitted in  
partial fulfillment of the requirements  
for the degree of Doctor of Philosophy

Carnegie Mellon University  
Department of Biological Sciences

Pittsburgh, PA

August 2018

CARNEGIE MELLON UNIVERSITY

Mellon College of Science

This dissertation was presented

by

Amanda Marie Willard

It was defended on

August 2018

and approved by

Robert S. Turner, Ph.D., Professor, Department of Neurobiology

Alison L. Barth, Ph.D., Professor, Department of Biological Sciences

Sandra J. Kuhlman, Ph.D., Associate Professor, Department of Biological Sciences

Dissertation Advisor: Aryn H. Gittis, Ph.D., Associate Professor, Department of

Biological Sciences

**A Novel Dopamine Depletion Paradigm: Investigation of Progressive Circuit  
Dysfunction in Parkinson's Disease**

By

Amanda Marie Willard

Carnegie Mellon University, 2018

The development of animal models of Parkinson's disease (PD) and assessing their electrophysiological differences has played a critical role in our understanding of basal ganglia function and the underlying mechanisms of PD. The wide range of animal models available and the quest to explore new ways to recover motor function have greatly enhanced our understanding of the remarkable reorganization that occurs in the brain following dopamine neurodegeneration. However, it remains unclear how and when pathophysiological features develop during the progression of the disease; information that could be critical to advancing the development of disease-modifying therapies. Here, we developed a novel paradigm for modeling progressive dopamine loss and used this paradigm, in addition to other well-studied animal models of PD, to investigate how and when basal ganglia activity changes in PD.

First, we developed a gradual dopamine depletion mouse model by injecting multiple low doses of the neurotoxin 6-OHDA over months to better recapitulate the slow progression of dopamine loss seen in PD. Behavioral assessment of these animals throughout the progression of dopamine loss revealed a differential degradation of motor symptoms, with vertical movement declining linearly while horizontal movement remained robust until late stages. Interestingly, we found that motor coordination was

significantly less impaired in animals that had undergone gradual depletions as opposed to acute depletions. These results establish a gradual depletion paradigm that can be used to study changes at various stages of dopamine loss, while modeling the progressive degeneration in PD so as not to preclude any compensatory plasticity that may be missing in more acute depletion models.

Next, we demonstrated a stereotyped, hierarchical progression of pathophysiology in the output nucleus of the basal ganglia using a number of animal models of PD. Briefly, firing rate changes occurred first at early stages of dopamine loss, followed by changes in firing pattern at more intermediate stages. The progression of pathophysiology was similar between two mechanistically different models of PD and end stage pathophysiology was similar regardless of the rate or lateralization of depletion. These results provided the first quantitative analysis of the trajectory with which the basal ganglia output physiology breaks down over the course of progressive dopamine depletion.

In the final chapter, we discuss the evolving field of animal models of PD and potential physiological correlates of motor function based on current treatments effects on physiology and other studies of pathophysiology leading up to motor symptom onset. Taken together, these results demonstrate the complex interplay between the onset and progression of various motor deficits and pathological basal ganglia activity that develop due to the progressive degeneration of dopamine.

## ACKNOWLEDGMENTS

Over the past six years I have received support, motivation, and inspiration from a number of incredible individuals. First, I would like to thank Dr. Aryn Gittis for accepting me as a rotation student before she even had a lab and allowing me to help build it from the ground up. We celebrated every success and persevered through every failure together. Your guidance, support, and trust through the many ups and downs of my project was instrumental to my success and I'm so proud of the work we have produced. I would also like to thank all those who served on my committee throughout my graduate career: Drs. Alison Barth, Sandra Kuhlman, Robert Turner, and Nathan Urban. I left each of our meetings feeling rejuvenated and inspired to think about my data in new and interesting ways. I am greatly appreciative of all of your advice and the ways in which you pushed me to be a better scientist, a more thoughtful writer, and a more effective communicator.

Being a part of the collaborative, innovative, and supportive environment that is the Great Hall of Brain Science has contributed immensely to my success as a graduate student. I am thankful for all of the intellectually stimulating discussions I have had with each member, in addition to the personal support I received as I navigated each academic and scientific hurdle. I look forward to continuing to celebrate all of your future successes, as I will always consider you members of my academic family.

The members of the Gittis lab have all played an essential role in my development as a scientist, mentor, and overall person. Rachel Bouchard has been my rock from day one, ensuring that the lab runs smoothly and helping me in whatever ways she could. I will cherish the countless hours we spent in the surgical and behavior spaces getting to know each other while troubleshooting our experiments. Dr. Kevin Mastro is my scientific partner. Our stimulating scientific discussions always left me feeling inspired and made each setback a little bit easier to overcome. I'm so proud of everything you have accomplished, and I cannot wait to celebrate your continued contributions to the scientific community. Kevin Zitelli, Victoria Corbit and Tim Whalen, I have learned so much from you all and your constructive feedback and unwavering support has continually steered me in the right direction. To my undergraduates, Amira Millette and Jen Thomas, you were both such a pleasure to mentor; thank you for all of your contributions and for actively engaging in my research. I'd like to thank Katrina Nguyen and Teresa Spix for always helping me laugh through the hard times and reminding me to celebrate each success. To the newest members of the lab, Ian Rosner, Liz Wendel, Jenna Schwenk, and Brian Isett, you are all extremely talented scientists and overall wonderful people. I have enjoyed our short time together and I wish you all the best with your academic journeys.

Thank you to all of my fellow graduate students, faculty, and administrators in the Department of Biological Sciences at Carnegie Mellon University. Each of you has contributed to my success as a graduate student. Dr. D.J. Brasier, thank you for letting me serve as your first teaching assistant and for giving me opportunities to research and experiment in the classroom. Your love of teaching is contagious and serving as your TA throughout my time at CMU was a true gift. Thank you to Allies Grad for serving as a catalyst for my involvement at the university level and helping me find my voice to advocate for a diverse graduate student body. A special thank you to the Graduate Student

Assembly (GSA) for electing me to serve the graduate community and providing me with a purpose outside of the lab. To each executive member I served with (Daniel Gingerich, Nicole Rafidi, Chetali Gupta, Stephanie Laughton, Rony Patel, Clive Newstead, and Jon Wilcox) thank you for all of the support you provided and for showing me what amazing things can be accomplished by working together as a team. To each of the staff, faculty, and administrators (Brittani McKenna, Dr. Amy Burkert, Gina Casalegno, Dr. Suzie Laurich-McIntyre, M. Shernell Smith, Jamie Rossi, Angie Lusk, Ashley Grice, and Jess Klein) I got to know during my term on GSA, thank you for being incredible mentors and serving as consistent advocates for all graduate students at CMU.

Last, but certainly not least, I would like to thank my family for everything they have done to encourage and support me throughout my academic journey. Special thanks to my father, Fred Willard, and my mother, Julie Willard, for always indulging my desire to learn and explore. Thank you to the incredible array of parents (MJ Willard, Anna Thomas, John Thomas, Colleen Thomas, and Gerald Mull) I have come to know and love and who have each taught me something special about the meaning of family. To my Pappap, Marco Ellena, and my grandmothers, Rose Ellena and Mary Willard, thank you for instilling me with a strong work ethic and for always believing in me and always showing up to support me in whatever way I needed it. Melinda Willard, Jen Thomas, Nick Thomas, Julia Blair, Sarah Blair, Nick Cottrell, Dan Donnelly and James Mackenzie, thank you for being amazing sisters and brothers and serving as a constant source of encouragement and laughter. To my game night family, Ben Shoemaker, Gina Sigler, and Christian Bruggeman, thank you for all of the amazing memories and for managing to stay in touch all these years despite all of our hectic lives.

Finally, I would like to give the biggest thank you to my wife, Dr. Jessica Thomas. You have stood by my side through every up and down, spent countless nights and weekends keeping me company in the lab, and listened intently when I would talk endlessly about my project. I would not have been able to complete this journey without you by my side, cheering me on every step of the way. Thank you.

## TABLE OF CONTENTS

ABSTRACT.....	iii
ACKNOWLEDGEMENTS.....	v
TABLE OF CONTENTS.....	vii
LIST OF FIGURES.....	xi
LIST OF TABLES.....	xiii
1.0 INTRODUCTION.....	1
1.1 ANIMAL MODELS OF PARKINSON'S DISEASE.....	2
1.1.1 Pharmacological models.....	3
1.1.2 Neurotoxin models.....	4
1.1.3 Genetic and $\alpha$ -synuclein models.....	6
1.2 PARKINSONIAN PATHOPHYSIOLOGY IN THE BASAL GANGLIA.....	8
1.2.1 Striatum.....	9
1.2.2 Globus pallidus externa (GPe) & subthalamic nucleus (STN).....	11
1.2.3 Globus pallidus interna (GPi) & substantia nigra pars reticulata (SNr).....	12
1.3 SUMMARY AND AIMS OF DISSERTATION .....	14
2.0 DIFFERENTIAL DEGRADATION OF MOTOR DEFICITS DURING GRADUAL DOPAMINE DEPLETION WITH 6-HYDROXYDOPAMINE IN MICE....	16
2.1 INTRODUCTION.....	17

2.2	EXPERIMENTAL PROCEDURES.....	20
2.2.1	Animals.....	20
2.2.2	Implantation of bilateral cannulas and 6-OHDA injection in the MFB.....	21
2.2.3	Behavioral assessment.....	22
2.2.4	Immunohistochemistry.....	23
2.2.5	Statistical analysis.....	25
2.3	RESULTS.....	25
2.3.1	Injections of 6-OHDA over time result in graded depletion of striatal dopamine.....	25
2.3.2	Effects of gradual depletion on dopamine metabolites and monoamines.....	29
2.3.3	Open field locomotor deficits develop suddenly during gradual depletions.....	31
2.3.4	Rearing deficits progress gradually as dopamine is depleted.....	34
2.3.5	Motor coordination is differentially affected in gradually vs. acutely depleted mice.....	35
2.3.6	Time course of gradual depletions can be varied and extended....	38
2.4	DISCUSSION.....	40
2.5	ACKNOWLEDGEMENTS.....	46
3.0	STEREOTYPED BASAL GANGLIA OUTPUT PATHOPHYSIOLOGY ACROSS DOPAMINE DEPLETION MODELS EMERGES PRIOR TO MOTOR DEFICITS.....	47

3.1	INTRODUCTION.....	48
3.2	METHODS.....	50
3.2.1	Animals.....	50
3.2.2	Cannula implantation.....	51
3.2.2	Stereotaxic $\alpha$ -synuclein injection.....	52
3.2.3	Implantation of head-fixation system.....	52
3.2.4	Head-fixation training and recording.....	53
3.2.5	Behavioral assessment.....	53
3.2.6	In vivo SNr recordings.....	55
3.2.7	Electrophysiology analysis.....	55
3.2.8	Synchrony analysis.....	56
3.2.9	Immunohistochemistry.....	57
3.2.10	Fluorescence quantification.....	58
3.2.11	Statistical analysis.....	58
3.2.12	Principal component analysis.....	59
3.2.13	Linear models.....	60
3.2.14	Linear classifier.....	61
3.3	RESULTS.....	62
3.3.1	SNr pathophysiology at end-stages of dopamine depletion in awake mice.....	62
3.3.2	Increased irregularity in firing pattern correlates with increased bursting activity.....	66

3.3.3	SNr pathophysiology proceeds in two phases during gradual dopamine depletion.....	68
3.3.4	Gradual dopamine depletion with 6-OHDA results in late onset of behavioral deficits.....	71
3.3.5	PFF $\alpha$ -synuclein drives gradual dopamine loss and behavioral changes that mirror the prodromal stage of 6-OHDA-treated mice.....	73
3.3.6	SNr pathophysiology progresses similarly in PFF $\alpha$ -syn mice and 6-OHDA-treated mice .....	75
3.3.7	Unilateral 6-OHDA SNr pathophysiology aligns to prodromal and end-stage bilateral pathophysiological phases.....	78
3.4	DISCUSSION.....	82
3.5	ACKNOWLEDGEMENTS.....	87
4.0	SUMMARY AND CONCLUSIONS.....	88
4.1	THE PATH TO A BETTER PARKINSON MODEL.....	90
4.1.1	Progressive models.....	90
4.1.2	Fusion models.....	92
4.2	PHYSIOLOGICAL CORRELATES OF MOTOR DYSFUNCTION....	94
4.2.1	Influencers of basal ganglia output physiology.....	95
4.2.2	Current treatments and their effect on physiology.....	99
4.2.3	Prodromal pathophysiology in Parkinson’s disease.....	101
4.3	FINAL REMARKS.....	103
	APPENDIX A.....	105
	BIBLIOGRAPHY.....	106

## LIST OF FIGURES

Figure 2.1. Gradual depletion paradigm linearly reduces dopamine over time.....	28
Figure 2.2. Levels of dopamine metabolites and other monoamines measured with HPLC during gradual dopamine depletion paradigm.....	30
Figure 2.3. Effects of gradual dopamine depletion on spontaneous locomotion in an open field.....	33
Figure 2.4. Effects of gradual dopamine depletion on rearing behavior.....	34
Figure 2.5. Effects of gradual dopamine depletion on motor coordination assessed with a vertical pole task.....	37
Figure 2.6. Time course of gradual depletions can be varied and extended over a month.....	39
Figure 2.7. Differential progression motor deficits in gradually depleted mice.....	41
Figure 3.1. 6-OHDA-induced acute bilateral dopamine depletions result in similar SNr pathophysiology as gradual bilateral dopamine depletions.....	65
Figure 3.2. Irregularity and bursting physiological parameters are correlated in control and 6-OHDA-induced bilateral dopamine depletions.....	67
Figure 3.3. 6-OHDA-induced bilateral gradual dopamine depletion causes early reduction of firing rate followed by increases in irregularity and bursts within the SNr.....	70
Figure 3.4. 6-OHDA-induced bilateral gradual dopamine depletion results in late stage onset of motor deficits.....	72
Figure 3.5. PFF $\alpha$ -syn-induced bilateral gradual dopamine depletion leads to hyperactivity and fails to reach end-stage motor impairments.....	74

Figure 3.6. PFF  $\alpha$ -syn-induced bilateral gradual dopamine depletion causes early reduction of firing rates followed by increases in irregularity and bursts within the SNr.....77

Figure 3.7. Unilateral 6-OHDA model pathophysiology aligns to prodromal and end-stage bilateral pathophysiology.....81

Figure 4.1. Propagation of pathophysiology in the basal ganglia in Parkinsonian conditions.....98

Figure A1. SNr pathophysiology in bilateral 6-OHDA dopamine depletions.....105

## LIST OF TABLES

Table 2.1 Striatal dopamine levels following 6-OHDA injections.....	26
---	----

## 1.0 INTRODUCTION

Laboratory animal models have played a crucial role in enhancing our ability to diagnose, manage, and treat diseases in humans. However, our progress in treating complex neurodegenerative diseases such as Parkinson's disease (PD) has been stalled due to our incomplete understanding of the etiology of the disease in humans (Olanow and Tatton, 1999). Over the last few decades, longitudinal studies in human patients with PD have aided in unveiling new information about the progression of disease pathology and new technologies have enabled physiological measurements to be obtained during treatment (Huang et al., 2007; Singh et al., 2016). This wealth of new information has revealed a wide array of changes in brain activity that occur following PD neurodegeneration and has subsequently led to a push for the development of new animal models that allow us to study how these activity patterns develop over the course of the disease. These models will be featured throughout the dissertation while shifting the attention from the development of animal models (see Reviews (Blesa et al., 2012; Chesselet and Richter, 2011; Dawson et al., 2010)) to utilizing these models to enhance our understanding of the patterns of activity that may be causal to the development of motor symptoms.

Here, we will first review animal models of PD and discuss how they have contributed to the advancements that have been made in understanding and treating PD. In doing so, we will highlight how these animal models have contributed to our current understanding of the basal ganglia and the role it plays in the manifestation of motor symptoms. Over the last 40 years, the development of better animal models coupled with new technologies has brought us closer to understanding the link between pathological brain activity and motor dysfunction.

## 1.1 ANIMAL MODELS OF PARKINSON'S DISEASE

In 1817, James Parkinson first described the key clinical features of what is now the second most common neurodegenerative disease afflicting approximately 1% of the population over 60 years of age (de Lau et al., 2006; Parkinson, 2002). There are two distinct pathologies that are typically described as hallmarks of Parkinson's disease (PD) (Olanow and Tatton, 1999). One diagnostic marker involves the presence of misfolded  $\alpha$ -synuclein proteins in the form of Lewy bodies. However, this pathology is not specific to PD; Lewy bodies are found in healthy elderly patients and patients with the pathology of Alzheimer's disease can also have Lewy bodies (Dickson et al., 2009; Gibb and Lees, 1988; Zaccai et al., 2008). Additionally, Lewy body pathology is highly variable in location and quantity. The other far more consistent pathological hallmark of PD is the degeneration of dopamine neurons in a region of the midbrain known as the substantia nigra pars compacta (SNc). This results in decreased dopamine signaling in the striatum, a major input nucleus of the basal ganglia, involved in the control of voluntary movement. Many motor symptoms of PD, including tremors, rigidity, bradykinesia, freezing, and balance instability (Betarbet et al., 2002; Dauer and Przedborski, 2003; Olanow and Tatton, 1999) are thought to arise due to initial dysfunction of neural circuits in the striatum propagating to other parts of the basal ganglia and outside brain areas. Motor symptoms typically do not become overt enough to diagnose PD until 80% of dopamine has been depleted from the striatum, but by this point, patients have likely been living with chronically low levels of dopamine for years and dysfunction in neural circuits may have already passed a point of no return.

At present, primary treatments such as L-DOPA and deep brain stimulation (DBS) are administered after the onset of motor symptoms and can have severe side effects or involve

invasive surgeries (Fasano et al., 2012; Poewe et al., 2010; Sgambato-Faure and Cenci, 2012). These limits to current therapies might be circumvented if treatments were applied earlier in the disease, before widespread dysfunction could spread throughout the basal ganglia and alter function in motor areas throughout the brain. PD is a complex neurological disorder that likely results from a combination of multiple genetic and environmental factors, making it difficult to elucidate a distinct mechanism for pathology. Symptoms of the disease involve both motor and non-motor features such as impaired cognition, depression, and constipation. Currently, no single animal model reproduces all features of the disease, but a number of animal models are available that reproduce a subset of symptoms and pathologies (Betarbet et al., 2002; Bové et al., 2005; Meredith et al., 2008a; Simola et al., 2007). Most of the available models fall under three main categories based on the method employed to replicate features of the human disease: 1) pharmacological models, 2) neurotoxin models, and 3) genetic and  $\alpha$ -synuclein models. While these models have greatly enhanced our understanding of how circuits are altered following a full dopamine lesion and what may be contributing to dopamine degeneration, we are still lacking key information about the how aberrant activity patterns develop over the course of progressive dopamine loss and how they ultimately contribute to the onset of motor dysfunction.

### **1.1.1 Pharmacological models**

One of the earliest advancements in treating PD can be attributed to the first animal model in 1957. Arvid Carlsson began studying a compound called reserpine, which when administered to mice and rabbits resulted in reduced motor activity. Upon further investigation of the mechanism behind reserpine's sedative effect, he showed that reserpine depleted brain dopamine and

injecting L-DOPA alleviated the parkinsonian state (Carlsson et al., 1957; Obeso et al., 2017). This provided the first evidence of the role of striatal dopamine in motor control and led to clinical trials that ultimately resulted in one of the most effective symptomatic treatments for PD (Fahn, 2015; Lees et al., 2015; Nagatsua and Sawadab, 2009). We now understand that reserpine mimics the disease biochemistry of PD by causing a transient (24 hour) decrease in monoamines (noradrenaline, 5-HT, and dopamine) by inhibiting the vesicular monoamine transporter (VMAT2) (Duty and Jenner, 2011).

The other pharmacological model of PD involves an injection of haloperidol which antagonizes dopamine receptors to block striatal dopamine transmission. Animals treated with haloperidol present with muscle rigidity and an inability to initiate movements (akinesia) within 60 minutes (Duty and Jenner, 2011; Francardo, 2018). Both the reserpine and haloperidol model fail to replicate the characteristic neurodegeneration associated with PD and their transient manifestation limits the ability to test long-term symptom relief of potential treatments. However, these models remain a popular choice for assessing the potential symptomatic efficacy of novel dopaminergic and non-dopaminergic drugs during the early screening process.

### **1.1.2 Neurotoxin models**

A decade after the discovery of the reserpine model, Urban Ungerstedt reported that stereotaxic injection of the toxin 6-hydroxydopamine (6-OHDA) into the substantia nigra could be used to produce unilateral dopamine loss (Obeso et al., 2017; Ungerstedt, 1968).

Traditional rodent models involve a single unilateral infusion of a high dose of 6-OHDA intracranially into various areas of the nigrostriatal pathway to induce a high degree of striatal

dopamine loss (Betarbet et al., 2002; Bové et al., 2005; Iancu et al., 2005; Schober, 2004; Schwarting and Huston, 1996a, 1996b; Simola et al., 2007). 6-OHDA selectively targets the dopamine transport system and induces non-apoptotic death of dopaminergic neurons (Jeon et al., 1995; Schober, 2004). High doses are used to produce 80-90% striatal dopamine loss in 2-3 days. Reducing dopamine levels unilaterally results in a robust quantifiable circling behavior in rodents that has been the gold standard in evaluating the effectiveness of potential therapies and neuroprotective strategies (Bové et al., 2005). The 6-OHDA model is commonly chosen due to the availability of well-established injection techniques and relatively low maintenance cost (Betarbet et al., 2002). Furthermore, recent studies have shown that bilaterally administering 6-OHDA results in key non-motor symptoms of PD, including anxiety, depression, olfactory deficits, and cognitive deficits (Bonito-Oliva et al., 2014; Campos et al., 2013). While this model presents sustained dopamine degeneration as well as other pathological features of PD, it produces acute damage rather than progressive neurodegeneration and it does not present Lewy body pathology (Francardo, 2018).

The other commonly used neurotoxin model of PD resulted from the discovery by J. William Langston and colleagues in 1983 that 1-methyl-4-phenyl-1,2,3,6-tetrahydropyridine (MPTP) caused irreversible parkinsonian symptoms (Langston et al., 1983). Since then, MPTP has been used to model PD in the laboratory by administering it systemically via subcutaneous or intravenous injections to non-human primates or mice (Przedborski et al., 2001). High doses of MPTP given over a short period of time result in bilateral dopamine neurodegeneration and pronounced motor deficits such as akinesia, bradykinesia, postural and gait abnormalities. Protocols have been developed to attempt to reproduce the progressive degeneration seen in PD by administering lower doses for longer periods (see Review: (Meredith and Rademacher,

2011)). Studies in MPTP-treated non-human primates in the early 1990s led to the development of the latest symptomatic breakthrough in the management of PD that is the surgical ablation and deep brain stimulation of the subthalamic nucleus and globus pallidus interna (Aziz et al., 1992; Benabid et al., 1994; Guridi et al., 1994; Obeso et al., 2017; Wichmann et al., 1994). The use of the MPTP model in rodents has been less successful, largely due to the large variability in behavioral and biochemical changes depending on mouse strain, age, gender, and body weight, and the fact that rats are resistant to the neurodegenerative effects of the toxin (Date et al., 1990; Francardo, 2018; Jackson-Lewis and Przedborski, 2007; Johannessen et al., 1985; Miller et al., 1998; Mitumoto et al., 1998; Schwarting et al., 1999; Sedelis et al., 2000). Both the 6-OHDA and MPTP models fail to present Lewy body pathology and most protocols result in acute neurodegeneration, however these models remain a popular choice for studying physiological and biochemical changes that result from sustained dopamine depletion. These models have also been useful in studying antiparkinsonian drugs as well as treatment-related complications such as L-DOPA-induced dyskinesia (Cenci and Lindgren, 2007; Iderberg et al., 2012).

### **1.1.3 Genetic and $\alpha$ -synuclein models**

The discovery of the first gene mutation associated with PD in 1997 led to a surge in the development of new animal models through the manipulation of the animal genome (Polymeropoulos et al., 1997). While only about 5% of PD cases are caused by genetic defects (Dauer and Przedborski, 2003), some argue that since both inherited and idiopathic forms of PD share common pathology, findings in genetic models could be relevant to all types of PD (Beilina and Cookson, 2015; Kumaran and Cookson, 2015; Mullin and Schapira, 2015).

Mutations affecting the  $\alpha$ -synuclein gene (SNCA) are the most commonly studied. Models with these mutations display widespread  $\alpha$ -synuclein containing Lewy-body pathology, similar to that seen in human patients with PD (Spillantini et al., 1997). Unfortunately, while these models have the pathological feature missing from pharmacological and neurotoxin models, they typically show quite subtle deficits, if any, due to a lack of significant degeneration of dopamine neurons (see Reviews (Betarbet et al., 2002; Chesselet et al., 2008; Dawson et al., 2010; Kreiner, 2015; Meredith et al., 2008a; Potashkin et al., 2010; Terzioglu and Galter, 2008)). These models may not be effective for testing neuroprotective strategies or efficacy of treatments aimed at alleviating motor symptoms, however we can still use these models to learn more about the mechanisms underlying non-motor symptoms and protein pathology (Dehay and Fernagut, 2016; Francardo, 2018).

Studies involving these  $\alpha$ -synuclein gene mutations have undoubtedly opened up new research avenues and represent a paradigm shift in the way we think about the pathogenesis of PD (Obeso et al., 2017). Findings from these models led to the hypothesis that misfolded  $\alpha$ -synuclein assemblies such as oligomers or fibrils are the toxic forms of the protein that can lead to neurodegeneration. This further inspired the development of new methods for generating  $\alpha$ -synuclein animal models involving viral vector delivery to overexpress  $\alpha$ -synuclein (Decressac et al., 2012a, 2012b; Lundblad et al., 2012) and injections of recombinant  $\alpha$ -synuclein pre-formed fibrils (Luk et al., 2012). Both of these models result in varying degrees of dopamine neuron degeneration as well as some detectable motor deficits (Lindgren et al., 2012; Volpicelli-Daley et al., 2016). These models provide further evidence that misfolded  $\alpha$ -synuclein may act as a pathological seed that promotes the misfolding of other  $\alpha$ -synuclein molecules, thereby propagating and enhancing the degenerative process of PD (Desplats et al., 2009; Giráldez-Pérez

et al., 2014; Kordower et al., 2008; Obeso et al., 2017; Valadas et al., 2015; Volpicelli-Daley et al., 2011). While these models offer new ways to study mechanisms of neurodegeneration, protein pathology, and early stages of dopamine loss, they may not be well-suited to studying end-stage PD pathology.

Together, this diverse array of animal models, in combination with the increasing availability of novel technologies in the field of neuroscience, allows for the investigation of the wide range of pathologies involved in PD and will provide invaluable insight into the underlying mechanisms of the disease. In doing so, we are continuing to unveil how dopamine regulates a vast number of complex processes. Further investigation into how aberrant activity patterns in key brain areas such as the basal ganglia develop in relation to dopamine loss and the onset of motor symptoms may enable us to develop disease-modifying strategies as well as more effective treatments for PD symptoms.

## **1.2 PARKINSONIAN PATHOPHYSIOLOGY IN THE BASAL GANGLIA**

The main motivation behind developing better animal models of PD is to identify the underlying mechanisms responsible for the debilitating symptoms. Advancements made in understanding the pathophysiology of PD, specifically within the basal ganglia circuit, have inspired the development of more effective treatment strategies. The basal ganglia are a group of subcortical nuclei that are an integral part of three main parallel processing loops: 1) motor, 2) associative-cognitive, and 3) emotional-limbic (Alexander et al., 1986, 1990; Kelly and Strick, 2004; Middleton and Strick, 2000). The motor loop has been the most highly studied because it is implicated in the motor symptoms of PD as well as a host of other movement disorders (DeLong,

1990). In the 1980s and early 1990s, findings from human patients combined with neuroanatomy and neurophysiology studies in animals culminated in the generation of a firing rate model of basal ganglia function in both health and disease (Albin et al., 1989; DeLong, 1983, 1990; Penney and Young, 1983). While this model has several limitations, it has provided both clinicians and basic scientists with an important framework with which to generate testable hypotheses regarding basal ganglia nuclei function in PD. Studies in which basal ganglia activity is monitored in vivo in an intact network have been the most promising in terms of identifying complex physiological changes such as synchrony between neurons within and across nuclei and oscillatory activity within and across nuclei. Each of the following sections will highlight key findings from each nuclei of the basal ganglia and how they have informed the development of novel treatment strategies.

### **1.2.1 Striatum**

The striatum is the nucleus most directly affected by the loss of dopaminergic neurons in the SNc during PD and it is critically involved in the production and control of volitional movement. The striatum acts as the major input nucleus of the basal ganglia, integrating information primarily from the cortex and thalamus (Bolam et al., 2000). Neurons within the striatum project differentially to downstream nuclei through two distinct pathways, the “direct” and “indirect”. The direct pathway is comprised of inhibitory projections to the output nuclei of the basal ganglia, the globus pallidus interna (GPi) and the substantia nigra pars reticulata (SNr). The indirect pathway is a multi-nuclei route through the globus pallidus externa (GPe), followed by the subthalamic nucleus (STN), that then terminates in the same output nuclei. Under healthy

conditions, dopamine regulates the activity in both of these pathways by altering excitability based on their differential expression of dopamine receptors (Gerfen and Surmeier, 2011). In the rate model of basal ganglia circuitry, the direct pathway aids in facilitating and initiating movements, while the indirect pathway is responsible for the inhibition or suppression of unwanted movements (Albin et al., 1989; Alexander and Crutcher, 1990; DeLong, 1990). It is theorized that a delicate balance between these two pathways allows for the appropriate selection of movements (Albin et al., 1989; DeLong, 1990; Galvan and Wichmann, 2007; Graybiel et al., 1994).

Based on the rate model, dopamine loss in PD would result in decreased activity of striatal neurons involved in the direct pathway, and increased activity of neurons in the indirect pathway. Since these neurons are heterogeneously interspersed throughout the striatum and dopamine alters transmission from the cortex to the striatum rather than spontaneous activity, it has been difficult to identify firing rate changes in vivo (Galvan and Wichmann, 2008). One study in anesthetized 6-OHDA-treated rats did show that direct pathway neurons were less active and indirect pathway neurons were more active compared to control animals (Mallet et al., 2006). A more recent study in humans reported an overall increase in firing rate in striatal neurons when compared to patients with essential tremor and isolated dystonia (Singh et al., 2016). Additionally, this study used a probability-based algorithm to detect “burst” firing activity which was also elevated in PD patients compared to other groups.

In terms of treatment, L-DOPA dopamine replacement therapy remains the most effective way to minimize motor deficits stemming from decreased dopamine signaling in the striatum. However, prolonged usage of L-DOPA leads to L-DOPA induced dyskinesias, characterized by unwanted involuntary movements, in the vast majority of PD patients (Obeso et al., 2000). These

side effects may be in part due to the non-specific nature of this type of therapy resulting in maladaptive plasticity of basal ganglia circuits. Designing future treatments with more specific targets could rescue motor deficits while avoiding negative side effects. Using the rate model in combination with documented physiological changes in striatal activity, one might predict that upregulating activity of the motor-facilitating direct pathway could help correct the pathway imbalance and ultimately rescue motor deficits. Using an animal model of PD, Kravitz and colleagues showed that optogenetic activation of the direct pathway was sufficient to restore motor function (Kravitz et al., 2010). These findings serve as an example of how understanding the pathophysiology underlying PD can unveil unique therapeutic targets for more effective treatments.

### **1.2.2 Globus pallidus externa (GPe) & subthalamic nucleus (STN)**

The globus pallidus externa (GPe) and the subthalamic nucleus (STN) are intermediary basal ganglia nuclei that are part of the indirect pathway. GPe receives inhibitory projections from the striatum and sends inhibitory projections mainly to STN. The STN receives input from the cortex as well as the GPe and sends excitatory projections both back to the GPe and onward to the basal ganglia output nuclei. The rate model predicts that in PD, over-activity of the indirect pathway results in decreased activity of the GPe, and increased activity of the STN.

Multiple studies in animal models of PD and human PD patients have reported decreased firing rates in the GPe, in addition to increased irregularity in firing pattern and increased burst firing (Boraud et al., 1998; Filion and Tremblay, 1991; Hutchison et al., 1994; Mastro et al., 2017; Pan and Walters, 1988; Wichmann and DeLong, 2003; Wichmann and Soares, 2006).

Another prominent pathophysiological feature seen in GPe in animal models of PD is an increase in synchronous firing and the presence of synchronized beta ( $\beta$ ) oscillations (13-30 Hz) (Mallet et al., 2008; Raz et al., 2000). In a recent study, Mastro and colleagues showed that global optogenetic activation of the GPe in an animal model of PD was unable to rescue motor function. Interestingly, transiently dissociating the activity of two subpopulations of GPe neurons, PV and Lhx6 was sufficient to induce recovery of movement. In fact, the length of time for which movement was recovered post-activation was significantly longer than when recovery was achieved through optogenetic activation of the direct pathway (Mastro et al., 2017).

In PD, STN firing rates are elevated, there is an increase in the irregularity of firing pattern as well as the presence of bursts, and there is also increased synchronous firing and  $\beta$ -oscillations (Bergman et al., 1994; Bevan et al., 2002; Kühn et al., 2005; Neumann et al., 2016; Wichmann and Soares, 2006). Currently, the STN is one of the most popular targets for DBS, which involves the surgical implantation of electrodes into the brain to supply high frequency electrical stimulation to the surrounding tissue and ameliorate motor symptoms. However, similar to L-DOPA, DBS does not prevent the progression of PD and can result in the appearance of other cognitive, mood, and motor complications.

### **1.2.3 Globus pallidus interna (GPi) & substantia nigra pars reticulata (SNr)**

The globus pallidus interna (GPi) and substantia nigra pars reticulata (SNr) are the output nuclei of the basal ganglia. They receive input from the striatum, GPe and STN and send inhibitory projections to motor areas of the thalamus. The overall consequence of all of the previously described predictions of the rate model is increased activity in GPi/SNr which leads to excessive

inhibition of downstream motor systems in the thalamus, cortex, and brainstem resulting in parkinsonian motor deficits.

Studies in human patients and animal models have reported predicted increases in firing rate, irregularity, bursting, synchrony, and  $\beta$ -oscillations in GPi/SNr (Filion and Tremblay, 1991; Galvan and Wichmann, 2008; Heimer et al., 2002; Hutchison et al., 1994; Wichmann et al., 2002). There are a number of studies, however, that report no changes or changes contradictory to the rate model (Leblois et al., 2007; Muralidharan et al., 2016; Raz et al., 2000; Soares et al., 2004; Wichmann and Soares, 2006) and even find differences in pathology between the GPi and SNr (Wichmann et al., 1999). Furthermore, findings in the output nuclei of rodent models of PD are even more heterogeneous and seem to vary based on the type of model, length of time between dopamine loss and recording, and even the anesthesia used during recordings (Lobb and Jaeger, 2015a; Lobb et al., 2013; Seeger-Armbruster and Von Ameln-Mayerhofer, 2013). While it remains unclear what physiological changes in the output nuclei contribute to motor dysfunction, treatments targeting the GPi have been successful in relieving symptoms in PD patients. Surgical ablation of the GPi was the predominate treatment for PD in the 1950s and 60s prior to the introduction of L-DOPA. A resurgence of this procedure occurred in the 1990s thanks to new surgical technologies and the severe side-effects associated with chronic L-DOPA treatments (Laitinen et al., 1992). Today, GPi remains a popular target for DBS and there is still an ongoing debate regarding the relative therapeutic benefits of GPi- vs. STN-DBS (Odekerken et al., 2016; Tan et al., 2016; Wang et al., 2016).

Overall, these results highlight how unveiling pathophysiology in PD has led to the development of promising new therapeutic strategies. However, all of these findings in addition to all of the proposed therapies, focus on patients who are symptomatic and therefore in the

advanced stages of the disease. Redirecting our efforts to focus on the progression of pathophysiology and the transition from asymptomatic to symptomatic PD may help us design strategies for slowing or stopping progression of the disease as opposed to simply minimizing debilitating symptoms.

### **1.3 SUMMARY AND AIMS OF DISSERTATION**

In summary, the development of new animal models has enabled us to start to piece together how network activity within the brain is altered in PD and provides new targets for therapeutic intervention. Much of what we know about how the basal ganglia function is due in large part to our investigation of its dysfunction in disease states. This dissertation represents the steps taken to understand when pathophysiology emerges within the basal ganglia in an intact network during the progression of dopamine loss in PD and how this relates to the onset of motor symptoms. In the following chapters, we will highlight the development of a novel dopamine depletion paradigm that allows us to recapitulate the progressive degeneration of dopaminergic neurons as well as the transition from asymptomatic to symptomatic PD. This study establishes that this new paradigm allows us to probe multiple stages of dopamine loss while still mirroring the severity of late stage motor deficits seen in other animal models. Additionally, it shows how certain aspects of motor performance may be differentially affected depending on the rate of dopamine loss. Secondly, we will demonstrate how we can use this new paradigm, in addition to other animal models, to determine how stereotyped pathophysiology is within the basal ganglia in an intact network and what features may be contributing to the onset of motor deficits. Lastly,

we will explore the two major themes within this document; animal models and the link between pathophysiology in the basal ganglia and the symptomatic onset of PD.

## **2.0 DIFFERENTIAL DEGRADATION OF MOTOR DEFICITS DURING GRADUAL DOPAMINE DEPLETION WITH 6-HYDROXYDOPAMINE IN MICE**

Parkinson's disease (PD) is a movement disorder whose cardinal motor symptoms arise due to the progressive loss of dopamine. Although this dopamine loss typically progresses slowly over time, currently there are very few animal models that enable incremental dopamine depletion over time within the same animal. This type of gradual dopamine depletion model would be useful in studies aimed at the prodromal phase of PD, when dopamine levels are pathologically low but motor symptoms have not yet presented. Utilizing the highly characterized neurotoxin 6-hydroxydopamine (6-OHDA), we have developed a paradigm to gradually deplete dopamine levels in the striatum over a user-defined time course – spanning weeks to months – in C57BL/6 mice. Dopamine depletions were achieved by administration of five low dose injections (0.75 µg) of 6-OHDA through an implanted intracranial bilateral cannula targeting the medial forebrain bundle. Levels of dopamine within the striatum declined linearly with successive injections, quantified using tyrosine hydroxylase immunostaining and high-performance liquid chromatography. Behavioral testing was carried out at each time point to study the onset and progression of motor impairments as a function of dopamine loss over time. We found that spontaneous locomotion, measured in an open field, was robust to loss of dopamine until ~70% of striatal dopamine was lost. Beyond this point, additional dopamine loss caused a sharp decline in motor performance, reaching a final level comparable to that of acutely depleted mice. Similarly, although rearing behavior was more sensitive to dopamine loss and declined linearly as a function of dopamine levels, it eventually declined to levels similar to that seen in acutely

depleted mice. In contrast, motor coordination, measured on a vertical pole task, was only moderately impaired in gradually depleted mice, despite severe impairments observed in acutely depleted mice. These results demonstrate the importance of the temporal profile of dopamine loss on the magnitude and progression of behavioral impairments. Our gradual depletion model thus establishes a new paradigm with which to study how circuits respond and adapt to dopamine loss over time, information which could uncover important cellular events during the prodromal phase of PD that ultimately impact the presentation or treatability of behavioral symptoms.

## 2.1 INTRODUCTION

Parkinson's disease (PD) is a neurodegenerative disease characterized by a progressive loss of dopamine neurons in the substantia nigra pars compacta (SNc) (Damier et al., 1999; Fearnley and Lees, 1991; Morrish et al., 1996). This results in decreased dopamine signaling in the striatum, a major input nucleus of the basal ganglia involved in the control of voluntary movement (Dauer and Przedborski, 2003; Marsden and Obeso, 1994; Mink, 1996; Olanow and Tatton, 1999). Motor symptoms such as tremors, rigidity, bradykinesia, freezing, and balance instability typically do not become overt enough to diagnose PD until dopaminergic loss exceeds 70% in the striatum (Bernheimer et al., 1973; Betarbet et al., 2002; Deumens et al., 2002; Fahn, 2003; Riederer and Wuketich, 1976). Unfortunately by this time, patients have likely been living with chronically low levels of dopamine for years and dysfunction in neural circuits may have already passed a point of no return. Attempts at treating motor symptoms through dopamine replacement have been shown to successfully restore motor function, however prolonged treatment ultimately results in additional motor complications (Poewe et al., 2010; Sgambato-

Faure and Cenci, 2012). Interruptions of pathological brain activity through deep brain stimulation have been effective at reducing bradykinesia, rigidity, and tremor but typically have little effect on gait and postural symptoms and can also result in other side effects (Fasano et al., 2012; Sgambato-Faure and Cenci, 2012). It has been proposed that the pre-symptomatic phase of PD, called the prodromal phase, is an ideal time to begin therapies (Olanow and Obeso, 2012; Schapira and Tolosa, 2010). Treatments administered prior to complete dopamine loss may prevent further neurodegeneration or delay the onset of motor deficits. In addition, further understanding of how and when motor systems begin to break down during this phase may lead to techniques for early detection and more effective therapies aimed at restoring circuit function (Little and Brown, 2014).

Current standard animal models of PD typically involve acute, rapid degeneration of dopamine neurons which does not recapitulate PD disease progression (for reviews see (Betarbet et al., 2002; Bové et al., 2005; Hisahara and Shimohama, 2010; Schober, 2004; Terzioglu and Galter, 2008)). These models preclude the development of pathogenic mechanisms and prevent studies of various stages of PD. This need for chronic models of dopamine degeneration has led to an increase in the number and availability of genetic models of PD, but only 5% of human PD cases are inherited and these models come with their own set of limitations, discussed at length in a number of reviews (Betarbet et al., 2002; Chesselet et al., 2008; Dauer and Przedborski, 2003; Dawson et al., 2010; Meredith et al., 2008a; Potashkin et al., 2010; Terzioglu and Galter, 2008). In contrast to genetic strategies, well-characterized neurotoxin models, and more recently, AAV-induced overexpression of  $\alpha$ -synuclein (Decressac et al., 2012a, 2012b; Lundblad et al., 2012), have been adapted to create alternative chronic models of dopamine depletion (Fleming et al., 2005; Goldberg et al., 2011, 2012; Greenamyre et al., 2003; Meredith

et al., 2008a). However, models using 1-methyl-4-phenyl-1,2,3,6-tetrahydropyridine (MPTP) require increased safety precautions when handling mice which has proven to be a deterrent for widespread application of these models. Furthermore MPTP has had questionable toxicity in various mouse strains and does not always result in persistent and progressive motor symptoms (Betarbet et al., 2002; Bezard et al., 1997a; Blesa et al., 2010; Blume et al., 2009; McNaught et al., 2004; Meredith et al., 2002; Przedborski et al., 2001; Schober, 2004; Schwarting et al., 1999). Other adapted models utilize 6-hydroxydopamine (6-OHDA), the neurotoxin used in the first animal model of PD associated with SNc dopaminergic neurodegeneration (Ungerstedt, 1968). In most models utilizing 6-OHDA, animals are dopamine depleted unilaterally or given various acute doses to model different stages (Ferro et al., 2005; Fleming et al., 2005; Kirik et al., 1998; Przedborski et al., 1995; Schwarting and Huston, 1996a, 1996b; Truong et al., 2006). While dopamine loss in human PD can be asymmetrical, it ultimately results in dopamine loss in both hemispheres (Deumens et al., 2002; Simola et al., 2007). There are also concerns regarding contralateral compensation in unilateral depletions and a lack of compensatory mechanisms in using acute doses to model different stages of the disease (Meredith and Kang, 2006; Potashkin et al., 2010; Schwarting and Huston, 1996a). Thus, there is a lack of behavioral data available for the prodromal phase, where dopamine is being depleted bilaterally and gradually within the same animal.

In this study, we adapt the traditional 6-OHDA model to produce a gradual, bilateral dopamine loss over a user-defined time course. By administering low doses of 6-OHDA bilaterally through an intracranial cannula targeting the medial forebrain bundle (MFB), we gradually depleted dopamine levels within the same animal over 2-7 weeks rather than 2-3 days. Using this technique, we were able to slowly deplete dopamine over a prolonged time course to

study the effects of gradual vs. acute depletion on the onset and progression of motor impairments. We find that certain aspects of motor behavior are altered differentially as dopamine is depleted. Furthermore, some behaviors were differentially affected in gradually vs. acutely depleted mice, suggesting the engagement of compensatory plasticity during gradual depletion that is not engaged with the more traditional, acute paradigm. This study demonstrates that the time course of dopamine loss can influence the final behavioral state of the animal and provides a paradigm with which to study how motor systems adapt to chronically low levels of dopamine over time.

## **2.2 EXPERIMENTAL PROCEDURES**

### **2.2.1 Animals**

Experiments were conducted in accordance with the guidelines from the National Institutes of Health and with approval from Carnegie Mellon University Institutional Animal Care and Use Committee. Male and female P30-P80 day old mice on a C57BL/6J background were used for experiments. Acutely depleted animals were P42-P59 at time of injection and were P47-P81 when they completed their last behavioral testing. Gradual(3day) depleted animals and littermate saline controls were P34-P61 at the time of their first injection and were P44-P80 when they completed their last behavioral testing. Gradual(7day) depleted animals and littermate controls were P41 at the time of their first injection and were P90 when they completed their last behavioral testing. After surgical implantation of the cannula, animals were housed separately to prevent damage to the cannula. Animals were provided with dishes of crushed high fat food

pellets moistened with water, additional hard food pellets on the floor of the cage, as well as access to a water bottle. All cages were placed half on/half off heating pads following surgery and each subsequent infusion of 6-OHDA. Cages remained on heating pads unless animals were observed resting mainly in the unheated portion of the cage. Each infusion of saline or 6-OHDA was performed while animals were lightly anesthetized on a heating pad, and all animals were injected with 0.1 cc of saline i.p. before being returned to their home cage. Animal's weights were tracked regularly and extra i.p. saline and softened food or trail mix were provided to encourage weight gain and proper hydration when appropriate.

### **2.2.2 Implantation of bilateral cannulas and 6-OHDA injection in the MFB**

Under ketamine/xylazine (100 mg/kg: 30 mg/kg, i.p.) anesthesia, the animals were placed on a stereotaxic frame (David Kopf Instruments) and maintained throughout surgery using 1-2% isoflurane. Bilateral internal cannulas (Plastics One) cut to target  $\pm 1.1$ mm lateral and -5.0mm ventral were implanted 0.45mm posterior to bregma and secured using superglue. 6-hydroxydopamine was prepared at a concentration of 5  $\mu\text{g}/\mu\text{L}$  in 0.9% NaCl for acute depletions and diluted further with 0.9% NaCl to 0.75  $\mu\text{g}/\mu\text{L}$  for gradual depletions (Sigma-Aldrich H116 6-Hydroxydopamine hydrobromide). Injections were performed using a 33-gauge cannula (Plastics One) attached to a 10  $\mu\text{L}$  Hamilton syringe within a syringe pump (GenieTouch; Kent Scientific) running at 0.5 $\mu\text{L}/\text{min}$ , to a total volume of 1 $\mu\text{L}/\text{side}$ . The injection cannula was left in place for 5 min following the injection. Control animals received the same volume of vehicle (0.9%NaCl), following the same procedure. 6-OHDA and vehicle were administered every 3 or

7 days, respectively, for gradual depletions and controls. Animals were sacrificed 72-80 h following the last given injection.

### **2.2.3 Behavioral assessment**

Following initial surgery and subsequent injections, animals were exposed to the following sequential behavioral tests: open field, rearing, and pole task. The minimum interval between two consecutive procedures was 30 min. All analysis and scoring was performed by observers blind to treatment. One individual assigned a random number to each animal at the time of initial surgery that identified their treatment group and analysis and scoring was performed by separate individuals who recorded data solely based on animal number.

*Open Field:* To determine overall spontaneous mobility, mice were placed in a 24 cm diameter clear cylindrical open field chamber with video monitoring from above. Mice were in the arena for a total of 20 m, with 10 m for acclimation, and 10 m for data acquisition. Positions of nose, tail, and center of mass of each mouse were tracked using EthoVision 9.0 software (Noldus).

Ambulation was defined as periods when the velocity of the animal's center point averaged more than 2.00 cm/s until the velocity was reduced to 1.75 cm/s. Two blind observers validated accuracy of this definition, and it excluded other fine movements such as rearing and sniffing.

Immobility was defined as continuous periods of time (at least 1 s) during which the average pixel change of the entire video image is less than 0.5%. This definition is very strict, such that any movement of the head, limbs, or tail would not be scored as immobility. Total time spent mobile, total time spent immobile, distance traveled, and average velocities were calculated using EthoVision 9.0. The arena was cleaned with 50% ethanol between each animal.

*Rearing:* To assess spontaneous vertical activity, mice were placed in a standard 1000 mL glass beaker with video monitoring from the side for a total of 10 min. The number of full extension rears was manually scored post-hoc by observers blind to treatment. The beaker was cleaned with 50% ethanol between each animal.

*Pole Task:* To evaluate coordination and bradykinesia, mice were placed head-upward at the top of a vertical gauze-wrapped circular wooden pole (diameter = 1 cm; height = 55 cm) with video monitoring from the side. To encourage descent, a 60-watt lamp was aimed at the top of the pole. Prior to surgery/testing mice were trained for 3-5 trials or until descent took < 30 s under testing conditions to ensure each mouse was able to perform the task with ease before dopamine depletion. The latency to turn downward (turn down latency = TDL), time from orientation downward until all four paws reached the ground (traverse time), and total time spent on the pole (total) was recorded with a maximum duration of 120 s for three trials. All measurements were manually scored offline by observers blind to treatment. Even if the mouse fell part way into its descent, the behavior was scored until it reached the ground. When the mouse was unable to turn downward and/or instead dropped from the pole, all latencies were recorded as 120 s (default value) because of the severity of motor dysfunction.

#### **2.2.4 Immunohistochemistry**

Degree of dopamine denervation was assessed at 72 h post-injection in 6-OHDA-treated mice by tyrosine hydroxylase staining. Following decapitation, brains were surgically removed and drop-fixed with 4% paraformaldehyde in phosphate buffered saline at 4°C for 24 h. After rinsing with phosphate buffered saline, brains were transferred to 30% sucrose in phosphate buffered saline

and stored at 4°C for at least 24 h prior to sectioning. Immunohistochemistry was carried out in free-floating coronal frozen sections (30 µm). Tissue was sectioned using a freezing microtome (Microm HM 430; Thermo Scientific), blocked with 10% normal donkey serum, and permeabilized with 0.5% Triton X-100 for 1 h. Primary antibody incubations were performed at room temperature for 24 h using rabbit anti-TH (1:500; Pel-Freez). Primary antibodies were detected with Alexa Fluor 647-conjugated donkey anti-rabbit (1:500, Vector Laboratories), incubated for 90 min at room temperature.

*Fluorescence Quantification:* Epifluorescent images (10x magnification) were taken from bilateral dorsal striatum in one coronal section between 0.62mm and 1.10 mm Bregma (according to Paxinos second edition Mouse Brain in Stereotaxic Coordinates). Pixel intensity over a 75 × 75 µm area (5625 µm<sup>2</sup>) from each hemisphere was measured using the pixel intensity measuring tool in ImageJ and normalized to the pixel intensities measured in saline control mice processed and imaged in parallel.

*High Performance Liquid Chromatography:* Levels of dopamine neurotransmitter were assessed at 72 h post-injection in 6-hydroxydopamine-treated mice by high performance liquid chromatography (HPLC). Following decapitation, brains were quickly placed in a Vibrotome and a 700 µm coronal section containing striatum was removed. Dorsal striatum from each side was dissected and flash frozen on dry ice immediately. These samples were randomly numbered and shipped on dry ice to CMN/KC Neurochemistry Core Laboratory at Vanderbilt University in Nashville, TN for analysis. Upon receipt of results, data was compared to immunohistochemistry results prior to un-blinding for analysis based on treatment group. In order to control for variability of dopamine, data from each animal was normalized to a same sex, same litter saline control.

### **2.2.5 Statistical analysis**

All data sets were tested for normality with the Shapiro-Wilk test prior to any statistical analysis.

Data are expressed as mean  $\pm$  standard error of mean (SEM) unless otherwise indicated.

Statistical analysis was performed using Kruskal-Wallis analysis of variance nonparametric test (KW) and any differences were further investigated by Kruskal-Wallis pairwise comparison between percentage dopamine remaining or injection number and saline controls with a Bonferroni correction for number of comparisons. Bar graphs comparing performance between saline, gradual, and acute depletions were also tested using KW and pairwise comparisons included gradual vs. acute. In Figure 2.1F comparison of dorsal and ventral dopamine was analyzed with a Student's t-test. Dopamine metabolites in Figure 2.2 were analyzed using a one-way analysis of variance (ANOVA) followed by a Dunnett T3 post hoc test (HVA, DOPAC, 3-MT) or a Dunnett t (2-sided) post hoc test (Nor, 5-HT). A *p*-value of 0.05 was considered statistically significant. All statistical procedures were performed using IBM SPSS Statistics, version 22.

## **2.3 RESULTS**

### **2.3.1 Injections of 6-OHDA over time result in graded depletion of striatal dopamine**

To develop a depletion paradigm where the rate of dopamine loss can be controlled over time in the same animal, we administered multiple, low doses of 6-OHDA through bilateral internal

guide cannulas implanted in the MFB (Fig. 2.1A). Bilateral cannulas cut to target the MFB at  $\pm$  1.1 mm medial/lateral and -5.0 mm ventral were implanted 0.45 mm posterior to bregma.

Targeting was confirmed post-hoc by analyzing Nissl-stained sections of tissue. Summaries of paired cannula locations within the MFB are shown in Figure 2.1B.

To determine an optimal concentration of 6-OHDA to use for our paradigm, we first tested the acute effects of different concentrations on striatal dopamine levels, assessed with immunostaining for tyrosine hydroxylase (TH) (Table 2.1). We chose to use a dose of 0.75  $\mu$ g because this reduced striatal dopamine by  $\sim$ 20% (TH-IR loss =  $21.3 \pm 7.5$  %, n = 8) and should therefore permit 4-5 injections to be administered before reaching full dopamine depletion. For the majority of experiments, injections were administered once every three days, but in Figure 2.6 we will show that the time in between doses can be increased to deplete dopamine over an even longer period.

Dose of 6-OHDA ( $\mu$ g)	% TH-IR Remaining (avg $\pm$ std dev)	% DA-HPLC Remaining (avg $\pm$ std dev)
0.5	88.14 $\pm$ 19.57	90.64 $\pm$ 12.11
0.75	78.70 $\pm$ 21.18	71.20 $\pm$ 20.37
1	54.15 $\pm$ 23.44	43.46 $\pm$ 26.06
5	15.80 $\pm$ 12.99	13.70 $\pm$ 13.90

**Table 2.1. Striatal dopamine levels following 6-OHDA injections.** Quantification of TH immunoreactivity (TH-IR) and high performance liquid chromatography (HPLC) detected levels of dopamine in the striatum normalized to saline controls following an injection of 0.5, 0.75, 1, and 5  $\mu$ g of 6-OHDA. Values are expressed as average percentage of dopamine remaining  $\pm$  standard deviation.

Over the course of our protocol, a subset of animals were sacrificed after each injection to analyze dopamine levels within the striatum. Dopamine levels within the dorsal striatum were quantified with two distinct methods: TH immunostaining to estimate the degree of dopaminergic innervation, and high performance liquid chromatography (HPLC) to measure

levels of dopamine neurotransmitter. Histological analysis of TH immunostaining revealed that repeated injections of 0.75  $\mu\text{g}$  resulted in a gradual and linear depletion ( $R^2 = 0.857$ ,  $p < 0.0001$ ) of dopamine levels within the striatum over the course of 5 injections, spanning 15 days (KW pairwise,  $p < 0.005$  from saline) (Fig. 2.1C-D). By the fifth injection, the degree of dopamine depletion was similar to that observed with the traditional acute method (5  $\mu\text{g}$ , 1 injection). Both the gradual and acute paradigms resulted in a more pronounced loss of dopamine in the dorsal striatum compared to the ventral striatum (Fig. 2.1E-F). Although dopamine levels declined somewhat in the accumbens over the course of our depletions, this was significantly less than the dopamine loss observed in the dorsal striatum (Student's t-test, D. Str. =  $16.9 \pm 2.5$  %,  $n = 20$ ; V. Str. =  $52.8 \pm 8.8$  %,  $n = 13$ ,  $p = 0.002$ ).

TH immunoreactivity often correlates tightly with dopamine levels, but this relationship may break down under dopamine depleted conditions (Zigmond et al., 1984), so dopamine levels were also measured directly with HPLC. HPLC analysis of dorsal striatum confirmed that levels of dopamine neurotransmitter were also gradually and linearly depleted ( $R^2 = 0.819$ ,  $p < 0.0001$ ), in strong accordance with our measurements of TH immunofluorescence (KW pairwise,  $p < 0.005$  from saline) (Fig. 2.1G). Combined, these results show that repeated injections of 0.75  $\mu\text{g}$  of 6-OHDA into the MFB gradually depletes dopamine to the same end-point achieved with the traditional 5  $\mu\text{g}$  acute model, although over a much longer time course.

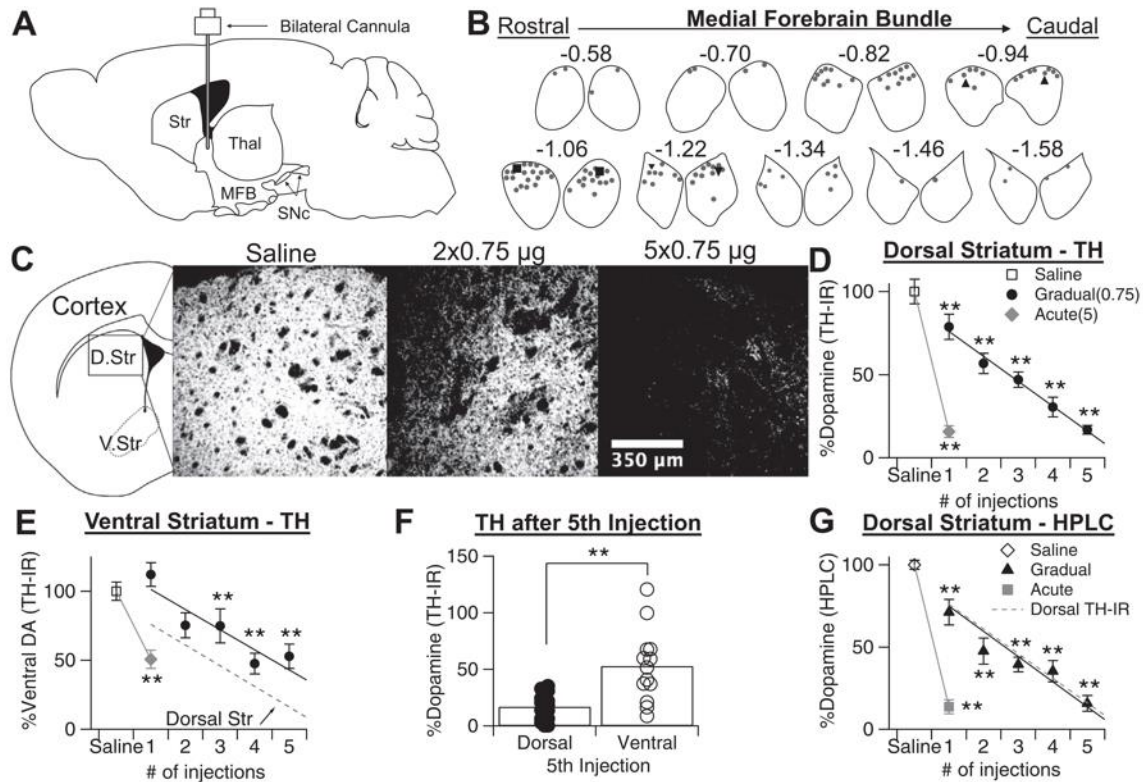


**Figure 2.1. Gradual depletion paradigm linearly reduces dopamine over time.** (A) Schematic of sagittal section of mouse brain showing the position of the infusion cannula in the MFB. Str = striatum, Thal = thalamus, MFB = medial forebrain bundle, SNc = substantia nigra pars compacta. (B) Cannulae placements in the MFB, confirmed postmortem. Left and right MFBs from coronal sections spanning the cannulae placements are shown, and Bregma coordinates are noted. Representative bilateral cannulae placements from three representative mice are indicated with triangles, squares, and inverted triangles. (C) Representative images of TH immunofluorescence (TH-IR), taken from the dorsal striatum of mice treated with saline, two doses of 0.75 µg 6-OHDA, or five doses of 0.75 µg 6-OHDA. (D) Quantification of TH-IR in the dorsal striatum, normalized to saline controls, following repeated injections of 0.75 µg or a single injection of 5 µg 6-OHDA. Values are expressed as percentage of dopamine remaining. Throughout figure, error bars are SEM. KW,  $\chi^2(6) = 106.218$ ,  $p < 0.0001$ , pairwise,  $**p < 0.005$  from saline. (E) Quantification of TH-IR in the ventral striatum, normalized to saline controls, following repeated injections of 0.75 µg or a single injection of 5 µg 6-OHDA. Values are expressed as percentage of dopamine remaining. KW,  $\chi^2(6) = 51.744$ ,  $p < 0.0001$ , pairwise,  $**p < 0.005$  from saline. (F) Quantification of TH-IR in the dorsal and ventral striatum following the 5th injection of 0.75 µg of 6-OHDA. Data from each mouse, as well as population averages are shown. Student's t-test,  $t = -3.896$ ,  $**p = 0.002$ . (G) Quantification of HPLC detected levels of dopamine in the dorsal striatum, normalized to saline controls, following repeated injections of 0.75 µg or a single injection of 5 µg 6-OHDA. Values are expressed as percentage of dopamine remaining. Fit line from the graph of TH-IR levels is overlaid for comparison. KW,  $\chi^2(6) = 69.554$ ,  $p < 0.0001$ , pairwise,  $**p < 0.005$  from saline.

### 2.3.2 Effects of gradual depletion on dopamine metabolites and monoamines

To test whether our gradual depletion paradigm produced any compensatory changes in dopamine metabolism, we used HPLC to measure levels of additional compounds in the tissue. Levels of the dopamine metabolites homovanillic acid (HVA), 3,4-Dihydroxyphenylacetic acid (DOPAC), and 3-methoxytyramine (3-MT) all showed similarly linear declines (HVA:  $r^2 = 0.762$ ,  $p < 0.0001$ ; DOPAC:  $r^2 = 0.776$ ,  $p < 0.0001$ ; 3-MT:  $r^2 = 0.602$ ,  $p < 0.0001$ ) to that of dopamine during our gradual depletion paradigm, but did not reach quite the same end stage values as seen during acute depletion (Fig. 2.2A). This suggests there may be a compensatory mechanism to slow dopamine metabolism that is engaged by gradual dopamine depletion, but this mechanism is not sufficient to boost dopamine levels by a significant amount (see Fig. 2.1G).

Because 6-OHDA can also kill noradrenergic neurons, a population of neurons that is also depleted in PD (Rommelfanger and Weinshenker, 2007), we used HPLC to measure norepinephrine (NE) levels in the striatum. NE levels dropped by 40% (NE loss =  $40.2 \pm 9.1$  %,  $n = 7$ , ANOVA with Dunnett  $t$ ,  $p = 0.042$  from saline) after the first injection, but then remained constant across subsequent injections, ending at the same level of depletion as seen in acutely depleted mice (Gradual NE =  $52.4 \pm 8.7$  %,  $n = 9$  vs. Acute NE =  $41.1 \pm 6.7$  %,  $n = 8$ ) (Fig. 2.2B). Finally, we examined levels of serotonin in our tissue. Although serotonin neurons are not directly affected by 6-OHDA, there have been conflicting reports about changes in serotonin levels in the dorsal striatum following dopamine depletion (Balcioglu et al., 2003; Breese et al., 1984; Carta et al., 2006; Commins et al., 1989; Frechilla et al., 2001; Karstaedt et al., 1994; Rylander et al., 2010) and this has been hypothesized to play a role in L-dopa induced

dyskinesias (Nagatsua and Sawadab, 2009; Rylander et al., 2010). Interestingly, serotonin levels remained constant until ~60% of dopamine had been lost, then suddenly increased by 10-20% (ANOVA with Dunnett t,  $p < 0.05$  from saline). The magnitude of serotonin increase was similar in both gradually and acutely depleted animals (Fig. 2.2C). These results suggest that monoamine levels are altered to the same extent in both gradually and acutely depleted animals, however, the trajectories of their changes differed compared to those for dopamine.

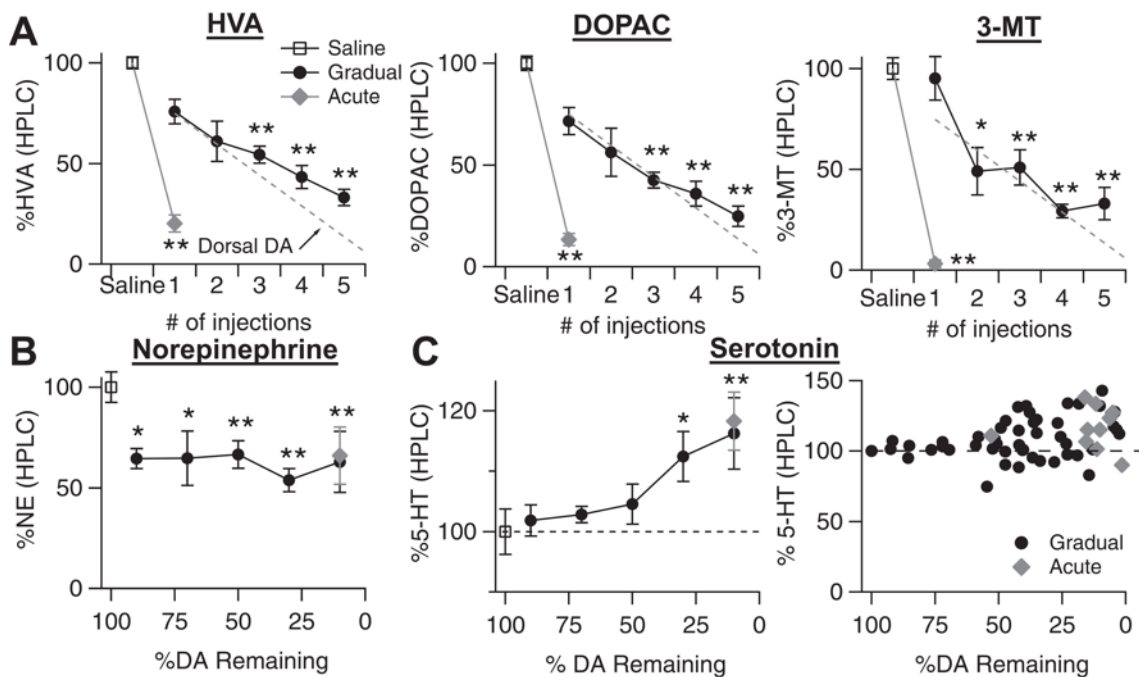


**Figure 2.2. Levels of dopamine metabolites and other monoamines measured with HPLC during gradual dopamine depletion paradigm.** (A) Quantification of HPLC detected levels of the dopamine metabolites homovanillic acid (HVA), 3,4-Dihydroxyphenylacetic acid (DOPAC), and 3-methoxytyramine (3-MT). Tissue samples were taken from the dorsal striatum of mice who received repeated injections of 0.75  $\mu$ g 6-OHDA or a single injection of 5  $\mu$ g of 6-OHDA. Values are normalized to saline controls for each time point. Throughout figure, error bars are SEM. Fit line from the graph of HPLC dopamine levels is overlaid for comparison. ANOVA, HVA:  $F[6,73] = 51.085$ ; DOPAC:  $F[6,73] = 55.560$ ; 3-MT:  $F[6,73] = 34.572$ , all  $p < 0.0001$ , Dunnett T3,  $*p < 0.05$  from saline;  $**p < 0.005$  from saline. (B) Quantification of HPLC detected levels of norepinephrine in the dorsal striatum at all time points of the gradual depletion paradigm and in acutely depleted mice. Values are normalized to saline controls. ANOVA,  $F[6,73] = 9.709$ ,  $p < 0.0001$ , Dunnett t,  $*p < 0.05$  from saline;  $**p < 0.005$  from saline. (C) Quantification of HPLC detected levels of serotonin in the dorsal striatum at all time points of the gradual depletion paradigm and in acutely depleted mice. Values are normalized to saline controls. ANOVA,  $F[6,73] = 4.083$ ,  $p = 0.01$ , Dunnett t,  $*p < 0.05$  from saline;  $**p < 0.005$  from saline. Serotonin levels in the dorsal striatum from each mouse, normalized to saline controls, plotted as a function of striatal dopamine levels.

### 2.3.3 Open field locomotor deficits develop suddenly during gradual depletions

The behavioral effects of our gradual dopamine depletion paradigm were first assessed by examining spontaneous locomotion in an open field arena (Ferro et al., 2005; Kravitz et al., 2010; Kreitzer and Malenka, 2007; Simola et al., 2007). Mice were placed in a clear walled, circular arena and allowed to habituate for 10 minutes. After the habituation period, their spontaneous behavior was monitored for an additional 10 minutes with overhead and side-mounted video cameras (Fig. 2.3A). For all of the behavioral tasks, our questions were two-fold: At what stage of dopamine loss would behavioral impairments first become apparent, and, would end-stage motor deficits differ between gradually and acutely depleted mice?

Using EthoVision behavioral tracking software (Noldus), we quantified movement parameters such as total distance traveled, average velocity, and time spent immobile (Fig. 2.3B-G). We measured parameters that would capture both mobility and immobility because these different aspects of motor function are believed to be controlled by distinct pathways within the basal ganglia and may be differentially affected by dopamine depletion (Albin et al., 1989; Day et al., 2006; DeLong, 1990; Galvan and Wichmann, 2007; Gittis et al., 2011; Graybiel et al., 1994; Kreitzer and Malenka, 2007; Mallet et al., 2006; Schwarting and Huston, 1996a, 1996b). Gradually depleted mice were grouped into five groups, based on percent dopamine remaining ( $89.8 \pm 2.4\%$ ,  $n = 10$ ;  $73.9 \pm 1.8\%$ ,  $n = 9$ ;  $51.8 \pm 1.3\%$ ,  $n = 22$ ;  $30.1 \pm 1.4\%$ ,  $n = 21$ ;  $14.1 \pm 1.7\%$ ,  $n = 12$ ). Dopamine levels decreased linearly with increasing number of injections of  $0.75 \mu\text{g}$  6-OHDA received ( $r^2 = 0.594$ ,  $p < 0.0005$ ). Saline-injected mice moved an average of  $2756 \pm 63$  cm ( $n = 28$ ) in 10 minutes. At early stages of gradual dopamine depletion ( $<20\%$ ), locomotion was actually increased ( $3381 \pm 132$  cm,  $n = 10$ , KW pairwise,  $p = 0.006$  from saline) (Fig. 2.3B). As our gradual depletion paradigm progressed, mice continued to show robust movement around

the arena until dopamine levels had dropped by ~70%, after which distance traveled sharply declined. At end-stage dopamine levels (dopamine loss >80%), locomotion had decreased by about 2-fold compared to saline and was similarly impaired in both gradually and acutely depleted mice (Gradual =  $1323 \pm 29$  cm, n=12; Acute =  $1534 \pm 324$  cm, n=14, KW pairwise,  $p = 1$ ) (Fig. 2.3C).

Average velocity during the 10-minute period followed a similar pattern. The average velocity of saline-treated mice was  $4.6 \pm 0.1$  cm/s and increased slightly after the initial injection, before declining sharply once dopamine loss exceeded ~70% (Fig. 2.3D). At end-stage dopamine levels, both gradually and acutely depleted animals showed a similar 2-fold decrease in velocity compared to saline control animals (Gradual =  $2.2 \pm 0.4$  cm/s; Acute =  $2.5 \pm 0.5$  cm/s, KW pairwise,  $p = 1$ ) (Fig. 2.3E). Finally, we also observed that mice spent relatively little time during this task immobile, until gradual depletions reached ~70%, after which immobility increased significantly (KW pairwise,  $p < 0.05$  from saline) (Fig. 2.3F). Immobility was defined such that any movement of the head, limbs, or tail did not count towards time spent immobile. By the time dopamine depletions were >80%, gradually depleted mice spent  $18.7 \pm 8.0\%$  of their time immobile, similar to the  $16.1 \pm 5.6\%$  of time acutely depleted mice were immobile (KW pairwise,  $p = 1$ ) (Fig. 2.3G). These results suggest that both mobile and immobile aspects of general locomotion remain intact until >70% dopamine is lost. Furthermore, animals that have lost >80% of their dopamine, either through gradual or the acute depletion paradigms, show the same degree of locomotor deficits on this task.

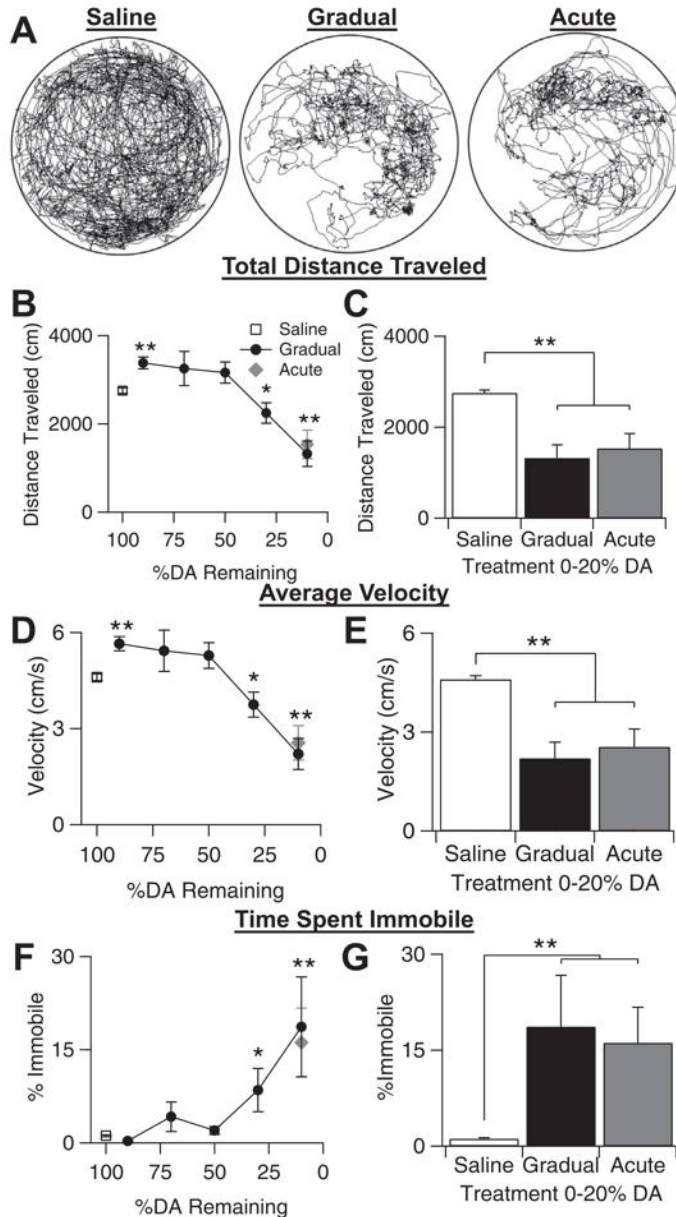


**Figure 2.3. Effects of gradual dopamine depletion on spontaneous locomotion in an open field.** (A) Example plot tracks from a saline control mouse, a gradually depleted mouse that has received 5 injections of 0.75  $\mu\text{g}$  6-OHDA, and an acutely depleted mouse that has received 1 injection of 5  $\mu\text{g}$  6-OHDA. (B) Total distance traveled over 10 minutes in saline control animals, gradually depleted animals, and acutely depleted animals. Throughout the figure, error bars are SEM. KW,  $\chi^2(6) = 49.674$ ,  $p < 0.0001$ , pairwise,  $*p = 0.012$  from saline;  $**p < 0.005$  from saline. (C) Total distance traveled by saline control animals compared to gradually and acutely depleted mice with 0-20% dorsal striatal dopamine remaining. KW,  $\chi^2(2) = 31.091$ ,  $p < 0.0001$ , pairwise,  $**p < 0.005$ . (D) Average velocity of saline control animals, gradually depleted animals, and acutely depleted animals. KW,  $\chi^2(6) = 49.642$ ,  $p < 0.0001$ , pairwise,  $*p = 0.012$  from saline;  $**p < 0.005$  from saline. (E) Average velocity of saline control animals compared to gradually and acutely depleted mice with 0-20% striatal dopamine remaining. KW,  $\chi^2(2) = 31.141$ ,  $p < 0.0001$ , pairwise,  $**p < 0.005$ . (F) Percentage of time spent immobile by saline control animals, gradually depleted animals, and acutely depleted animals. KW,  $\chi^2(6) = 40.429$ ,  $p < 0.0001$ , pairwise,  $*p < 0.05$  from saline;  $**p < 0.005$  from saline. (G) Percentage of time spent immobile in saline control animals compared to gradually and acutely depleted animals with 0-20% striatal dopamine remaining. KW,  $\chi^2(2) = 31.679$ ,  $p < 0.0001$ , pairwise,  $**p < 0.005$ .

### 2.3.4 Rearing deficits progress gradually as dopamine is depleted

Although movement in the open field can detect general deficits in locomotion, this task is very broad and does not reveal deficits to any particular system. In contrast, vertical movement, assessed with rearing tasks, has been suggested to correlate strongly with dorsolateral striatal function (Drago et al., 1994; Jicha and Salamone, 1991; Schwarting et al., 1999). To assess how rearing behavior changed over the course of our gradual dopamine depletion, mice were placed in a 1000 mL beaker for 10 minutes, and the number of rears were counted over this period (Fig. 2.4A).

The number of rears in gradually depleted mice decreased linearly (grouped data:  $R^2 = 0.314$ ,  $p < 0.0001$ ; raw data:  $R^2 = 0.287$ ,  $p < 0.0001$ ) with decreasing levels of dopamine (Fig. 2.4B,C). At end-stage dopamine levels (depletion  $>80\%$ ), acute and gradually depleted mice showed similar reductions in rearing frequency compared to saline controls that had been tested a similar number of times (Saline =  $52.9 \pm 2.8$ ,  $n = 24$ ; Gradual =  $13.8 \pm 5.7$ ,  $n = 10$ ; Acute =  $12.8 \pm 5.9$ ,  $n = 13$ , KW pairwise, saline vs. gradual and acute,  $p < 0.006$ , gradual vs. acute,  $p = 1$ ) (Fig. 2.4C).

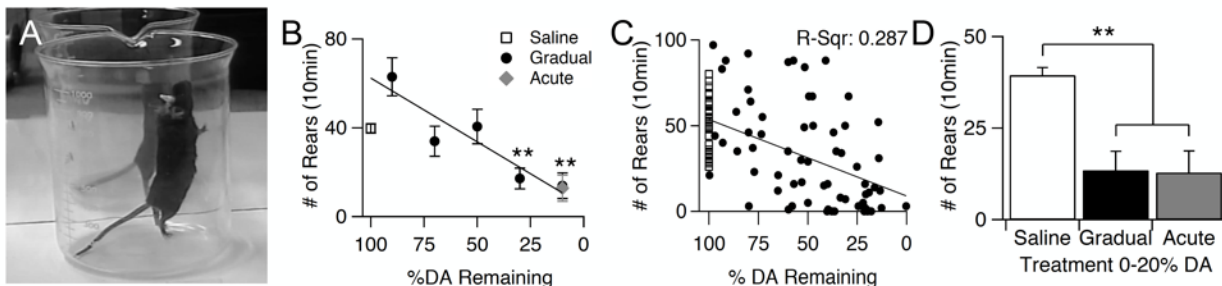


**Figure 2.4. Effects of gradual dopamine depletion on rearing behavior.** (A) Example of a full extension rear. (B) Average number of rears of saline control animals, gradually depleted animals across all dopamine levels, and acutely depleted animals during 10 minutes in beaker. Throughout the figure, error bars are SEM. KW,  $\chi^2(6) = 42.623$ ,  $p < 0.0001$ , pairwise,  $**p < 0.005$  from saline. (C) Scatter plot of individual animals rearing performance. (D) Average number of rears of saline control animals, gradually depleted animals with 0-20% dorsal striatal dopamine, and acutely depleted animals with 0-20% dorsal striatal dopamine. KW,  $\chi^2(2) = 23.977$ ,  $p < 0.0001$ , pairwise,  $**p < 0.005$ .

### 2.3.5 Motor coordination is differentially affected in gradually vs. acutely depleted mice

Both open field and rearing tasks assess different aspects of spontaneous gross motor function in mice, but neither provides a measurement of fine movement or coordination, behaviors which detect early motor deficits in some mouse models of disease (Fernagut et al., 2003; Fleming et al., 2004; Matsuura et al., 1997; Ogawa et al., 1985; Sedelis et al., 2001). To assess fine motor coordination in gradually depleted mice, animals were subjected to a pole task. While less commonly utilized than open field and rearing, the pole task is a well-established technique used to assess motor skills in many animal models of diseases that result in motor dysfunction (Credle et al., 2015; Hickey et al., 2008; Matsuura et al., 1997). The task involves placing an animal face upward on a tall vertical pole with small diameter (1 cm) and measuring the time it takes for the animal to turn facing downward (Turn down latency = TDL), the time from turning downward to finish traversing the pole (Traverse), and the total time spent on the pole (Total) (Fig. 2.5A).

Intriguingly, although acutely depleted mice were severely impaired on this task, gradually depleted mice maintained a level of performance similar to that of saline controls (KW pairwise,  $p > 0.12$  from saline) (Fig. 2.5B). The total time gradually depleted animals spent on the pole increased slightly with decreasing levels of striatal dopamine, but even at end-stage dopamine levels, gradually depleted mice significantly outperformed acutely depleted mice (KW pairwise,  $p = 0.00495$ ), and their time spent on the pole was not significantly different from that of saline controls (KW pairwise,  $p = 0.102$ ) (Saline =  $23.0 \pm 2.0$ ,  $n = 26$ ; Gradual =  $46.3 \pm 10.7$ ,  $n = 11$ ; Acute =  $107.4 \pm 5.7$ ,  $n = 15$ ) (Fig. 2.5C).

To differentiate between the two different components of this task: orienting downward after being placed at the top of the pole, and descending to the bottom, we separately analyzed

the time needed to complete these two phases of the task. Turn down latency of gradually depleted mice remained similar to that of saline controls throughout dopamine depletion (KW pairwise,  $p > 0.318$  from saline) (Fig. 2.5D-E). In contrast, acutely depleted mice displayed a significantly increased turn down latency (Saline =  $11.0 \pm 1.7$ ; Gradual =  $18.4 \pm 6.5$ ; Acute =  $96.3 \pm 9.4$ ; KW pairwise,  $p < 0.005$  from saline and gradual). In many cases, acutely depleted animals either could not turn downward on their own, or it took them over half of the total time allotted for the task. Gradually depleted mice showed a significant impairment on this task during the traverse phase, where the amount of time it took them to walk to the bottom was significantly greater than that of saline controls (KW pairwise,  $p = 0.012$ ), but still much faster than that of acutely depleted mice (KW pairwise,  $p = 0.0012$ ) (Saline =  $12.3 \pm 0.7$ ; Gradual =  $32.4 \pm 9.6$ ; Acute =  $88.7 \pm 9.6$ ) (Fig. 2.5F-G). In many cases, acutely depleted animals either fell from the pole, unable to complete the task, or circled around the pole many times as they descended, resulting in traversal times over half of the allotted time for the task. Gradually depleted animals also circled around the pole as they descended; however they were still significantly faster than acutely depleted animals.

These results suggest that certain aspects of an animal's behavior may adapt differently when dopamine is depleted gradually rather than acutely. Gradually depleted animals show little or no deficits on the pole task, whereas acutely depleted animals show severe deficits on the same task.

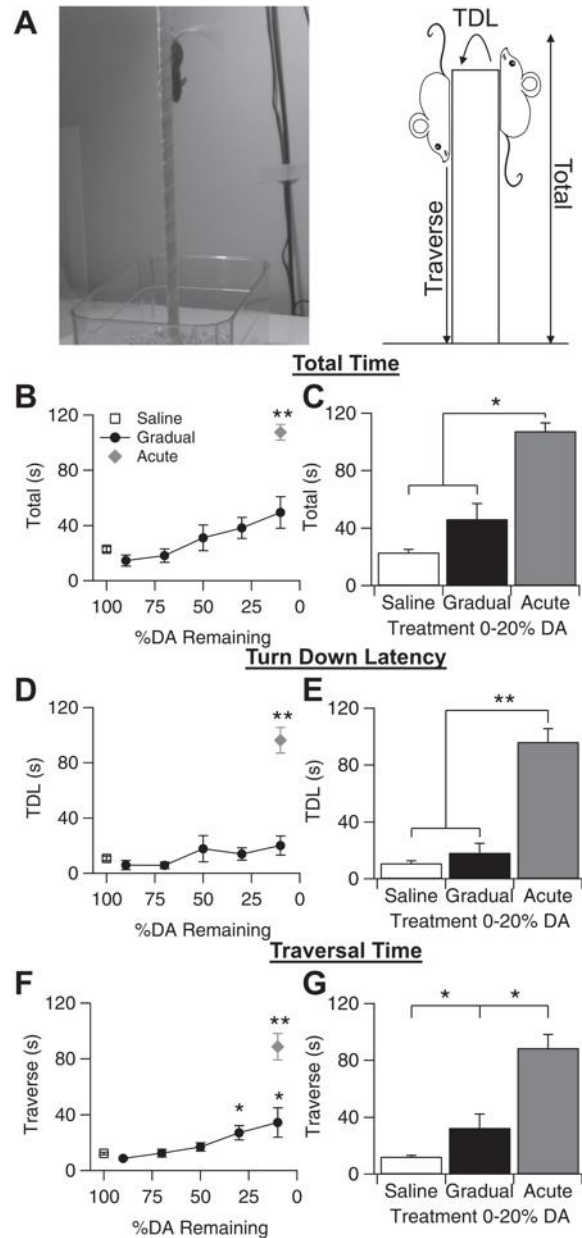


**Figure 2.5. Effects of gradual dopamine depletion on motor coordination assessed with a vertical pole task.** (A) Image of mouse descending pole and schematic of timed parameters of pole task. (B) Average time needed to complete the entire task for saline control animals, gradually depleted animals, and acutely depleted animals. Throughout the figure, error bars are SEM. KW,  $\chi^2(6) = 52.592$ ,  $p < 0.0001$ , pairwise,  $**p < 0.005$  from saline. (C) Average total time of saline control animals compared to gradually and acutely depleted animals with 0-20% striatal dopamine remaining. KW,  $\chi^2(2) = 39.537$ ,  $p < 0.0001$ , pairwise,  $*p < 0.05$ . (D) Average turn down latency (TDL) of saline control animals, gradually depleted animals, and acutely depleted animals. KW,  $\chi^2(6) = 37.667$ ,  $p < 0.0001$ , pairwise,  $**p < 0.005$  from saline. (E) Average TDL of saline control animals compared to gradually and acutely depleted animals with 0-20% dorsal striatal dopamine, and acutely depleted animals with 0-20% striatal dopamine remaining. KW,  $\chi^2(2) = 29.908$ ,  $p < 0.0001$ , pairwise,  $**p < 0.005$ . (F) Average traversal time of saline control animals, gradually depleted animals, and acutely depleted animals. KW,  $\chi^2(6) = 58.834$ ,  $p < 0.0001$ , pairwise,  $*p < 0.05$  from saline;  $**p < 0.005$  from saline. (G) Average traversal time of saline control animals compared to gradually and acutely depleted animals with 0-20% striatal dopamine remaining. KW,  $\chi^2(2) = 43.068$ ,  $p < 0.0001$ , pairwise,  $*p < 0.05$ .

### **2.3.6 Time course of gradual depletions can be varied and extended**

The gradual paradigm used for this study involved injections every three days for a total of 15 days. This is five times longer than the traditional acute depletion, however this is still a relatively short time span compared to the slow progression of PD in humans. Therefore, we wanted to determine whether dopamine could be fully depleted using a longer time course. We therefore spaced our injections of 0.75  $\mu\text{g}$  6-OHDA every seven days, instead of every three days, for a total of 35 days. Subsets of animals were sacrificed after three injections and five injections to analyze TH levels in the dorsal striatum (Fig. 2.6A). In contrast to our findings with injections every three days, five injections spaced every seven days was not sufficient to fully deplete dopamine from the striatum (Fig. 2.6A). However, increasing the number of injections to seven, for a total of 49 days, resulted in full striatal dopamine depletion (KW pairwise,  $p < 0.0001$  from saline) (Fig. 2.6B).

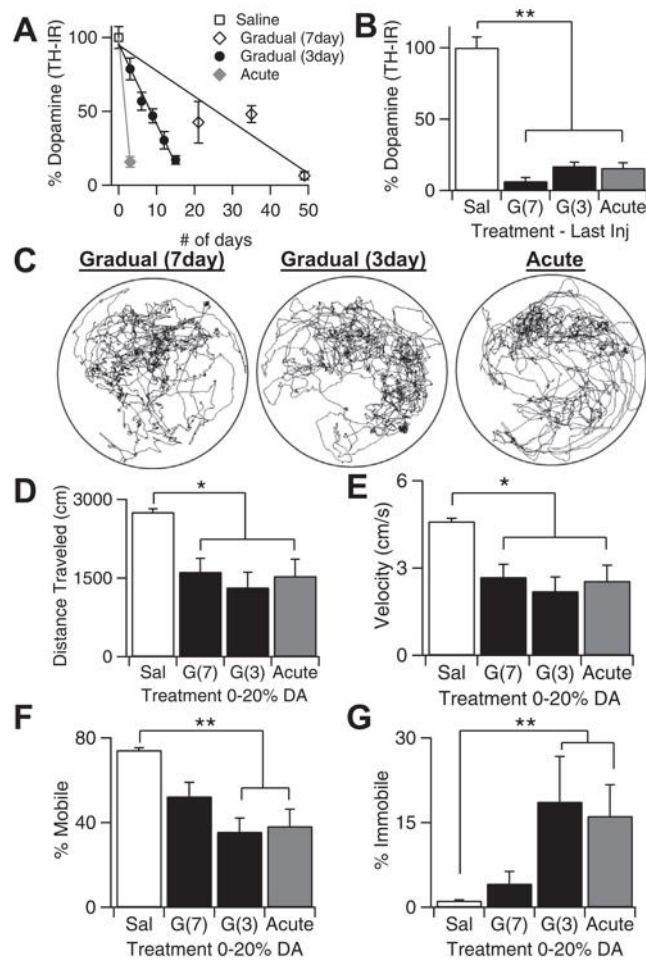


**Figure 2.6. Time course of gradual depletions can be varied and extended over a month.** (A) Quantification of TH-IR in the dorsal striatum normalized to saline controls following repeated injections of 0.75  $\mu\text{g}$  6-OHDA, administered every seven days, every three days, or a single injection of 5  $\mu\text{g}$  of 6-OHDA. Values are normalized to saline controls and expressed as percentage of dopamine remaining. Throughout the figure, error bars are SEM. (B) Quantification of TH-IR in the dorsal striatum, normalized to saline controls, following the last injection of the gradual seven-day, gradual three-day, and acute paradigms. KW,  $\chi^2(3) = 110.653$ ,  $p < 0.0001$ , pairwise,  $**p < 0.005$ . (C) Example plot tracks from a gradually depleted mouse that has received seven injections of 0.75  $\mu\text{g}$  6-OHDA every seven days, a gradually depleted mouse that has received five injections of 0.75  $\mu\text{g}$  every three days, and an acutely depleted mouse that has received one injection of 5  $\mu\text{g}$ . (D) Total distance traveled during 10 minutes in the open field arena by saline control animals compared to mice with 0-20% dopamine remaining that were depleted with the seven-day gradual, three-day gradual, or acute dopamine depletion paradigms. KW,  $\chi^2(3) = 36.831$ ,  $p < 0.0001$ , pairwise,  $*p < 0.05$ . (E) Average velocity of saline control animals compared to animals with 0-20% dopamine that were depleted with the seven-day gradual, three-day gradual, or acute dopamine depletion paradigms. KW,  $\chi^2(3) = 36.881$ ,  $p < 0.0001$ , pairwise,  $*p < 0.05$ . (F) Percentage of time spent mobile in saline control animals and animals with 0-20% dopamine that received 0.75  $\mu\text{g}$  every 7 days, 0.75  $\mu\text{g}$  every 3 days, or a single injection of 5  $\mu\text{g}$  of 6-OHDA during open field. KW,  $\chi^2(3) = 40.548$ ,  $p < 0.0001$ , pairwise,  $**p < 0.005$ . (G) Percentage of time spent immobile in saline control animals and animals with 0-20% dopamine that received 0.75  $\mu\text{g}$  every 7 days, 0.75  $\mu\text{g}$  every 3 days, or a single injection of 5  $\mu\text{g}$  of 6-OHDA during open field. KW,  $\chi^2(3) = 34.129$ ,  $p < 0.0001$ , pairwise,  $**p < 0.005$ .

At end-stage dopamine depletions (>80%), spontaneous locomotion of seven-day gradually depleted mice in the open field was compared to that of three-day gradually depleted and acutely depleted mice (Fig. 2.6C). Distance traveled and velocity were decreased in seven-day depleted animals compared to saline (KW pairwise,  $p = 0.018$  from saline), to a similar extent as that seen in three-day gradual and acutely depleted mice (KW pairwise,  $p < 0.002$  from saline,  $p = 1$  from 7day) (Fig. 2.6D-E). Although immobility tended to increase in seven-day depleted mice compared to saline, this increase was not as dramatic as that seen with the acute and three-day gradual paradigm (KW pairwise,  $p = 0.24$  from saline), suggesting there may be additional compensatory mechanisms engaged during the longer seven-day depletion paradigm resulting in a smaller reduction in mobility (Saline =  $1.1 \pm 0.1$  %,  $n = 40$ ; Gradual(7day) =  $4.1 \pm 2.1$  %,  $n = 4$ ; Gradual(3day) =  $18.6 \pm 8.0$  %,  $n = 12$ ; Acute =  $16.1 \pm 5.5$  %,  $n = 14$ ) (Fig. 2.6F-G). Percentage of time spent performing fine movements was also analyzed, however there were no differences between mice that underwent the seven-day paradigm, three-day paradigm, or acute paradigm (data not shown).

## 2.4 DISCUSSION

Using a progressive model of dopamine depletion, we show that the time course of dopamine loss can impact the severity of motor symptoms. Furthermore, progressive dopamine loss reveals dissociable rates of behavioral impairment for different types of motor tasks (Fig. 2.7A-B). Spontaneous locomotion in the open field remained normal until rapidly declining with depletions >70%; rearing behavior declined steadily as a function of decreasing dopamine levels; and performance on the pole task remained robust in gradually depleted mice, despite severe

deficits on this task in acutely depleted mice. Taken together, these data suggest that our gradual depletion paradigm provides an experimental platform to study circuit changes during early dopamine loss, including mechanisms of compensatory plasticity that may be precluded in traditional acute models.

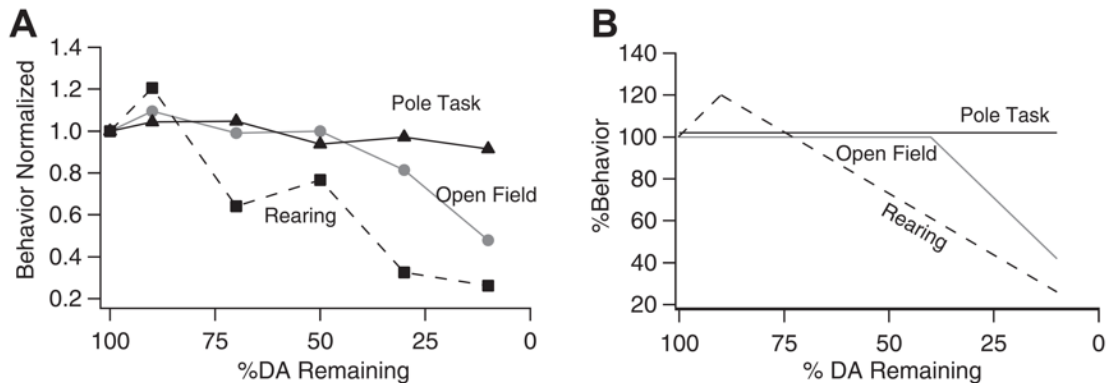


**Figure 2.7. Differential progression motor deficits in gradually depleted mice.** (A) Normalized behavior of gradually depleted animals plotted as a function of striatal dopamine levels. Percentage of time spent mobile normalized to saline controls is plotted as a representative of open field activity, total number of rears normalized to saline controls is plotted for rearing, and turn down latency normalized to saline controls is plotted as a representative of pole task performance. (B) Schematic showing the differential degradation of behavior of animals whose dopamine was gradually depleted.

A major challenge in treating PD is that the hallmark motor symptoms of the disease typically do not present until the majority of dopamine (>70%) has been depleted from the system (Bernheimer et al., 1973; Deumens et al., 2002; Fahn, 2003; Olanow and Obeso, 2012; Riederer and Wuketich, 1976). Therefore, by the time of diagnosis, physiological progression of the disease may have already reached a point where it cannot be reversed (Bezard and Gross, 1998; Bezard et al., 2003; Schapira and Tolosa, 2010). This early phase of the disease, when dopamine levels have started to decline but overt motor symptoms have not yet presented, is called the prodromal phase, and is likely an ideal window in which to begin therapy (Bezard et al., 2003; Tolosa et al., 2009). However, our understanding of the physiological changes occurring during prodromal PD are sparse, and there is no clear understanding of when and where to best intervene during this period to maximize therapeutic outcome.

This knowledge gap is exacerbated by the fact that most mouse models of PD are not suitable for study of the prodromal phase because they rely on administration of an acute dose of 6-OHDA, or other neurotoxins, to produce a certain degree of depletion (Ferro et al., 2005; Kirik et al., 1998; Meredith et al., 2008a; Przedborski et al., 1995; Schwarting and Huston, 1996a, 1996b; Truong et al., 2006). Although the acute 6-OHDA model has unveiled many differences in the brain following full dopamine depletion (Day et al., 2006; Gittis et al., 2011; Iancu et al., 2005; Jeon et al., 1995; Kravitz et al., 2010; Kreitzer and Malenka, 2007; Mallet et al., 2006; Schober, 2004; Schwarting and Huston, 1996b; Taverna et al., 2008), this technique fails to capture what is happening to the behavior of an animal as dopamine is gradually and consistently depleted within the same system, similar to the pathology of human PD (Bernheimer et al., 1973; Meredith et al., 2008a; Potashkin et al., 2010; Savitt et al., 2006). One promising progressive model involves AAV-induced overexpression of  $\alpha$ -synuclein. This model results in considerable loss of dopamine, as well as gradual motor impairments and proteinaceous inclusions (Decressac et al., 2012a, 2012b; Lundblad et al., 2012). These vector injections may shed more light on the role of  $\alpha$ -synuclein inclusions in the degeneration of dopamine and appearance of motor deficits, however optimization and characterization of this model is still on-going (see review (Lindgren et al., 2012)).

By administering repeated, low doses of 6-OHDA to the MFB, we were able to linearly deplete dopamine levels over a user-defined time course of 15-49 days, based on the spacing of injections. Using this approach, we induced behavioral deficits at end-stages of dopamine depletion (>80%), that were comparable to that of acutely depleted mice in both locomotor open field and rearing tasks. The only difference we observed between gradually and acutely depleted mice on these tasks was that mice who had been gradually depleted over 49 days showed less

immobility in the open field, largely because they spent more of their time moving, which was more similar to the behavioral patterns observed in saline-treated mice. The fact that we observed a greater difference in immobility than mobility, suggests that there may be different degrees of compensatory plasticity within separate pathways of the basal ganglia that differentially control these distinct aspects of movement (DeLong and Wichmann, 2007; Gerfen and Surmeier, 2011; Kravitz et al., 2010; Smith et al., 1998). The lack of immobility in seven-day depleted mice compared to three-day depleted mice may indicate compensatory mechanisms that are engaged over weeks rather than days.

Through assessment of exploratory rearing, we found that impairments in this behavior appear even at early stages of dopamine loss, and continue to progress as a direct function of dopamine levels. This linear decrease in rearing has been noted in previous studies using genetic or graded toxin models (Fleming et al., 2004; Goldberg et al., 2011). This behavior relies heavily on dorsolateral striatal function and therefore suggests that dorsolateral striatum is being progressively impaired over the course of our depletion protocol. The dorsolateral striatum is thought to be the source for many motor symptoms of PD – because it is the nucleus most directly affected by the loss of dopaminergic neurons in the SNc – and is critically involved in motor behaviors (Albin et al., 1989; Bolam et al., 2000; DeLong, 1990). The different trajectories of behavioral impairments on the open field vs. rearing tasks could be due to a number of reasons. While rearing appears to be most directly related to decreasing levels of striatal dopamine, mobility in the open field may be temporarily preserved due to compensation or adaptation in the dopamine system (Zigmond and Hastings, 1997; Zigmond et al., 1984, 2002), altered activity of nuclei within the basal ganglia (Bezard et al., 1997b, 1999; Maneuf et

al., 1994; Qiu et al., 2014), or compensation outside of the basal ganglia (Bezard et al., 2003; Brooks, 1999; Brotchie and Fitzer-Attas, 2009; Schroll et al., 2014).

An intriguing discovery of our study is that performance on the pole task, which relies on fine motor control and coordination, was dramatically different in severely dopamine depleted animals (>80%), depending on whether mice were gradually or acutely depleted. Previous studies using other models of dopamine depletion have shown severe deficits in performing this task (Fleming et al., 2004, 2006; Matsuura et al., 1997; Ogawa et al., 1985). Consistent with these previous studies, acutely depleted animals either could not perform the task, or took longer than half the allotted time for the task. In contrast, gradually depleted animals showed almost no deficits when compared to saline controls. This suggests that the improved performance on the pole task is due specifically to the time course of dopamine depletion. These results lend further support to the notion that the brain compensates or adapts differently to decreased levels of dopamine when dopamine loss occurs gradually over weeks instead of acutely over days. While the pole task may not be a good test of basal ganglia function, another possibility is that performance on this task can be regulated by a number of interacting motor systems (Brooks and Dunnett, 2009; Thullier et al., 1997), some of which can compensate when basal ganglia function is impaired. Many studies have shown the cerebellum as well as the supplementary motor area (SMA) may contribute to motor coordination and fine motor skills and show different activity patterns in human PD patients (Bezard et al., 2003; Bostan and Strick, 2010; Debaere et al., 2001; Ramnani et al., 2001; Rascol et al., 1997; Rosin et al., 2015; Thach et al., 1992; Wu and Hallett, 2005, 2013; Yu et al., 2007). These outside brain areas may be recruited only when dopamine is gradually depleted from the system and could account for the differences seen on the pole task. This difference in pole task performance highlights the importance of developing

and analyzing models where dopamine is depleted gradually within the same animal in a manner that is more consistent with PD pathology.

Although toxin models do not replicate all symptoms of human PD, most notably Lewy body inclusions, they are critical tools for gaining better mechanistic insights into circuit changes underlying the motor symptoms of the disease. In particular, toxin models are useful for studies directed at cell-specific mechanisms of circuit dysfunction, especially in mice where genetic labeling and manipulation of cells and circuits is unparalleled compared to any other mammalian system. By developing toxin paradigms that better replicate the chronic dopamine loss seen in human PD, we can gain a better understanding of how the temporal progression of dopamine loss alters neural circuits and ultimately motor function. A thorough understanding of how neural circuits adapt to decreasing levels of dopamine could lead to more effective therapies targeted at restoring circuit function in addition to restoration of dopamine levels.

In summary, we have shown that 6-OHDA can be utilized to gradually deplete dopamine within the same animal over time. This model has allowed us to uncover differential trajectories of motor degradation due to gradual dopamine depletion. Furthermore, this gradual model does not show the same extent of motor deficits seen in traditional acute models of dopamine depletion, suggesting that compensation may have a bigger impact on behavior when dopamine is gradually reduced within the same animal over time. This gradual depletion model can be manipulated to further uncover important aspects of how the brain adapts during the prodromal phase of PD and may lead to better methods of diagnosing and treating this neurodegenerative disease.

## 2.5 ACKNOWLEDGEMENTS

The authors would like to thank Michael Zigmond and Sandy Castro for helpful discussion. We also thank Amira Millette and Alexis Willis for their assistance with immunohistochemistry, behavioral scoring, and imaging. This work was supported by a NARSAD Young Investigator Grant from the Brain & Behavior Research Foundation, National Institutes of Health Grants R00 NS076524 and T32 NS007433, and a grant from the Disruptive Healthcare Technology Institute.

### **3.0 STEREOTYPED BASAL GANGLIA OUTPUT PATHOPHYSIOLOGY ACROSS DOPAMINE DEPLETION MODELS EMERGES PRIOR TO MOTOR DEFICITS**

Parkinson's disease (PD) is characterized by the progressive loss of dopamine in the basal ganglia that drastically alters circuit physiology and motor function. While dopamine levels in individuals with PD are gradually reduced over many years, motor deficits do not appear until ~70-80% of dopamine is lost. Theoretical models propose that changes in firing rate and/or firing pattern in basal ganglia output are likely responsible for the transition from asymptomatic to symptomatic PD. Here, to determine the onset and progression of pathophysiology in the basal ganglia during progressive dopamine loss, we recorded neural activity in the output nucleus at different stages of dopamine loss in two progressive mouse models of PD – a gradual 6-hydroxydopamine (6-OHDA) toxin model and a gradual pre-formed fibrils  $\alpha$ -synuclein (PFF  $\alpha$ -syn) model. We found that pathophysiology progresses in a stereotyped, hierarchical manner with firing rate changes occurring at early stages of dopamine loss, followed by changes in firing pattern that emerge at intermediate stages of dopamine loss. No one physiological parameter predicted motor deficits, however, principal component analysis revealed a biphasic transition in basal ganglia output physiology from healthy to end-stage. Due to the gradual and bilateral nature of these models, we also compared the degree of the pathophysiology seen in these models to two additional well-studied 6-OHDA mouse models – a bilateral acute 6-OHDA model with a much faster time course and a unilateral 6-OHDA model with preserved dopamine levels on the contralateral hemisphere. We found that the severity of pathophysiology was similar across all models regardless of time course or method of depletion, suggesting that

compensatory mechanisms in the basal ganglia become overwhelmed at end-stages of dopamine loss.

### 3.1 INTRODUCTION

Parkinson's disease (PD) is a movement disorder caused by the progressive degeneration of dopamine neurons in the substantia nigra pars compacta (SNc). The main projection targets of SNc dopamine neurons are motor territories of the basal ganglia, especially the dorsal striatum (Björklund and Dunnett, 2007; Lavoie et al., 1989). As a result, the hallmark symptoms of PD are predominantly motor, including resting tremor, postural abnormalities, gait disturbances, and decreased/slowed movement. Physiological indicators of basal ganglia dysfunction in the parkinsonian state include changes in both neuronal firing rates and patterns. The 'rate model' posits that motor symptoms are the result of elevated firing rates of basal ganglia output neurons under dopamine depleted conditions (DeLong, 1990; Fillion and Tremblay, 1991; Kravitz et al., 2010; Wichmann and DeLong, 2011). However, changes in both the magnitude and sign of firing rates vary widely across studies, suggesting that rates alone do not account entirely for motor deficits (Leblois et al., 2007; Nelson and Kreitzer, 2014; Seeger-Armbruster and Von Ameln-Mayerhofer, 2013; Wichmann et al., 1999). An alternative model is that motor deficits are more closely related to changes in neuronal firing patterns (Guridi and Alegre, 2017; Hammond et al., 2007). Under dopamine depleted conditions, basal ganglia output neurons fire more irregularly and synchronously than under normal conditions (Fillion and Tremblay, 1991; Galvan and Wichmann, 2008; Heimer et al., 2002; Hutchison et al., 1994; Wichmann et al., 2002). These aberrant firing patterns are hypothesized to disrupt information encoding which

impairs movement, but the correlation between firing patterns and motor deficits remains controversial.

Despite a vast literature describing basal ganglia pathophysiology at end-stages of dopamine loss, the question of *when* deficits emerge over the course of progressive depletion is poorly understood. PD is a gradual, neurodegenerative disorder and motor symptoms rarely present until late stages of dopamine loss (~20-30% striatal dopamine remaining) (Bernheimer et al., 1973; Fahn, 2003; Riederer and Wuketich, 1976). At this stage, treatments are limited to those that minimize symptoms rather than disease-modifying therapies. Diagnosing and treating patients during the presymptomatic, or ‘prodromal’ phase of the disease – when dopamine levels have started to decline but motor symptoms are not yet present – would increase options for treatment and result in better patient outcomes (Olanow and Obeso, 2012; Schapira and Tolosa, 2010; Tolosa et al., 2009). However, we know very little about the physiological trajectory of basal ganglia circuits as they transition from the healthy to the diseased state. Do pathophysiological changes emerge all at once, or is there a hierarchical progression? Does their severity worsen monotonically, or are there discrete inflection points that predict the transition from asymptomatic to symptomatic stages of the disease? Answering these questions is critical to develop therapeutic strategies for early intervention.

To study the onset and progression of basal ganglia pathophysiology during progressive dopamine loss in an intact network, we recorded neural activity in vivo from the substantia nigra pars reticulata (SNr) of mice at different stages of dopamine depletion, induced at rates ranging from 3 days – 6 months, using both toxin and neurodegenerative models. We found that across depletion models, SNr pathophysiology progressed in a stereotyped, hierarchical manner: firing rate change occurred first, at early stages of depletion, followed by changes in firing patterns that

emerged at more intermediate stages of depletion. Although no physiological parameters could predict motor deficits in isolation, in aggregate, we found that the transition from the asymptomatic to symptomatic stage was accompanied by a sharp increase in interactions with synchrony. Finally, at end-stages of depletion, the physiology of SNr neurons could not be discriminated across models or time course of depletion, suggesting that at end-stage, compensatory mechanisms become overwhelmed, supported by findings that unilaterally depleted mice and bilaterally depleted mice exhibit similar pathophysiology at end-stages of dopamine loss.

## **3.2 METHODS**

### **3.2.1 Animals**

Experiments were conducted in accordance with the guidelines from the National Institutes of Health and with approval from Carnegie Mellon University Institutional Animal Care and Use Committee. Male and female mice 8-15 weeks old weighing at least 20g prior to initial surgery on a C57BL/6J background were used for experiments. Co-housed littermates of the same sex were randomly assigned to experimental groups. After surgical implantation of the cannula or head-bar, animals were housed separately to prevent damage to the cannula or head-bar. Animals were provided with dishes of crushed high fat food pellets moistened with water, additional hard food pellets on the floor of the cage, as well as access to a water bottle. All cages were placed half on/half off heating pads following surgery and each subsequent infusion of 6-OHDA. Cages remained on heating pads unless animals were observed resting mainly in the unheated portion of

the cage. Each infusion of saline or 6-OHDA was performed while animals were lightly anesthetized on a heating pad, and all animals were injected with 0.1 cc of saline i.p. before being returned to their home cage. Animal's weights were tracked regularly and extra i.p. saline and softened food or trail mix were provided to encourage weight gain and proper hydration when appropriate. All animals prior to cannula or head-bar implant were group housed (2-6 per group) in a 12-h/12-h light dark cycle and all experiments were completed during the light cycle.

### **3.2.2 Cannula implantation**

Under ketamine/xylazine (100 mg/kg: 30 mg/kg, i.p.) anesthesia, the mice were placed on a stereotaxic frame (David Kopf Instruments) and maintained throughout surgery using 1-2% isoflurane. Bilateral internal cannulas (Plastics One) cut to target  $\pm 1.1$  mm lateral and -5.0 mm ventral were implanted 0.45 mm posterior to bregma and secured using superglue. 6-hydroxydopamine was prepared at a concentration of 5  $\mu\text{g}/\mu\text{L}$  in 0.9% NaCl for unilateral and bilateral acute depletions and diluted further with 0.9% NaCl to 0.75  $\mu\text{g}/\mu\text{L}$  for bilateral gradual depletions (Sigma-Aldrich H116 6-Hydroxydopamine hydrobromide). Injections were performed using a 33-gauge cannula (Plastics One) attached to a 10  $\mu\text{L}$  Hamilton syringe within a syringe pump (GenieTouch; Kent Scientific) running at 0.5  $\mu\text{L}/\text{min}$ , to a total volume of 1  $\mu\text{L}/\text{side}$ . The injection cannula was left in place for 5 min following the injection. Control animals received the same volume of vehicle (0.9% NaCl), following the same procedure. 6-OHDA and vehicle were administered every 5 days, respectively, for gradual depletions and controls. Subsets of gradually depleted animals were used for SNr recordings after each injection with a buffer period of 5 days following their last injection before behavior and

recordings were performed. Bilaterally depleted animals were used for experiments 4-5 days following the last given injection, whereas unilaterally depleted animals were used for experiments 4-7 weeks following 6-OHDA injection.

### **3.2.2 Stereotaxic $\alpha$ -synuclein injection**

Animals undergoing the gradual PFF  $\alpha$ -Syn paradigm underwent the same surgical preparation described above and received 1.5  $\mu$ L injections of 4  $\mu$ g/ $\mu$ L recombinant mouse  $\alpha$ -synuclein pre-formed fibrils bilaterally into the striatum (AP: +0.5, ML: +/-, DV: -2.6 mm). Injections were performed as described above with an adjusted pump speed of 1.5 $\mu$ L/7 min. PFF  $\alpha$ -Syn animals were recorded from 2-6 months after injection.

### **3.2.3 Implantation of head-fixation system**

Following dopamine depletion protocol, animals underwent surgery to prepare them for head-fixed *in vivo* physiology. Mice underwent anesthesia as described above and bilateral craniotomies were created over the SNr (-2.4 to -3.6 mm anterior, 0.9 to 2.1 mm lateral to bregma). Animals were then implanted with a copper head-bar fixed to the anterior portion of the skull (approximately at bregma) using a combination of superglue and dental cement. Dental cement was extended from the head-bar to surround the extent of both craniotomies to form a well. This well was then filled with silicone elastomer (Kwik-sil, WPI) that prevented infection and damage to the exposed brain tissue. During the recording, this well was filled with 0.9% NaCl and used as a ground reference.

### **3.2.4 Head-fixation training and recording**

Mice were clamped into place above a running wheel and allowed to run freely for 60 min the day prior to recording. Movement was tracked for the entirety of the recording using an inverted optical computer mouse and custom MATLAB script. Craniotomies were cleaned in preparation for recordings the following day and the silicone elastomer was replaced.

### **3.2.5 Behavioral assessment**

Prior to in vivo electrophysiological recordings, animals were exposed to the following sequential behavioral tests: open field, rearing, pole task, and wire hang. The minimum interval between two consecutive procedures was 30 min. Mice were habituated to the testing room for 20 minutes before testing.

*Open Field:* To determine overall spontaneous mobility, mice were placed in the center of a 1,600 cm<sup>2</sup> clear square open field chamber with video monitoring from above. Mice were in the arena for a total of 20 m, with 10 m for acclimation to the arena, and 10 m for data acquisition. Positions of nose, tail, and center of mass of each mouse were tracked using EthoVision 9.0 software (Noldus). Distance traveled and average velocities for the 10 m data acquisition period were calculated using EthoVision 9.0. The arena was cleaned with 50% ethanol in between animals.

*Rearing:* To assess spontaneous vertical activity, mice were placed in a standard 1000 mL glass beaker with video monitoring from the side for a total of 10 min. The number of full extension

rears was manually scored post-hoc by observers blind to treatment. The beaker was cleaned with 50% ethanol between each animal.

*Pole Task:* To evaluate coordination and bradykinesia, mice were placed head-upward at the top of a vertical gauze-wrapped circular wooden pole (diameter = 1 cm; height = 55 cm) placed inside a clean home cage with video monitoring from the side. To encourage descent, a 60-watt lamp was aimed at the top of the pole. Mice were given a total of 6 trials, the first 3 for training, the last 3 for testing. The latency to turn downward (turn down latency = TDL), time from orientation downward until all four paws reached the ground (traverse), and the total time spent on the pole (total) was recorded with a maximum duration of 120 s each for TDL and traverse time. All measurements were manually scored offline by observers blind to treatment. Even if the mouse fell part way into its descent, the behavior was scored until it reached the ground. When the mouse was unable to turn downward and/or instead dropped from the pole, TDL and traverse latencies were recorded as 120 s (default value) because of the severity of motor dysfunction.

*Wire Hang:* Mice were placed on the top of a standard wire cage lid. The lid was slightly shaken to cause animals to grip the wires and then the lid was turned upside down and suspended ~50 cm above a standard animal cage with fresh bedding. The latency of mice to fall off the wire hang was measured up to 15 min, and average values were computed from two trials (15 min apart). Trials were stopped if the mouse remained on the lid after 15 min.

### **3.2.6 In vivo SNr recordings**

On the day of recording, animals were fixed to the top of the wheel and allowed 15 min to acclimate to the head-fixed position. The silicone elastomer was removed and the craniotomies were cleaned. A linear 16-channel silicon probe with sites spaced 50  $\mu\text{m}$  apart (Neuronexus) pre-coated with DiI stain (ThermoFisher) was attached to the micromanipulator and centered on lambda. The probe was slowly advanced (5-7  $\mu\text{m}/\text{s}$ ) until the top of the SNr ( $\sim 4.2$   $\mu\text{m}$  from the top of the brain) was found. SNr activity was distinguished based on a combination of physiological features: presence of putative dopamine neurons, presence of putative GABAergic neurons, and lack of spindle-like activity (thalamic). Post-mortem tissue analysis for craniotomy placements as well as DiI stain surrounding the probe tract were further evidence of proper targeting. Additionally, tissue from a subset of animals was stained for Iba-1 positive activated microglia (Wako) that allowed us to visualize the entire recording track within the SNr. Once a population of SNr units was identified, 5-10 min of activity was recorded following a 5 min waiting period to ensure stability of the identified units.

### **3.2.7 Electrophysiology analysis**

Data was filtered at 150-8000 Hz for spiking activity and 0.7-300 Hz for local field potentials (LFP). Spike detection was completed using the Plexon offline sorter where principal component analysis was used to delineate single and multi-units. To be classified as a single unit, the following criteria will be utilized: (a) PCA clusters are significantly different ( $p < 0.05$ ); (b) J3-

statistic is greater than 1; (c) percent of ISI violations ( $< 1$  ms) is less than 0.7%; (d) Davies Bouldin test statistic is less than 0.5.

Following spike-sorting, data was processed with NeuroExplorer software in addition to custom scripts in MATLAB. *Rest period analysis*: Periods of rest were analyzed to quantify firing rates (FR) and coefficient of variation of the interspike intervals ( $CV_{ISI}$ ) (Fig. A1A). *Burst analysis*: Using the Poisson Surprise method (surprise = 5; at least 4 spikes in a burst), bursts were identified in single-unit SNr activity (Fig. A1B). ‘Bursty units’ were defined as units with  $>1\%$  of total spikes occurring within a burst but less than 1 median absolute deviation above the median (1-3.92%), while ‘highly bursty’ units were defined as units with  $> 1$  median absolute deviation above the median of all recorded units ( $>3.92\%$ ).

### **3.2.8 Synchrony analysis**

We modified traditional cross-correlation analysis to correct for nonstationarities within a unit’s firing pattern and to allow for direct comparisons across pairs of units regardless of their firing rates. We performed cross-correlation with a bin size of 10 milliseconds over 12-second-long windows with 4-seconds of overlap, excluding any window in which we detected movement on the running wheel. In each window, we zeroed the first and last 4 seconds of the 2<sup>nd</sup> train and only calculated out to a maximum lag of 4 seconds, thereby ensuring that each window would have a constant level of zero-padding across all calculated lags. This ensured a consistent level of baseline synchrony at long lags, which we used to normalize the cross-correlogram - specifically, we divided each window’s cross-correlogram by the mean correlation value from 0.5 to 4 seconds on both sides. These normalized windows were each averaged together to achieve the

final, normalized cross-correlation, whose values represent the proportion of synchronous spikes relative to the local chance level of synchrony (chance = 1). We calculated a 99% confidence interval from 0.5 to 4 seconds on both sides of the normalized cross-correlation and called a pair ‘synchronous’ if its normalized cross-correlation at zero lag exceeded this confidence interval (Fig. A1B). To calculate the fraction of synchronous pairs at each stage of dopamine loss, we required that at least 2 units be recorded simultaneously, and the minimum number of simultaneously recorded pairs from an animal had to exceed 4. For the purposes of looking at the relationship between recorded physiological parameters, we assigned each single-unit a ‘synchrony peak’ value that is equal to the average of cross-correlogram peak values across all pairwise comparisons for that unit (see Fig. 3.2 C,E,F).

### **3.2.9 Immunohistochemistry**

Degree of dopamine denervation was assessed with tyrosine hydroxylase staining in all animals, in vivo probe track was assessed with Iba-1 activated microglia staining, and plaque pathology in PFF  $\alpha$ -syn was assessed with phosphor-S129- $\alpha$ -synuclein staining. Shortly after electrophysiological recordings, animals were sacrificed and perfused transcardially with phosphate-buffered saline (PBS), followed by 4% paraformaldehyde (PFA) in PBS. Brains were retrieved and post-fixed in 4% PFA for 24 h before being rinsed with PBS, transferred to 30% sucrose in PBS, and stored at 4°C for at least 24 h prior to sectioning. Immunohistochemistry was carried out in free-floating coronal frozen sections (30  $\mu$ m). Tissue was sectioned using a freezing microtome (Microm HM 430; Thermo Scientific), blocked with 10% normal donkey serum, and permeabilized with 0.5% Triton X-100 for 1 h. Primary antibody incubations were

performed at room temperature for 24 h using rabbit anti-TH (1:500; Pel-Freez), rabbit anti-phospho-S129- $\alpha$ -synuclein [EP1536Y] (1:100; AbCam), or rabbit anti-Iba-1 (1:1000, Wako). Primary antibodies were detected with Alexa Fluor 647-conjugated donkey anti-rabbit (1:500, Vector Laboratories), incubated for 90 min at room temperature, or Alexa Fluor 488 donkey anti-rabbit (1:500, Vector Laboratories), incubated for 3 hours at room temperature.

### **3.2.10 Fluorescence quantification**

Epifluorescent images (10x magnification) from TH staining were taken from bilateral dorsal striatum in one coronal section between 0.62mm and 1.10 mm Bregma (according to Paxinos second edition Mouse Brain in Stereotaxic Coordinates). Pixel intensity over a  $75 \times 75 \mu\text{m}$  area ( $5625 \mu\text{m}^2$ ) from each hemisphere was measured using the pixel intensity measuring tool in ImageJ and normalized to the pixel intensities measured in saline control mice processed and imaged in parallel.

### **3.2.11 Statistical analysis**

All data sets were tested for normality with the Shapiro-Wilk test and equal variance with Levene's test prior to any statistical analysis. Data are expressed as median  $\pm$  median absolute deviation (MAD) unless otherwise indicated. N values reported in text are formatted as follows:  $n = \#$  of neurons/ $\#$  of animals. Statistical analysis regarding firing rate and  $\text{CV}_{\text{ISI}}$  was performed using Kruskal-Wallis analysis of variance (ANOVA) nonparametric test (KW) and any differences were further investigated by Kruskal-Wallis pairwise comparison between condition

of interest and saline controls with a Bonferroni correction for number of comparisons. Statistical analysis regarding proportion of bursting units across conditions was performed using a Pearson Chi-Square Test (Pearson) and any further differences were investigated by z-test comparison of column proportions (z-test) between condition of interest and saline controls with a Bonferroni correction for number of comparisons. Statistical analysis regarding the average percentage of synchronous pairs was performed using a one-way ANOVA followed by a Dunnett t (2-sided) post hoc test with the exception of the asymmetric condition which was not normally distributed, thus we ran a KW test as described above. Results of initial statistical tests can be found in the figure legends, whereas any post-hoc testing is reported in results text where appropriate. A  $p$ -value of 0.05 was considered statistically significant. All statistical procedures were performed using IBM SPSS Statistics, version 24.

### **3.2.12 Principal component analysis**

Physiology: We performed centered, standardized PCA on single unit firing rate,  $CV_{ISI}$ , % spikes in bursts, and % synchronous pairs (pca( ), MATLAB 2016a). Coefficients were corrected for orthonormality. For consistency, we applied a sign convention so that positive and negative PC scores roughly corresponded to Control and Depleted physiology states, respectively. Next, single unit physiological PC scores were averaged within mice for each component. Finally, we fit a polynomial model to mouse PC scores as a function of dopamine (see: Linear Modeling). The best fit for PC1 was typically a 3<sup>rd</sup> degree polynomial, and the best fit for PC2 was typically a 1<sup>st</sup> degree polynomial. All units in each mouse (or hemisphere, in unilateral mice) were assigned the same % synchronous pairs value in this analysis. Skewed data ( $CV_{ISI}$ , bursts,

synchrony) were log-transformed prior to PCA ( $\log_{10}()$ , MATLAB). PCA was performed separately in Fig. 3.3 and Fig. 3.5 to capture the respective axes of variation in each. PCA was run jointly on all animal models in Fig. 3.7, and also included all pair-wise multiplicative interactions of the original 4 physiological measurements as inputs.

Behavior: We performed centered, standardized PCA on mouse open field velocity, # of rears in 10 minutes, total time on pole task and wire hang latency ( $\text{pca}()$ , MATLAB 2016a). Coefficients were corrected for orthonormality. For consistency, we applied a sign convention so that positive and negative PC scores roughly corresponded to hyperactive and hypoactive states, respectively. Next, we fit a polynomial model to mouse behavioral PC scores as a function of dopamine (see: Linear Modeling). The best fit for behavior PC1 was typically a 2<sup>nd</sup> degree polynomial. Behavioral data were log-transformed prior to PCA to correct for skew ( $\log_{10}()$ , MATLAB).

“Normalized scores”: To aid visual comparison of behavior and physiology PCA, we z-scored physiology and behavior PC scores and then fit a polynomial model as described above. We zeroed these fits to the Ctl fit value (Figs. 3.4E, 3.6I,J). In Fig. 3.7O & P, mean unilateral scores were zeroed to the bilateral Ctl fit value.

### **3.2.13 Linear Models**

Polynomial fits were performed in MATLAB 2016a using linear least-squares regression ( $\text{fit}()$ ). 95% confidence intervals represent non-simultaneous bounds of the model fit. Models were selected on the basis of adjusted  $R^2$  values (reported in figures).

### 3.2.14 Linear Classifier

To predict depletion state from single unit physiological features, we first fit a cross-validated multinomial regression (`mnrfit()`, MATLAB 2016a). The model was trained to predict depletion state from firing rate, bursting, irregularity, synchrony and all pair-wise multiplicative interactions of these parameters. We used a jackknife procedure for cross-validation: in each iteration, a different mouse was held out and the model was fit with the single unit data from all remaining mice. During this procedure, we controlled for bias in the number of units and mice used in the training set by resampling the number of single units to match the median number of single units per mouse and resampling the training set of mice to maintain equal numbers between classes ( $n = 500$  permutations). This allowed us to measure true performance against chance performance ( $100 * 1 / n$  classes). To predict the held-out mouse's depletion state, we used the held-out single units as inputs to the fitted model and then summed the depletion state probabilities predicted from each single unit to assign depletion state using a Winner-Take-All threshold. Chance performance was verified by fitting a null model using scrambled mouse depletion state on each iteration (plotted as a dashed line on applicable figures). We measured whether depletion states could be discriminated above chance by performing a paired t-test on the mean prediction accuracy for each mouse compared to the mean prediction of the null model.

### 3.3 RESULTS

#### 3.3.1 SNr pathophysiology at end-stages of dopamine depletion in awake mice

To establish the electrophysiological parameters that define SNr pathophysiology at end-stages of dopamine loss, we performed *in vivo* recordings from the SNr of awake, bilaterally depleted mice (Fig. 3.1A-C). Depletions were induced by infusing 6-hydroxydopamine (6-OHDA) into the bilateral medial forebrain bundle (MFB), either in a single, high-dose infusion ('acute'; ~3 days), or through a series of repeated, low-dose infusions, spaced 5 days apart ('gradual'; 38 ± 15 days) (Fig. 3.2A-B). In all mice, depletion severity was quantified using tyrosine hydroxylase (TH) immunoreactivity in the striatum, a metric that is well correlated with tissue dopamine levels (Willard et al., 2015). Mice were considered to be at 'end-stage' when striatal TH levels were <20% that of littermate controls on both sides: Acute ('A5%'): 4.1 ± 2.6%; Gradual ('G5%'): 3.7 ± 4.4%; t-test,  $p = 0.847$ .

At end-stages of dopamine depletion, SNr physiology in both acutely and gradually depleted mice differed markedly from that of dopamine-intact controls (Fig. A1). SNr firing rates were significantly lower in dopamine depleted mice (Median ± MAD: Ctl: 35 ± 11 Hz,  $n = 262$  neurons/7 animals; A5%: 25 ± 11 Hz,  $n = 245$  neurons/7 animals; G5%: 26 ± 11 Hz,  $n = 293$  neurons/9 animals) (KW pairwise, Ctl vs. A5%, G5%,  $p < 0.0001$ ) (Fig. 3.1D and Fig. A1A).

Firing patterns of SNr neurons were also significantly altered by dopamine loss. The tonic firing of SNr neurons became more irregular, quantified as a significant increase in the coefficient of variation of the interspike interval ( $CV_{ISI}$ ) (Median ± MAD: Ctl: 0.54 ± 0.13; A5%: 0.76 ± 0.24; G5%: 0.68 ± 0.16, KW pairwise, Ctl vs. A5%, G5%,  $p < 0.0001$ ) (Fig. 3.1E

and Fig. A1A). We also found that burst firing became more prevalent in dopamine depleted mice, quantified using the Poisson Surprise method (Soares et al., 2004) (see Methods, Fig. 3.1F and Fig. A1B). Based on the percentage of spikes falling within a burst, SNr neurons could be subdivided into three categories: (1) ‘not bursty’, where  $< 1\%$  of spikes were in a burst; (2) ‘bursty’ where  $1-3.9\%$  ( $\leq$  median + MAD) of spikes were in a burst; or ‘highly bursty’ where  $> 3.9\%$  ( $>$  median + MAD) of spikes were in a burst. As shown in Fig. 3.1F, the fraction of SNr neurons with 'highly bursty' activity was significantly increased in depleted mice compared to controls: (Ctl: 17.5% (46/262 neurons across 7 animals); A5%: 48.2% (118/245 across 7 animals); G5%: 43.0% (126/293 across 9 animals) (z-test, Ctl vs. A5%, G5%,  $p < 0.001$ ).

To assess physiological changes at the population level, we first inspected the spectral power of local field potentials (LFPs). Increased spectral power in the beta frequency range (13-30 Hz,  $\beta$ -oscillations) is seen in human patients and has been described in a number of animal models of PD. However, in mouse SNr, we saw no evidence of elevated  $\beta$ -oscillations under dopamine depleted conditions in either acutely or gradually depleted mice (Fig. 3.1G), nor in subsequent recordings from unilaterally depleted mice, 4 weeks after depletion (data not shown). These findings are consistent with results of Lobb and Jaeger (2015), who also reported no increase in  $\beta$ -oscillations from awake mouse SNr. These results suggest that elevated  $\beta$ -oscillations are not a robust feature of SNr pathophysiology in mice.

To examine more directly whether spiking synchrony is affected by dopamine depletion, we computed cross-correlations between pairs of neurons. In brief, we calculated the cross-correlation of pairs of spike trains over short time windows and normalized each window to account for nonstationarities in neuronal firing rates over a recording session. We then calculated a 99% confidence interval for each pair. A pair was termed “synchronous” if its correlation at

zero lag exceeded this confidence interval (see Methods, Fig. 3.1H and Fig. A1B). We found that the average percentage of synchronous pairs was  $8.6 \pm 7.8\%$  ( $n = 7$  animals) in control mice but increased to  $30.6 \pm 11.4\%$  ( $n = 7$  animals) and  $28.0 \pm 22.6\%$  ( $n = 9$  animals) in acutely and gradually depleted mice, respectively (Dunnett, Ctl vs. A5%, G5%,  $p < 0.05$ ) (Fig. 3.1H).

Taken together, our results confirm the presence of multiple physiological changes in SNr neurons under dopamine depleted conditions. Although none of the parameters examined individually could reliably distinguish between gradually and acutely depleted mice, it is possible that simultaneous changes in multiple parameters distinguish the two conditions. To test this possibility, we trained a classifier to discriminate 'acute' from 'gradual' depleted mice using the pathophysiological metrics described above (Fig. 3.1I, and see Methods). The classifier was unable to discriminate these conditions above chance levels ( $58.7\% \pm 26\%$  CI<sub>95</sub>, paired t-test,  $p = 0.25$ ) (Fig. 3.1J). By contrast, retraining the same model to discriminate end-stage mice from control mice resulted in classification well above chance ( $81.8\% \pm 15.3\%$  CI<sub>95</sub>, paired t-test,  $p = 0.0002$ ) (Fig. 3.1K). Examination of the model coefficients show that successful discrimination largely depended on the pathophysiological changes described above, as well as increased interactions between FR and spike patterns (Fig. 3.1L). These results suggest that stereotyped changes in SNr physiology occur at end-stages of dopamine loss, regardless of whether dopamine is depleted slowly over a month, or acutely, over days.

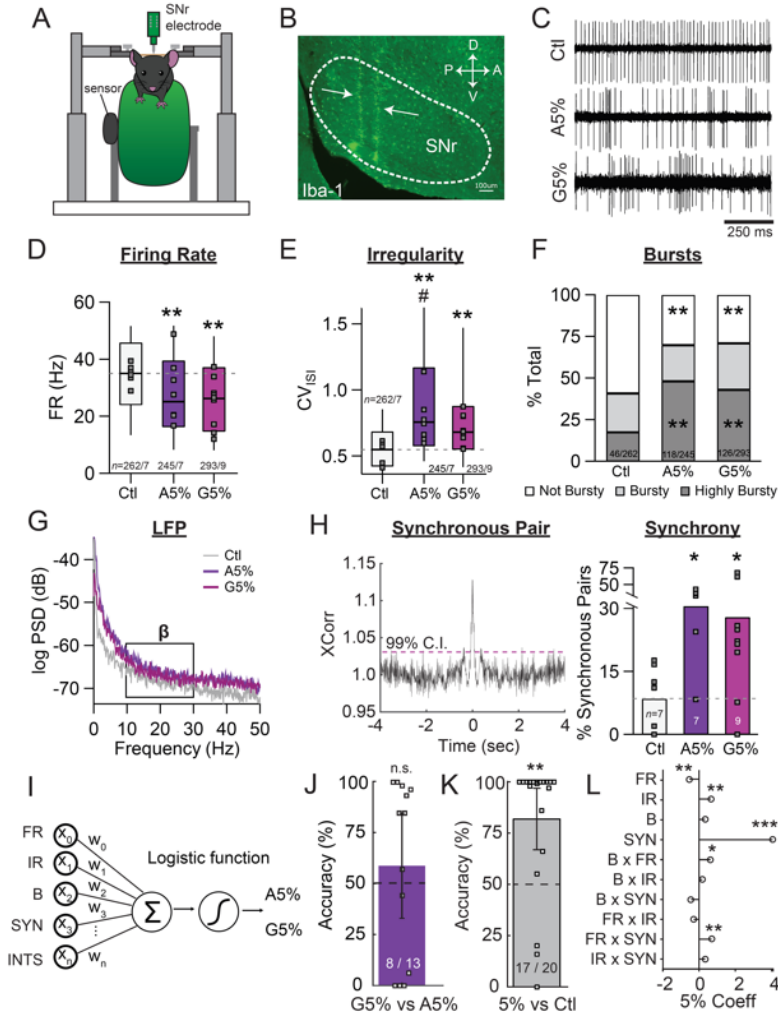


**Figure 3.1. 6-OHDA-induced acute bilateral dopamine depletions result in similar SNr pathophysiology as gradual bilateral dopamine depletions.** (A) Schematic of in vivo recording setup depicting head-restrained mouse on top of a freely moving wheel with a sensor to record wheel movement and a linear silicone probe to record SNr units. (B) Example sagittal image showing immunoreactive Iba-1-positive activated microglia surrounding the recording track within the SNr. Scale Bar = 100  $\mu$ m. (C) Representative example 1 s raw traces from control (Ctl), end-stage acute (A5%), and end-stage gradual conditions (G5%). (D) Box plot of firing rates of all single units recorded in each condition. Grey squares indicate animal medians. KW,  $\chi^2(2) = 40.463$ ,  $p < 0.0001$ , pairwise, \*\*  $p < 0.005$  from Ctl. (E) Box plot of  $CV_{ISI}$  of all single units recorded in each condition. Grey squares indicate animal medians. KW,  $\chi^2(2) = 101.830$ ,  $p < 0.0001$ , pairwise, \*\*  $p < 0.005$ , #  $p < 0.005$  from G5%. (F) Proportion of ‘not bursty,’ ‘bursty,’ and ‘highly bursty’ units in each condition. Pearson,  $\chi^2(4) = 80.591$ ,  $p < 0.0001$ , z-test, \*\*  $p < 0.005$  from Ctl. (G) Representative example LFP spectrograms from Ctl, A5%, and G5% with box highlighting  $\square$  frequency range (13-30 Hz). (H) Example cross-correlogram of a synchronous pair of simultaneously recorded SNr units. Horizontal dotted line is 99% confidence interval used as threshold for determining if a pair was synchronous (left). Average proportion of synchronous pairs in each condition; grey squares indicate animal proportions. ANOVA,  $F(2) = 3.992$ ,  $p = 0.035$ , Dunnett, \*  $p < 0.05$  from Ctl (right). (I) Schematic of cross-validated logistic regression trained to discriminate A5% from G5% animals using single unit spiking properties and pair-wise spike property interactions (INTS) (see: Methods) . (J) Mean cross-validated accuracy of predicting the model that led to end-stage in each mouse ( $\pm$  CI<sub>95</sub>). Paired t-test,  $p = 0.207$ , from permuted data  $n = 13$  mice. Grey squares indicate mean prediction for each mouse. (K) Same as J but predicting A5% and G5% combined (5%) vs Ctl. Paired t-test,  $p < 0.0001$ , from permuted data,  $n = 20$  mice. (L) Model coefficients from K that allow 5% to be discriminated Ctl. \*  $p < 0.05$ , \*\*  $p < 0.01$ , \*\*\*  $p < 0.001$

### 3.3.2 Increased irregularity in firing pattern correlates with increased bursting activity

To assess how the physiological parameters we are measuring influence each other, we plotted each single-unit physiological parameter against one other in the Ctl, A5%, and G5% condition. There was a moderate statistically significant negative correlation between firing rate and  $CV_{ISI}$  across all three conditions, where neurons that had low firing rates were more likely to have a more irregular firing pattern (Ctl:  $r = -0.33$ ,  $R^2 = 0.11$ ,  $p < 0.00001$ ; A5%:  $r = -0.40$ ,  $R^2 = 0.16$ ,  $p < 0.00001$ ; G5%:  $r = -0.38$ ,  $R^2 = 0.15$ ,  $p < 0.00001$ ) (Fig. 3.2A). There was a similar correlation between firing rate and the percentage of spikes in burst across all three conditions (Ctl:  $r = -0.40$ ,  $R^2 = 0.16$ ,  $p < 0.00001$ ; A5%:  $r = -0.33$ ,  $R^2 = 0.11$ ,  $p < 0.00001$ ; G5%:  $r = -0.29$ ,  $R^2 = 0.08$ ,  $p < 0.00001$ ) (Fig. 3.2B). Additionally, we observed a small but statistically significant positive correlation between firing rate and synchrony in gradually depleted animals that was not seen in control or acutely depleted animals (Ctl:  $r = 0.09$ ,  $R^2 = 0.008$ ,  $p = 0.156$ ; A5%:  $r = 0.012$ ,  $R^2 = 0.0002$ ,  $p = 0.847$ ; G5%:  $r = 0.23$ ,  $R^2 = 0.05$ ,  $p = 0.00007$ ) (Fig. 3.2C).

Given the similar correlations between firing rate and  $CV_{ISI}$  and firing rate and burst activity, we also analyzed at the relationship between  $CV_{ISI}$  and the percentage of spikes in bursts. Approximately 55% of the total variation in  $CV_{ISI}$  can be explained by the linear relationship between  $CV_{ISI}$  and bursting activity (Ctl:  $r = 0.76$ ,  $R^2 = 0.58$ ,  $p < 0.00001$ ; A5%:  $r = 0.68$ ,  $R^2 = 0.46$ ,  $p < 0.00001$ ; G5%:  $r = 0.79$ ,  $R^2 = 0.63$ ,  $p < 0.00001$ ) (Fig. 3.2D).

Based on observations that bouts of synchrony appeared to coincide with periods of irregular and/or burst firing, we additionally analyzed the relationship between these parameters (Fig. A1B). Since synchrony was measured between pairs, we created a ‘synchrony peak’ value for each unit that was equal to the average of cross-correlogram peak values across all pairwise

comparisons for that unit (see Methods). There was a small but statistically significant positive correlation between  $CV_{ISI}$  and synchrony in acutely depleted animals that was not seen in control or gradually depleted animals (Ctl:  $r = 0.07$ ,  $R^2 = 0.005$ ,  $p = 0.262$ ; A5%:  $r = 0.19$ ,  $R^2 = 0.04$ ,  $p = 0.003$ ; G5%:  $r = -0.06$ ,  $R^2 = 0.004$ ,  $p = 0.290$ ) (Fig. 3.2E). We found no significant correlations between burst activity and synchrony (Ctl:  $r = 0.10$ ,  $R^2 = 0.01$ ,  $p = 0.09$ ; A5%:  $r = 0.09$ ,  $R^2 = 0.008$ ,  $p = 0.168$ ; G5%:  $r = -0.07$ ,  $R^2 = 0.005$ ,  $p = 0.219$ ) (Fig. 3.2F). Taken together, these results suggest that measures of irregularity in firing pattern and burst activity are highly correlated with one another and this relationship is consistent across control and 6-OHDA-induced bilateral dopamine depleted animals.

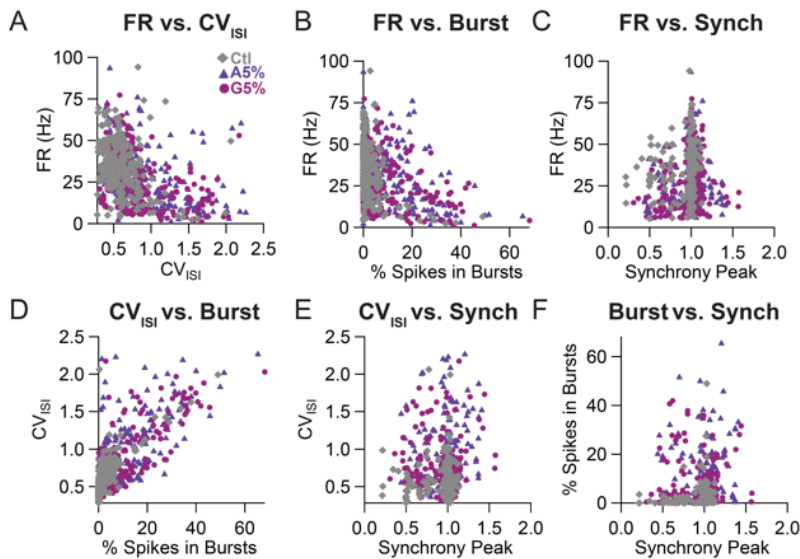


**Figure 3.2 Irregularity and bursting physiological parameters are correlated in control and 6-OHDA-induced bilateral dopamine depletions.** (A) Scatter plot of firing rate (FR) vs.  $CV_{ISI}$  for all units across Ctl, A5%, and G5% conditions. (B) Scatter plot of FR vs. % spikes in bursts (Burst) for all units across conditions. (C) Scatter plot of FR vs. average cross-correlogram synchrony peak (Synch) for all units across conditions. (D) Scatter plot of  $CV_{ISI}$  vs. Burst for all units across conditions. (E) Scatter plot of  $CV_{ISI}$  vs. Synch for all units across conditions. (F) Scatter plot of Burst vs. Synch for all units across conditions.

### 3.3.3 SNr pathophysiology proceeds in two phases during gradual dopamine depletion

To determine how SNr pathophysiology develops over the course of gradual dopamine loss, we performed *in vivo* recordings from mice at various stages of depletion (Fig. 3.3A). Because precise quantification of depletion stage required postmortem analysis, data at each depletion stage are from different groups of mice (TH immunoreactivity relative to control): ‘G85%’ =  $86 \pm 9\%$ ; ‘G60%’ =  $61 \pm 12\%$ ; ‘G30%’ =  $28 \pm 18\%$ ; ‘G5%’ =  $3.7 \pm 4.4\%$ .

Even at early stages of dopamine depletion, SNr physiology was altered relative to control. The most sensitive parameter was firing rate, which was significantly reduced at the first depletion stage examined (Median  $\pm$  MAD: Ctl:  $35 \pm 11$  Hz,  $n = 262$  neurons/7 animals; G85%:  $26 \pm 12$  Hz,  $n = 272$  neurons/5 animals; G60%:  $27 \pm 14$  Hz,  $n = 318$  neurons/7 animals; G30%:  $30 \pm 10$  Hz,  $n = 318$  neurons/8 animals; G5%:  $26 \pm 11$  Hz,  $n = 293$  neurons/9 animals) (KW pairwise, Ctl vs. G85%, G60%, G30%, G5%,  $p < 0.001$ ) (Fig. 3.3C).

A small change in firing pattern was apparent at the first depletion stage but increased in severity slightly later in the depletion process. A modest increase in firing irregularity ( $CV_{ISI}$ ) first emerged in mice with ~85% dopamine remaining (Median  $\pm$  MAD: Ctl:  $0.54 \pm 0.13$ ; G85%:  $0.59 \pm 0.15$ ; G60%:  $0.65 \pm 0.20$ ; G30%:  $0.71 \pm 0.22$ ; G5%:  $0.68 \pm 0.16$ ) (KW pairwise, Ctl vs. G85%, G60%, G30%, G5%,  $p < 0.005$ ) and increased in severity in mice with <30% dopamine remaining (KW pairwise, G85% vs. G30%, G5%,  $p < 0.01$ ) (Fig. 3.3D). A similar pattern was seen for burst firing. The proportion of ‘highly bursty’ neurons was relatively unchanged at early stages of depletion, but increased at later stages (Ctl: 17.5% (46/262 across 7 animals); G85%: 26.5% (72/272 across 5 animals); G60%: 34.9% (111/318 across 7 animals); G30%:

37.1% (118/318 across 8 animals); G5%: 43.0% (126/293 across 9 animals)) (z-test, Ctl vs. G60%, G30%, G5%,  $p < 0.001$ ) (Fig. 3.3E).

Spike synchrony at each stage of depletion was calculated as described in Fig. 3.1. The fraction of pairs firing synchronously in each animal tended to increase at intermediate stages of depletion, but did not reach statistical significance until end-stage (Ctl:  $8.6 \pm 7.8\%$   $n = 7$  animals; G85%:  $18 \pm 14\%$   $n = 5$  animals; G60%:  $7.3 \pm 7.3\%$   $n = 7$  animals; G30%:  $15 \pm 11\%$   $n = 8$  animals; G5%:  $28 \pm 23\%$   $n = 9$  animals) (Dunnett, Ctl vs. G5%,  $p = 0.04$ ) (Fig. 3.3F). We found no significant change in the fraction of  $\beta$  power at any stage of depletion (data not shown).

To determine whether capturing changes across all of these parameters simultaneously would reveal different physiological states over the course of depletion, we performed principal component (PC) analysis on these physiological parameters (see Methods). Physiology PC1 explained 52.6% of neural variability. This component primarily captured variation in firing rate, irregularity, and bursting (Fig. 3.3G). To visualize the trajectory of this component over the full spectrum of dopamine depletion, we plotted each mouse's physiology PC1 score as a function of its striatal TH level (Fig. 3.3I). We observed that the physiological transition from the control to the fully depleted state followed a biphasic progression (Fig. 3.3I). The first transition occurred early in the depletion process, reflecting an acute sensitivity of SNr physiology to even small changes in dopamine levels. After this initial drop, physiology PC1 remained relatively stable across subsequent depletion stages, but underwent a second sharp drop as mice reached the end-stage of depletion. At end-stage, the physiology PC1 score calculated from acutely depleted mice overlapped almost identically with that calculated from gradually depleted mice (Fig. 3.3I, triangle).

Changes in neural synchrony were best captured by physiology PC2, which explained 25.6% of neural variability (Fig. 3.3H). Unlike physiology PC1, PC2 showed little relationship with dopamine (adjusted  $R^2 = 0.019$ ), with a weak monotonic trend of decreasing as a function of dopamine loss (Fig. 3.3J). Nonetheless, acutely depleted mice showed a similar decrease in physiology PC2 scores (higher synchrony) at end-stage (Fig. 3.3J, triangle).

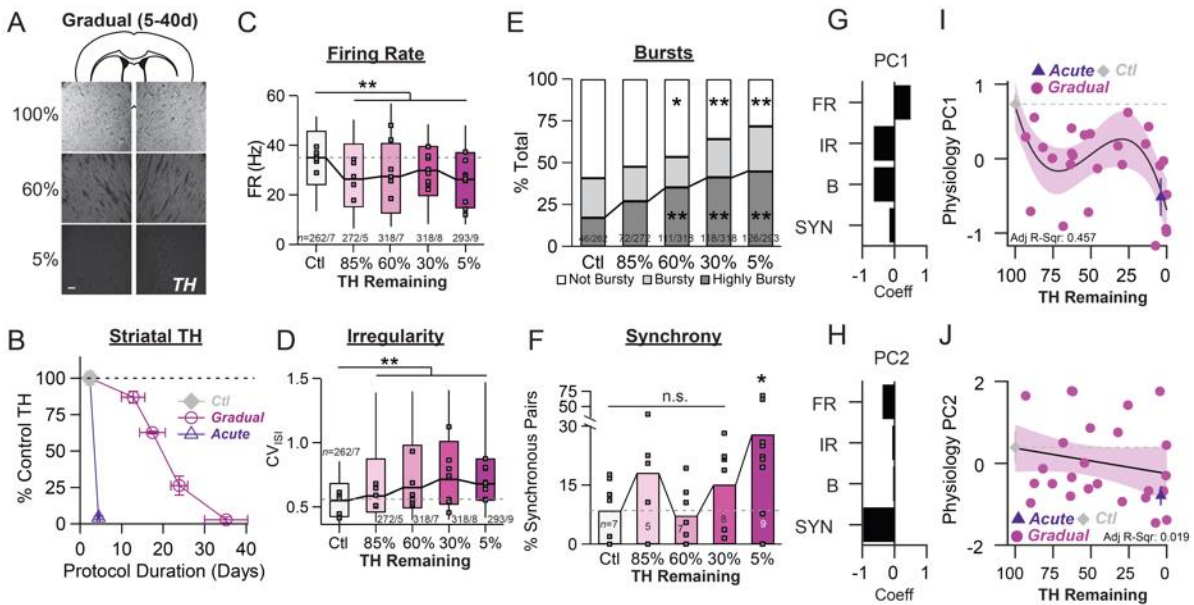


**Figure 3.3. 6-OHDA-induced bilateral gradual dopamine depletion causes early reduction of firing rate followed by increases in irregularity and bursts within the SNr.** (A) Schematic of coronal section of mouse brain showing representative images of TH immunoreactivity (TH-IR) in the dorsal striatum of mice treated with saline or multiple bilateral injections of 6-OHDA (3x0.75  $\mu$ g or 6x0.75  $\mu$ g). Scale Bar = 100  $\mu$ m. (B) Scatter plot showing the quantification of percent TH remaining, relative to saline controls, and time between initial surgery and in vivo recording across the bilateral gradual and acute 6-OHDA models. (C) Box plot of firing rates of all single units recorded in each condition. Grey squares indicate animal medians. KW,  $\chi^2(4) = 41.846$ ,  $p < 0.0001$ , pairwise, \*\*  $p < 0.005$  from Ctl. (D) Box plot of CV<sub>ISI</sub> of all single units recorded in each condition. Grey squares indicate animal medians. KW,  $\chi^2(4) = 72.039$ ,  $p < 0.0001$ , pairwise, \*\*  $p < 0.005$  from Ctl. (E) Proportion of 'not bursty,' 'bursty,' and 'highly bursty' units in each condition. Pearson,  $\chi^2(8) = 78.856$ ,  $p < 0.0001$ , z-test, \*  $p < 0.05$  and \*\*  $p < 0.005$  from Ctl. (F) Average proportion of synchronous pairs in each condition, grey squares indicate animal proportions ANOVA,  $F(4) = 2.753$ ,  $p = 0.045$ , Dunnett, \*  $p < 0.05$  from Ctl. (G) 1<sup>st</sup> principal component coefficients ('Coeff') from PCA performed on Ctl, Gradual and Acute single unit physiology: FR, firing rate; IR, irregularity; B, bursting; SYN, synchrony (see: Methods). (H) Same as G but for 2<sup>nd</sup> principal component. (I) Mean animal physiology PC1 scores as a function of dopamine loss with model fit to Ctl and Gradual animals. Shaded region indicates CI<sub>95</sub> of fit (see: Methods); Avg  $\pm$  SEM for Ctl and Acute also shown. (J) Same as I but for mean animal PC2 scores.

### **3.3.4 Gradual dopamine depletion with 6-OHDA results in late onset of behavioral deficits**

To investigate the relationship between SNr pathophysiology and symptomatic onset over the course of gradual dopamine depletion, mice were given a battery of behavioral tests one day prior to *in vivo* recordings. Behavioral performance on individual tasks followed a variety of trends in relation to dopamine loss (Fig. 3.4). Early dopamine loss often resulted in hyperactivity relative to control mice, followed by hypoactivity e depletion stages, as observed in open field velocity (Fig. 3.4A). Velocity and total time taken to complete the pole task were preserved until late stages of dopamine loss, while rearing performance initially increased relative to control animals during early dopamine loss, then preceded to monotonically decrease as a function of decreasing dopamine levels (Fig. 3.4B). Finally, wire hang was the most sensitive test, showing a high degree of variability in performance at early stages of dopamine loss that sharply declined at around 50% dopamine loss (Fig. 3.4B).

To summarize these behavioral changes, we used PCA to identify the best single axis of behavioral change across animals and fit a model to the scores from control and gradually depleted mice (Fig. 3.4C, see Methods). Behavioral scores were robust to dopamine loss until levels dropped below 30%, at which point behavioral performance declined rapidly (Fig. 3.4D). This is similar to the pattern of symptomatic onset observed in human PD patients (Bernheimer et al., 1973; Betarbet et al., 2002; Deumens et al., 2002; Fahn, 2003; Riederer and Wuketich, 1976).

By comparison to Ctl values, this behavioral analysis establishes 'prodromal' and 'symptomatic' stages of gradual dopamine depletion. We next asked whether changes in SNr

physiology were correlated with changes in behavior. As shown in Fig. 3.4E, early physiological changes related to firing rate/irregularity/bursting (PC1) were negatively correlated with behavior throughout the prodromal period, but became positively correlated at the transition from the prodromal to symptomatic stage, at ~30% dopamine remaining. At the same time, firing synchrony (physiological PC2) continued to decline (Fig. 3.4E). Thus, distinct prodromal and end stage behavioral phenotypes are reflected in distinct physiological states in the SNr.

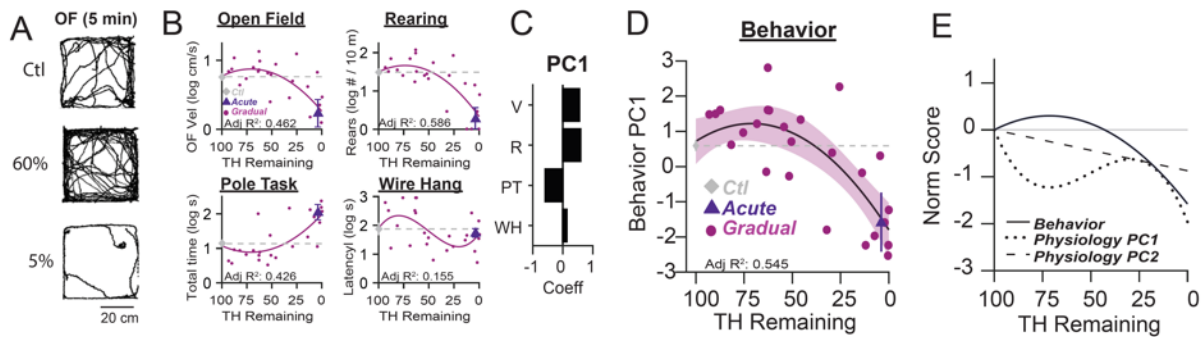


**Figure 3.4. 6-OHDA-induced bilateral gradual dopamine depletion results in late stage onset of motor deficits.** (A) Example raw open field movement traces from a Ctl, G60%, G5% mouse for a 5 minute period. (B) Scatter plots showing mean mouse open field velocity, rearing, pole task, and wire hang behavior vs. percent TH remaining across the bilateral gradual 6-OHDA model. Avg  $\pm$  SEM for Ctl and Acute also shown. Fits performed on Ctl and Gradual data. (C) 1<sup>st</sup> principal component coefficients for behavioral metrics. V, velocity; R, rearing; PT, pole task; WH, wire hang. (D) Mean animal behavior PC1 scores as a function of dopamine loss with model fit to Ctl and Gradual animals. Shaded region indicates CI<sub>95</sub> of fit (see: Methods). Avg  $\pm$  SEM for Ctl and Acute also shown. (E) Normalized behavioral PC fit from D overlaid with physiology PC fits (replotted from Fig. 3.3I,J) (see: Methods).

### **3.3.5 PFF $\alpha$ -synuclein drives gradual dopamine loss and behavioral changes that mirror the prodromal stage of 6-OHDA-treated mice**

Our results in 6-OHDA treated mice reveal a hierarchical progression of SNr pathophysiology over the course of gradual dopamine depletion. While most physiological deficits emerged well before the onset of motor symptoms, dimensionality reduction exposed distinct physiological states for the prodromal and symptomatic stages. To determine whether the onset and progression of SNr pathophysiology is robust across depletion models, we transitioned from a toxin model to a neurodegenerative model.

The protein  $\alpha$ -synuclein plays a central role in the pathogenesis of PD and is a major component of Lewy bodies in PD. A misfolded, fibrillar form of  $\alpha$ -syn has been shown to propagate throughout the brain via cell-to-cell transmission and drive neurodegeneration of SNc dopamine neurons and the formation of Lewy body-like inclusions (Luk et al., 2012; Mao et al., 2016; Volpicelli-Daley et al., 2014). Striatal inoculation with preformed fibrils of  $\alpha$ -syn (PFF  $\alpha$ -syn) resulted in progressive dopamine loss and the formation of Lewy body-like inclusions in a number of brain areas (Fig. 3.5A-B). Postmortem analysis of TH immunoreactivity in the striatum was used to group mice into discrete depletion categories (TH immunoreactivity relative to control): ‘Syn85%’ =  $85 \pm 10\%$ ; ‘Syn60%’ =  $60 \pm 11\%$ ; ‘Syn30%’ =  $30 \pm 5\%$ . Even after 6 months, striatal TH levels did not drop below 30%, a depletion severity sufficient to impair performance on the wire hang task, but not open field locomotion, consistent with previous results (Luk et al., 2012).

Behavioral scores were calculated for each mouse from their performance on a battery of behavioral tasks (Fig. 3.5C) and plotted as a function of depletion stage (Fig. 3.5D-E). Although

PFF  $\alpha$ -syn mice did not reach end-stage depletion levels and therefore did not transition into the symptomatic stage, their behavioral scores were similar to that of 6-OHDA-treated mice at similar stages of depletion, including slight elevations at intermediate stages of depletion, driven by hyperactivity in the open field, more rearing, and decreased time on the pole task (Fig. 3.5C).

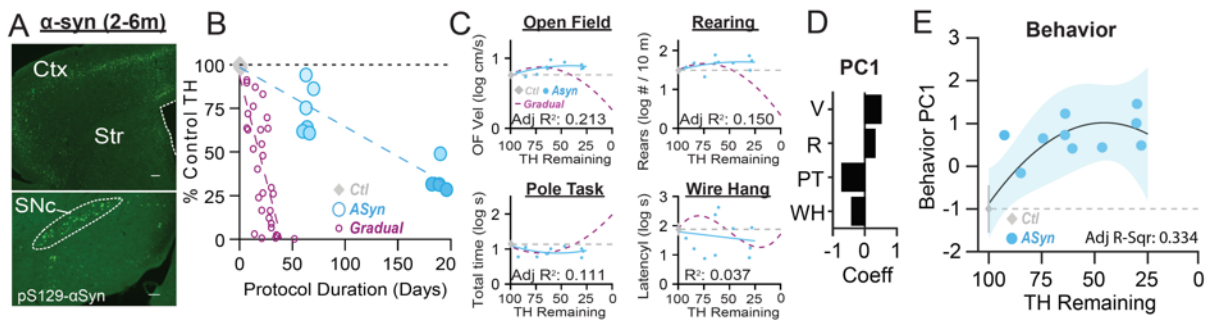


**Figure 3.5. PFF  $\alpha$ -Syn-induced bilateral gradual dopamine depletion leads to hyperactivity and fails to reach end stage motor impairments.** (A) Representative images of  $\alpha$ -syn inclusions present in the cortex (Ctx), striatum (Str), and substantia nigra pars compacta (SNc). Scale Bars = 100  $\mu$ m (top), 200  $\mu$ m (bottom). (B) Scatter plot showing the quantification of TH remaining, relative to saline controls, and time between initial surgery and in vivo recording across the PFF  $\alpha$ -Syn model. (C) Scatter plots showing mean open field velocity, rearing, pole task, and wire hang behavior vs. percent TH remaining in PFF  $\alpha$ -Syn-induced bilateral depletion animals. Fits performed on Ctl and PFF  $\alpha$ -Syn data with Gradual fits from Fig. 3.4C replotted for comparison. Avg  $\pm$  SEM for Ctl also shown. (D) 1<sup>st</sup> principal component coefficients for behavioral metrics. V, velocity; R, rearing; PT, pole task; WH, wire hang. (E) Mean animal behavior PC1 scores as a function of dopamine loss with model fit to Ctl and  $\alpha$ -Syn animals. Shaded region indicates CI<sub>95</sub> of fit.

### 3.3.6 SNr pathophysiology progresses similarly in PFF $\alpha$ -syn mice and 6-OHDA-treated mice

The onset and severity of SNr pathophysiology in PFF  $\alpha$ -syn mice was strikingly similar to that seen in 6-OHDA-treated mice. SNr firing rates were significantly reduced even at the earliest stage of depletion, and this decrease persisted across subsequent stages of depletion (Median  $\pm$  MAD: Ctl:  $35 \pm 11$  Hz,  $n = 262$  neurons/7 animals; Syn85%:  $26 \pm 11$  Hz,  $n = 98$  neurons/3 animals; Syn60%:  $25 \pm 9$  Hz,  $n = 155$  neurons /4 animals; Syn30%:  $25 \pm 8$  Hz,  $n = 150$  neurons/3 animals) (KW pairwise, Ctl vs. Syn85%, Syn60%, Syn30%,  $p < 0.0001$ ) (Fig. 3.6A).

Changes in firing patterns emerged at later stages of depletion, mirroring the progression observed in 6-OHDA-treated mice. Increases in firing irregularity ( $CV_{ISI}$ ) emerged in mice with  $<60\%$  dopamine remaining (Median  $\pm$  MAD: Ctl:  $0.54 \pm 0.13$ ; Syn85%:  $0.54 \pm 0.10$ ; Syn60%:  $0.73 \pm 0.19$ ; Syn30%:  $0.67 \pm 0.22$ ) (KW pairwise, Ctl, Syn85% vs. Syn60%, Syn30%,  $p < 0.001$ ) (Fig. 3.6B). The proportion of 'highly bursty' neurons was also significantly increased relative to control at later stages of depletion, but not at early stages (Ctl: 17.5% (46/262 neurons across 7 animals); Syn85%: 23.5% (23/98 neurons across 3 animals); Syn60%: 31.0% (48/155 neurons across 4 animals); Syn30%: 34.7% (52/150 neurons across 3 animals) (z-test, Ctl vs. Syn60%, Syn30%,  $p < 0.05$ ). The proportions of 'bursty' and 'highly bursty' neurons were similar between PFF  $\alpha$ -syn and 6-OHDA-treated mice (Fig. 3.6C).

At the population level, we saw a trend towards more synchronized spiking, but as was the case in 6-OHDA-treated mice, this effect never reached statistical significance during the prodromal period (Ctl:  $8.6 \pm 7.8\%$   $n = 7$  animals; Syn85%:  $10.4 \pm 2.6\%$   $n = 3$  animals; Syn60%:  $13.7 \pm 11.5\%$   $n = 4$  animals; Syn30%:  $16.2 \pm 19.4\%$   $n = 3$  animals) (ANOVA,  $F(4) = 0.491$ ,  $p =$

0.742) (Fig. 3.6D). Additionally, there was no increase in  $\beta$  power at any stage of dopamine depletion (data not shown).

To ask whether SNr pathophysiology, as a whole, progresses along a similar trajectory in PFF  $\alpha$ -Syn mice compared to 6-OHDA-treated mice, we performed PC analysis. In PFF  $\alpha$ -Syn mice, the majority of physiological variability was once again captured by two PCs, with PC1 capturing variations in firing rate, irregularity, and bursting (51.8% variability) (Fig. 3.6E,G) and PC2 capturing variations in synchrony (25.2% variability, Fig. 3.6F,H). In PFF  $\alpha$ -Syn mice, PC1 showed a monophasic progression, (Fig. 3.6G), presumably due to a lack of end-stage pathology. As in 6-OHDA-treated mice, the first phase consisted of an initial drop in physiology PC1 score followed by a slight increase (Fig. 3.6I). Interestingly, the initial drop occurred more gradually in PFF  $\alpha$ -Syn mice. The PC2 score (neural synchrony), changed monotonically as a function of dopamine loss with a similar rate to 6-OHDA, although this fit was not significant (Fig. 3.6J). These results suggest that the progression of SNr pathophysiology depends more on the stage of dopamine depletion than the mechanism of depletion.

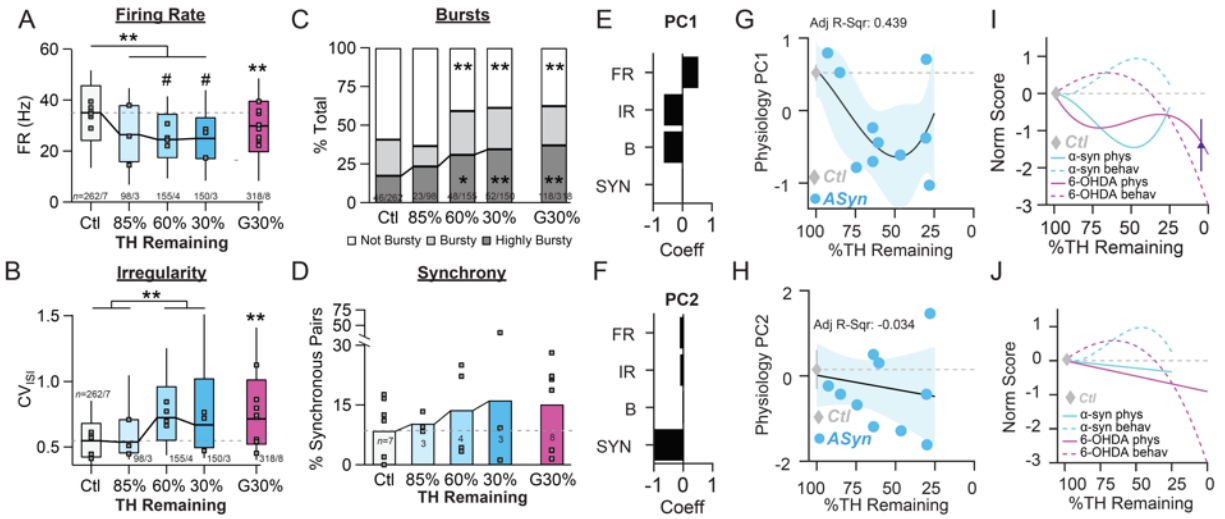


**Figure 3.6. PFF  $\alpha$ -Syn-induced bilateral gradual dopamine depletion causes early reduction of firing rates followed by increases in irregularity and bursts within the SNr.** (A) Box plot of firing rates of all single units recorded in each condition. Grey squares indicate animal medians. KW,  $\chi^2(4) = 53.274$ ,  $p < 0.0001$ , pairwise, \*\*  $p < 0.005$  from Ctl, #  $p < 0.05$  from G30%. (B) Box plot of CV<sub>ISI</sub> of all single units recorded in each condition. Grey squares indicate animal medians. KW,  $\chi^2(4) = 83.119$ ,  $p < 0.0001$ , pairwise, \*\*  $p < 0.005$  from Ctl and Syn85%. (C) Proportion of ‘not bursty,’ ‘bursty,’ and ‘highly bursty’ units in each condition. Pearson,  $\chi^2(8) = 77.286$ ,  $p < 0.0001$ , z-test, \*  $p < 0.05$  and \*\*  $p < 0.005$  from Ctl. (D) Average proportion of synchronous pairs in each condition. Grey squares indicate animal proportions ANOVA,  $F(4) = 0.491$ ,  $p = 0.742$ . (E) 1<sup>st</sup> principal component coefficients (‘Coeff’) from PCA performed on Ctl and  $\alpha$ -Syn single unit physiology: FR, firing rate; IR, irregularity; B, bursting; SYN, synchrony (see: Methods). (F) Same as E but for 2<sup>nd</sup> principal component. (G) Mean animal physiology PC1 scores as a function of dopamine loss with model fit to Ctl and  $\alpha$ -Syn animals. Shaded region indicates CI<sub>95</sub> of fit (see: Methods); Avg  $\pm$  SEM for Ctl also shown. (H) Same as G but for mean animal PC2 scores. (I) Normalized behavioral and physiological PC1 fits from  $\alpha$ -Syn mice (Fig. 3.5E, Fig 3.6G) overlaid with gradual 6-OHDA fits (replotted from Fig. 3.4E) (See: Methods). (J) Normalized behavioral PC1 and physiological PC2 fits from  $\alpha$ -Syn mice (Fig. 3.5E, Fig 3.6H), overlaid with gradual 6-OHDA (replotted from Fig. 3.4E).

### 3.3.7 Unilateral 6-OHDA SNr pathophysiology aligns to prodromal and end-stage bilateral pathophysiological phases

This far, our study has examined the progression of SNr pathophysiology in bilaterally depleted mice. However in human PD, dopamine loss often begins asymmetrically (Gelb et al., 1999; Hoehn and Yahr, 1967; Hughes et al., 1992), and the contralateral hemisphere might play an important role in compensation. Indeed, most studies of compensation under dopamine depleted conditions are conducted in unilaterally depleted animals (Chu et al., 2017; Escande et al., 2016; Fan et al., 2012; Fieblinger et al., 2014; Fuller et al., 2014; Gittis et al., 2011; Taverna et al., 2008).

To test whether compensatory plasticity from the opposite hemisphere can influence the nature or severity of pathophysiology in the SNr pathophysiology, we performed experiments in two additional models: 'unilateral' (Fig. 3.7A-B) and 'asymmetric' (Fig. 3.7F-G).

'Unilateral' mice received a single, high dose infusion of 6-OHDA (5 mg/mL) into the MFB on only one side and SNr pathophysiology was measured 4-7 weeks later ( $39 \pm 6$  days), to match the final time point used for bilaterally depleted mice. Depletion severity in the striatum ipsilateral to 6-OHDA injection was confirmed with TH immunoreactivity (Avg  $\pm$  SD:  $1.6 \pm 2.6\%$  striatal TH remaining;  $n = 6$  animals) (Fig. 3.7B). Intriguingly, we saw a significant increase in TH immunoreactivity on the contralateral side ( $211 \pm 91\%$ ,  $n = 5$  animals) (Fig. 3.7B).

Firing rates of SNr neurons in the depleted hemisphere were reduced relative to control (Median  $\pm$  MAD: Ctl:  $35 \pm 11$  Hz,  $n = 262$  neurons/7 animals; Ipsi<sub>uni</sub>:  $26 \pm 9$  Hz,  $n = 136$  neurons/ 6 animals, KW pairwise, Ctl vs. Ipsi<sub>uni</sub>,  $p < 0.0001$ ), and the magnitude of this change was similar to that seen in bilaterally depleted mice (KW pairwise, Ipsi<sub>uni</sub> vs. G5%,  $p = 0.842$ ) (Fig. 3.7C). No firing rate changes were observed in the contralateral, dopamine intact hemisphere (Median  $\pm$  MAD: Ctl:  $35 \pm 11$  Hz  $n = 262$  neurons/7animals; Contra<sub>uni</sub>:  $37 \pm 14$  Hz  $n = 94$  neurons/5 animals, KW pairwise, Ctl vs. Contra<sub>uni</sub>,  $p = 0.712$ ) (Fig. 3.7C). In contrast to changes in firing rates which were restricted to the dopamine depleted hemisphere, changes in firing patterns occurred in both hemispheres. Firing irregularity ( $CV_{ISI}$ ) was significantly elevated in both hemispheres (Median  $\pm$  MAD: Ctl:  $0.54 \pm 0.13$   $n = 262$  neurons/ 7 animals;

Contra<sub>uni</sub>:  $0.72 \pm 0.22$   $n = 94$  neurons/5 animals; Ipsi<sub>uni</sub>:  $0.86 \pm 0.30$   $n = 136$  neurons/6 animals, KW pairwise, Ctl vs. Ipsi<sub>uni</sub>, Contra<sub>uni</sub>,  $p < 0.0001$ ). On the ipsilateral side, irregularity was more pronounced than in bilaterally depleted mice (Ipsi<sub>uni</sub>:  $0.86 \pm 0.30$   $n = 136$  neurons/6 animals; G5%:  $0.68 \pm 0.16$   $n = 293$  neurons/9 animals, KW pairwise, Ipsi<sub>uni</sub> vs. G5%,  $p < 0.0001$ ), whereas on the contralateral side, firing irregularity was similar to that seen in bilaterally depleted mice (Contra<sub>uni</sub>:  $0.72 \pm 0.22$   $n = 94$  neurons/5 animals; G5%:  $0.68 \pm 0.16$   $n = 293$  neurons/9 animals, KW pairwise, Contra<sub>uni</sub> vs. G5%,  $p = 0.979$ ) (Fig. 3.7D). Similar effects were seen for the fraction of highly bursty units (data not shown). In both hemispheres, we saw a trend towards more synchronous spiking between pairs of neurons (Ctl:  $8.6 \pm 7.8\%$   $n = 7$  animals; Contra<sub>uni</sub>:  $14.8 \pm 13.0\%$   $n = 5$  animals; Ipsi<sub>uni</sub>:  $21.0 \pm 28.2\%$   $n = 6$  animals), but this value did not reach significance (Dunnett, Ctl vs. Contra<sub>uni</sub>,  $p = 0.930$ , Ctl vs. Ipsi<sub>uni</sub>,  $p = 0.567$ ) (Fig. 3.7E). Finally, there was no increase in fractional  $\beta$  power in either hemisphere (data not shown).

Because the extreme dichotomy of the unilateral model is an exaggeration of the asymmetry sometimes observed in human PD (Gelb et al., 1999; Hoehn and Yahr, 1967; Hughes et al., 1992), we also looked at SNr pathophysiology in an 'asymmetric' model, in which 6-OHDA was infused bilaterally but produced asymmetric depletions, in which the difference in TH levels between the two hemispheres was  $>20\%$  (Avg  $\pm$  SD =  $77 \pm 40\%$ ). On average, TH immunoreactivity was  $11 \pm 14\%$  relative to control in the ipsilateral hemisphere (Ipsi<sub>asym</sub>,  $n = 11$  animals) and  $96 \pm 44\%$  in the contralateral hemisphere (Contra<sub>asym</sub>,  $n = 11$  animals) (Fig. 3.7F-G).

In both hemispheres, firing rates of SNr neurons were significantly reduced compared to control (KW pairwise, Ctl vs. Ipsi<sub>asym</sub>, Contra<sub>asym</sub>,  $p < 0.0001$ ), and the magnitude of this effect was similar to that in bilaterally depleted mice (KW pairwise, Contra<sub>asym</sub> vs. G5%,  $p = 0.154$ , Ipsi<sub>asym</sub> vs. G5%,  $p = 0.740$ ) (Fig. 3.7H). Firing irregularity (CV<sub>ISI</sub>) was significantly elevated in both hemispheres (KW pairwise, Ctl vs. Contra<sub>asym</sub>, Ipsi<sub>asym</sub>,  $p < 0.0001$ ) (Fig. 3.7I), as well as the fraction of 'highly bursty' neurons (data not shown). In the ipsilateral hemisphere, but not the contralateral hemisphere, we saw a trend towards more synchronous spiking between pairs of neurons, but this value did not reach statistical significance (KW pairwise, Ctl vs. Ipsi<sub>asym</sub>,  $p = 0.337$ ) (Fig. 3.7J). Finally, there was no increase in fractional  $\beta$  power in either hemisphere (data not shown).

When considered individually, physiological changes in the SNr at end-stages of dopamine loss appear to be similar regardless of the depletion strategy used. To test whether this is the case when all physiological parameters are considered simultaneously, we trained a multinomial classifier to classify mice into each of four end-stage categories (A5%, G5%, Ipsi<sub>uni</sub> and Ipsi<sub>asym</sub> conditions), using single unit physiology and all pair-wise interactions (See: Methods). The classifier was unable to discriminate end-stage physiology above chance levels ( $26.1 \pm 6.3$  % accuracy, right-tail t-test vs. chance, 25%;  $p = 0.446$ ;  $n = 29$  mice) (Fig. 3.7K). Ipsi<sub>uni</sub> and Ipsi<sub>asym</sub> mice were confused with each other 37.5% of the time (6 / 16 Ipsi mice), and as a combined group (Ipsi<sub>all</sub>), could be discriminated from Ctl mice with  $71.9 \pm 6.0$  % accuracy (right-tail t-test vs. chance, 50%;  $p = 0.0006$ ;  $n = 29$  mice). When combined into a single end-stage category ('ES'), these groups were well-discriminated from Ctl mice ( $72.5 \pm 5.6$  % correct; right-tail t-test vs. chance, 50%;  $p = 0.00015$ ;  $n = 36$  mice) (Fig. 3.7L).

The results of our classifier suggest that regardless of depletion trajectory, the SNr transitions to a stereotyped state of severe pathophysiology. Ipsi and Contra physiology aligned with severe and control states respectively, when we performed PCA on physiology and behavior on all mice used in the study. Physiology PCA included all single unit spiking properties and pairwise multiplicative interactions (see: Methods) (Fig. 3.7M-N). PC1 again captured variability in firing rate, irregularity, and bursting, with the addition of how these parameters interacted (Fig. 3.7M). PC2 again captured variability in synchrony, but also captured when firing rate co-varied with synchrony (Fig. 3.7N). Due to their similarity, unilateral and asymmetric mice with behavior measurements and paired Ipsi and Contra recordings were pooled into Ipsi<sub>all</sub> and Contra<sub>all</sub> conditions ( $n = 7$  Contra<sub>asym</sub> and 7 Ipsi<sub>asym</sub> paired hemispheres; 5 Contra<sub>asym</sub> and 5 Ipsi<sub>asym</sub> paired hemispheres, 12 mice total). As shown in Fig. 3.7O, depleted hemispheres showed significantly lower PC1 scores than intact hemispheres (paired t-test,  $p = 0.037$ ,  $n = 12$  mice), and overlapped with PC1 scores from both gradually and acutely depleted mice. Intriguingly, PC1 scores for the contralateral hemisphere did not overlap with those of control mice, but rather with PC1 scores from the prodromal phase of PFF  $\alpha$ -Syn and 6-OHDA-treated mice (Fig. 3.7O). PC2 scores were not different between depleted and intact hemispheres (paired t-test,  $p = 0.54$ ,  $n = 12$  mice).

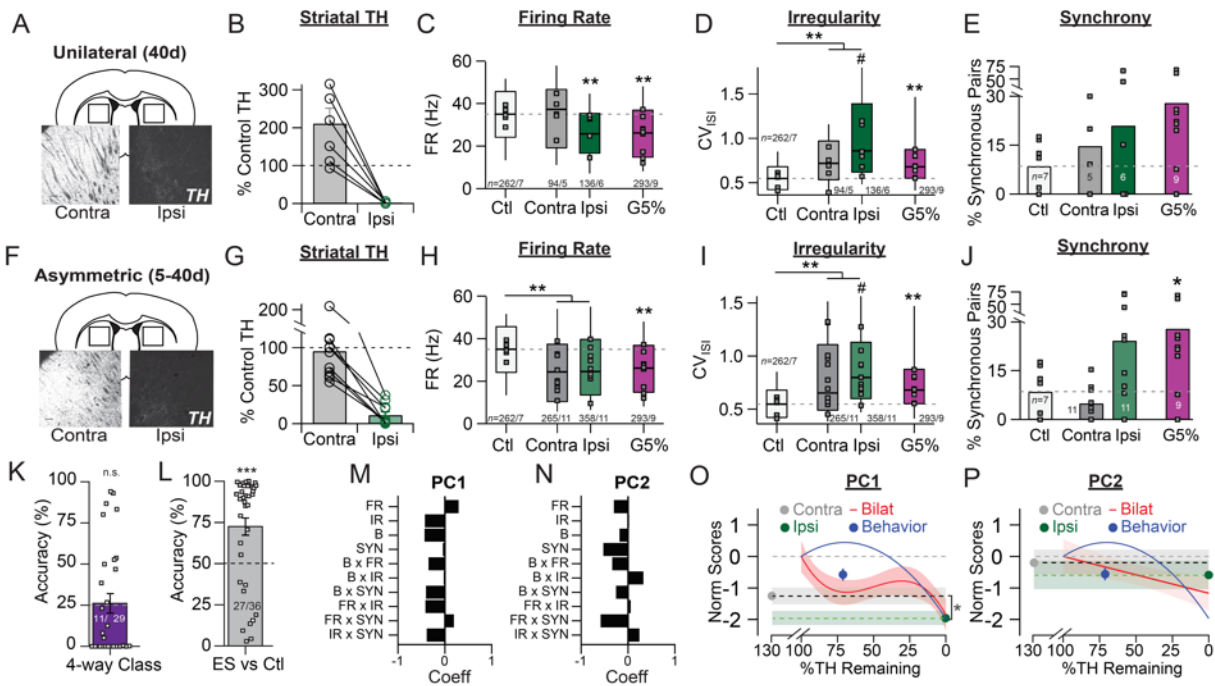


**Figure 3.7. Unilateral 6-OHDA model pathophysiology aligns to prodromal and end-stage bilateral pathophysiology.** (A) Example coronal sections showing TH-IR in the dorsal striatum of unilaterally depleted mice. Scale bar, 100  $\mu$ m. (B) Quantification of ipsilateral ('Ipsi') and contralateral ('Contra') percent TH remaining relative to saline controls in unilaterally depleted mice. (C) Box plots of single unit firing rates across conditions. Grey squares indicate animal medians. KW,  $\chi^2(3) = 5.488$ ,  $p < 0.0001$ , pairwise, \*\*  $p < 0.005$  from Ctl. (D) Box plots of single unit  $CV_{ISI}$  across conditions. Grey squares indicate animal medians. KW,  $\chi^2(3) = 110.685$ ,  $p < 0.0001$ , pairwise, \*\*  $p < 0.005$  from Ctl, #  $p < 0.005$  from G5%. (E) Average proportion of synchronous pairs in each condition. Grey squares indicate animal proportions. ANOVA,  $F(3) = 1.297$ ,  $p = 0.300$ . (F-J) Same as A-E but for asymmetrically depleted mice. Briefly, (F) Example coronal sections showing TH-IR in the dorsal striatum of asymmetrically depleted mice. Scale bar, 100  $\mu$ m. (G) same as B but for asymmetrically depleted mice. (H) Box plot of single unit firing rates. Grey squares indicate animal medians. KW,  $\chi^2(3) = 55.317$ ,  $p < 0.0001$ , pairwise, \*\*  $p < 0.005$  from Ctl. (I) Box plots of single unit  $CV_{ISI}$  across conditions. Grey squares indicate animal medians. KW,  $\chi^2(3) = 119.892$ ,  $p < 0.0001$ , pairwise, \*\*  $p < 0.005$  from Ctl, #  $p < 0.005$  from G5%. (J) Average proportion of synchronous pairs in each condition. Grey squares indicate animal proportions. KW,  $\chi^2(3) = 8.782$ ,  $p = 0.032$ , \*  $p < 0.05$  from Ctl. (K) Average classification performance for G5%, A5%, Ipsi<sub>uni</sub>, Ipsi<sub>asym</sub> mice ('4-way class') using single unit physiology. Right-tail t-test vs. chance (25%),  $p = 0.446$ ,  $n = 29$  mice. White squares, individual mouse classification accuracy. Inset, # mice predicted > chance / total mice. (L) Same as K but for classifying Ctl from all end-stage mice in 4-way class ('ES'). Right-tail t-test vs. chance (50%),  $p = 0.00015$ ,  $n = 26$  mice, \*\* $p < 0.005$ . (M) Physiology PC1 coefficients from all single units in study. (N) Same as M but for PC2. (O) Normalized bilateral physiology PC1 and behavior PC1. Shaded region indicates  $CI_{95}$  of fit. Contra and Ipsi hemisphere physiology PC1 scores overlaid, shaded area indicates  $\pm$ SEM. Paired t-test,  $p=0.037$ , \*  $p < 0.05$ ,  $n = 12$  mice. Blue dot, mean behavior PC1 score vs. average TH remaining across hemispheres in unilateral mice. (P) same as O but for physiology PC2 scores.

### 3.4 DISCUSSION

Results from 5 different depletion models, representing different mechanisms, rates, and patterns of dopamine depletion, show that SNr pathophysiology emerges at early stages of dopamine loss, well before the onset of motor symptoms, and its severity is independent of the rate of dopamine depletion. Firing rates of SNr neurons were the most sensitive to dopamine loss; with as little as ~15% dopamine loss, SNr firing rates were reduced to levels seen in fully depleted mice.

Aberrant firing patterns in the SNr, including loss of regularity and increased burst firing, emerged at later stages of depletion, once ~40% dopamine had been lost. At the network level, firing synchrony became more pronounced, particularly at late stages of dopamine loss, but amplified  $\beta$ -oscillations were never observed in any of our depletion models. Using dimensionality reduction to represent the progression of SNr pathophysiology along a single axis, we observed a sharp, stepwise transition from the intact to the depleted state that remained relatively stable across subsequent depletion stages and underwent a second sharp drop as mice reached the end-stage of depletion. These results suggest that regardless of the model or rate of depletion used, compensatory mechanisms do not maintain function of basal ganglia output into late-stages of the disease. These results provide the first quantitative analysis of the trajectory with which basal ganglia output physiology breaks down over the course of gradual dopamine depletion.

One of the major challenges in treating PD is that patients typically do not have overt motor symptoms until the late stages of dopamine neurodegeneration (Bernheimer et al., 1973; Fahn, 2003; Riederer and Wuketich, 1976). Thus, by the time a diagnosis is made, options for treatment are usually limited to those that minimize symptoms, rather than disease-modifying

therapies. Diagnosing and treating patients during the prodromal stage, when dopamine levels have started to decline but motor symptoms are not yet present, would increase options for treatment and likely result in better patient outcomes. Identifying the progressive changes leading up to the appearance of symptoms would also allow us to determine which adaptations are compensatory and develop pre-clinically and which are responsible for the onset of severe motor symptoms. However, our understanding of the physiological changes in the prodromal stage of PD is sparse.

Contributing to this lack of knowledge is the wide range of PD animal models used in research; none of which recapitulate all aspects of the disease (Betarbet et al., 2002; Bové et al., 2005; Meredith et al., 2008b; Simola et al., 2007). Even studies focused on the end stages of the disease, after dopamine has been fully depleted, have reported strikingly different and sometimes conflicting findings (Lobb and Jaeger, 2015a; Lobb et al., 2013; Seeger-Armbruster and Von Ameln-Mayerhofer, 2013). Furthermore, the fervor with which some researchers value one animal model over another can make it difficult to determine which model is best-suited for a given study. This led us to ask: What can we learn by leveraging these models against one another? The answer: we could see what factors (mechanism, rate, or lateralization of dopamine loss) are most influential in maintaining basal ganglia function and thus motor function. The unexpected outcome was that across models, canonical basal ganglia output developed stereotyped pathophysiology that onset early in disease progression prior to the onset of motor deficits.

With as little as ~15% dopamine loss, we saw a drastic decrease in the firing rates of SNr neurons. Although decreases in firing rate are contradictory to the classic rate model of the basal ganglia (DeLong, 1990), this effect was consistent across all depletion models used in our study

and with findings of other groups (Delaville et al., 2012; MacLeod et al., 1990; Murer et al., 1997; Rohlf's et al., 1997; Seeger-Armbruster and Von Ameln-Mayerhofer, 2013; Tseng et al., 2005). This decrease in firing rate may be explained by the presence of type 3 canonical transient receptor potential (TRPC3) channels on mouse SNr projection neurons. In particular, a previous study showed that SNc dopamine release tonically excites SNr neurons via D<sub>1</sub> – D<sub>5</sub> receptor coactivation that enhances tonically active TRPC3 channels (Zhou et al., 2009). Therefore, when dopamine release is reduced, TRPC3 channel activation is likely also reduced causing a decrease in firing frequency and increase in firing irregularity, similar to what is seen when these channels are pharmacologically inhibited (Zhou et al., 2008). While firing rates were abruptly reduced at early stages of dopamine loss, firing pattern changes such as irregularity and bursting seemed to gradually increase at more moderate stages of dopamine loss (~40%). Finally, synchronous firing patterns emerged only at end stages of 6-OHDA depletion models.

Interestingly, the time-course of these pathological features was highly conserved in both the gradual 6-OHDA dopamine depletion model and the PFF  $\alpha$ -Syn model. While these models both result in a progressive dopamine depletion, this loss is achieved through different mechanisms over different time courses and result in different motor deficits. Thus, it is surprising to see remarkably similar pathophysiology at comparable time points. We also found that the severity of pathophysiology in the SNr of mice was similar across many variations of dopamine depletion models, including the rapid bilateral acute 6-OHDA model, as well as the chronic unilateral 6-OHDA model. Our results further validate that end-stage pathophysiology, at least within canonical basal ganglia output, is similar regardless of time during depletion, time post depletion, or bilateral vs. unilateral exposure.

Based on these results, moderate SNr pathophysiology is present prior to the onset of motor deficits and was not very predictive of symptomatic severity. What other circuits could be involved in preserving motor function in prodromal PD? One possibility is the other output nuclei of the basal ganglia. In human and non-human primates, the output nuclei of the basal ganglia consist of the SNr and the internal segment of the globus pallidus (GPi). In this study, we focused our attention on the properties of neurons located in the SNr rather than the rodent homolog of the GPi, the entopeduncular nucleus (EPN), mainly due to the difference in projection targets. SNr likely serves a greater role in motor control in rodents as it sends canonical inhibitory projections to brainstem motor nuclei and thalamus (Oh et al., 2014), whereas cell populations in the EPN have been shown to send glutamatergic inputs to the lateral habenula (Wallace et al., 2017), suggesting a greater role in limbic processing. Another possibility is that intermediary nuclei, such as the external globus pallidus (GPe) or subthalamic nucleus (STN), within the basal ganglia are playing a greater role in influencing other motor circuits. Anatomical studies have shown that GPe and STN projections are not limited to downstream basal ganglia output. GPe projects to areas of the thalamus, amygdala, parasubthalamic nucleus, and cortex (Hazrati and Parent, 1991; Mastro et al., 2014), while STN projects to areas of the thalamus, frontal cortex, substantia innominata, pedunculopontine tegmental nucleus, dorsal raphe nucleus, and pontine reticular formation (Jackson and Crossman, 1981a, 1981b; Kita and Kitai, 1987; Rico et al., 2010). Additionally, recent studies have unveiled a disynaptic projection from the STN to the cerebellum (Bostan et al., 2010; Jwair et al., 2017) and it has been shown that therapeutic STN-deep brain stimulation in parkinsonian rats results in increased activity in cerebellar nuclei (Sutton et al., 2015). This finding, along with other studies looking at different activity patterns in human PD patients (Bezard et al., 2003; Rascol et al.,

1997; Wu and Hallett, 2005, 2013; Yu et al., 2007), highlights the possibility that motor circuits outside the basal ganglia, such as the cerebellum and supplementary motor area, may also be contributing to the preservation of motor function.

Many suspect a hierarchy of compensation is involved in the preservation of movement until late stages of dopamine loss. First up are dopamine-related mechanisms, followed by non-dopamine-mediated mechanisms within the basal ganglia, and finally mechanisms outside the basal ganglia (Bezard et al., 2010). What remains unclear are the exact thresholds of the transitions between each of these families of compensatory mechanisms and how they relate to the appearance of Parkinsonian motor abnormalities. Our results combine awake in vivo physiology with two types of progressive depletion models and show that basal ganglia output progresses through three distinct physiological states: normal, moderate pathophysiology, and severe pathophysiology. Additionally, transitions between these states depend on the amount, but not rate or mechanism of dopamine depletion. No single physiological parameter predicted the onset of motor deficits, but analysis of the relationship between parameters revealed that the transition from asymptomatic to symptomatic was accompanied by a sharp increase in the interaction of other parameters with synchrony. These findings suggest that regardless of the time course of method of depletion, compensatory mechanisms within the basal ganglia become overwhelmed at end-stages of dopamine loss.

### 3.5 ACKNOWLEDGEMENTS

The authors would like to thank Jennifer Thomas (Seton Hill University) for her assistance with behavioral scoring and data analysis, and Xiaobo Mao and Ted Dawson (John Hopkins University School of Medicine) for their collaboration and supply of mouse  $\alpha$ -synuclein pre-formed fibrils. This work was supported by National Institutes of Health Grants F31 NS093944 (A.M.W.), F31 NS090745 (K.J.M.), and R00 NS076524, NSF grant DMS 1516288, and grants from the Brain and Behavior Research Foundation (National Alliance for Research on Schizophrenia and Depression Young Investigator Grant), the Parkinson's Disease Foundation, and the NIH Intramural Research Program.

## 4.0 SUMMARY AND CONCLUSIONS

Through the combination of developing improved animal models and interrogating how and when pathophysiology develops during the course of PD, we are starting to get a clearer picture of the underlying mechanisms of the disease. As discussed in the introduction, the wide range of animal models available and the quest to explore new ways to recover motor function have greatly enhanced our understanding of remarkable reorganization that occurs in the brain following dopamine neurodegeneration. Here, we developed a novel paradigm for modeling progressive dopamine loss and used this paradigm in addition to other well-studied animal models of PD to investigate how and when basal ganglia activity changes in PD.

In Chapter 2, we inject multiple bilateral low doses of the neurotoxin 6-OHDA over time to better recapitulate the slow progression of the dopamine loss seen in PD. This model displayed a monotonic decrease in striatal dopamine levels that resulted in the differential degradation of motor symptoms. While spontaneous horizontal movement remained robust until late stages of dopamine loss, spontaneous vertical movement in the form of rearing declined linearly as a function of dopamine loss. Interestingly, we found that motor coordination assessed via the pole task was preserved in gradually depleted animals whereas animals that underwent an acute depletion in only a few days displayed significant deficits. This study established a gradual depletion paradigm that provides an experimental platform to study changes at various stages of dopamine loss, while modeling the progressive degeneration in PD so as not to preclude any compensatory plasticity that may be missing in more acute depletion models.

The role of the basal ganglia in the onset of motor deficits in PD is still poorly understood (Galvan and Wichmann, 2008). Therefore, we assessed the onset and progression of

pathophysiology in the output nucleus of the basal ganglia using a number of animal models of PD. We performed in vivo electrophysiological recordings in the SNr of awake animals at various stages of dopamine loss induced by different methods at rates ranging from 3-6 months to determine which pathological features contributed to the onset of motor dysfunction. As shown in Chapter 3, we observed a stereotyped, hierarchical progression of pathophysiology in the SNr. Specifically, firing rate changes occurred first at early stages of dopamine loss, followed by changes in firing pattern at more intermediate stages. No single physiological parameter predicted the onset of motor deficits, but analysis of the relationship between parameters revealed that the transition from asymptomatic to symptomatic was accompanied by a sharp increase in the interaction of other parameters with synchrony. Furthermore, onset and progression of pathophysiology was highly consistent across various models, suggesting that the amount of dopamine determines the degree of pathology, rather than the rate or mechanism of depletion. These results provide the first quantitative analysis of the trajectory with which basal ganglia output physiology breaks down over the course of progressive dopamine depletion.

Taken together, these results demonstrate the complex interplay between the onset and progression of various motor deficits and pathological basal ganglia activity. The main goal of this discussion is two-fold: 1) discuss the future of developing improved animal models of PD and 2) provide possible avenues for developing new therapeutic strategies based on what we currently know about the prodromal phase of PD. Though animal models of PD and theoretical models of basal ganglia circuitry have their limitations and caveats, they provide us with a great framework through which to study how the basal ganglia contributes to motor function and dysfunction in health and disease.

## **4.1 THE PATH TO A BETTER PARKINSON MODEL**

In the last few decades, the increasing array of animal models of PD has led every researcher to ask: which is the best? Unfortunately, there is no simple answer and choosing a model for a particular study requires careful consideration of the validity, benefits, and limitations of the current options. Animal models have allowed us to make considerable progress in understanding the biochemical, molecular, and physiological changes associated with late-stage PD. However, there is still a lot we do not understand about the pathology of disease progression and the physiological changes leading up to the onset of motor symptoms. In recent years, this knowledge gap has inspired the redesign of classic models in addition to the development of new models. The goal of the following section is to highlight some of the promising new avenues for future development of better animal models of PD. PD is characterized as a chronic progressive neurodegenerative disorder that is likely a result of a combination of multiple genetic and environmental factors. The latest development of new animal models involves those that recapitulate the progressive nature of PD, and those that blend methodology to better capture the complex pathology of PD.

### **4.1.1 Progressive models**

The degeneration of dopamine neurons in PD occurs over a number of years prior to the onset of motor deficits. Until recently, estimates based on postmortem analysis of brain tissue and striatal dopamine imaging suggested a 5-6 year preclinical or prodromal period (Fearnley and Lees, 1991; Hilker et al., 2005; Morrish et al., 1996, 1998). Studies of Lewy body pathology in other

areas of the brain as well as epidemiologic studies of non-motor symptoms suggest that the preclinical period may extend 20 years prior to the onset of motor dysfunction (Savica et al., 2010). Animal models that better simulate this slow disease progression are needed to study this extensive prodromal period, the transition to symptomatic PD, and test potential neuroprotective strategies.

One strategy used to study various stages of dopamine loss involves altering the delivery of traditional neurotoxins. 6-OHDA has been used to model earlier stages of PD by administering lower doses to produce various degrees of dopamine loss in rats (Truong et al., 2006). Other studies have reported that injecting 6-OHDA directly into the striatum results in a more progressive degeneration of dopamine neurons (Fleming et al., 2005; Przedborski et al., 1995; Sauer and Oertel, 1994). As discussed in Chapter 2, we demonstrated that injecting multiple small doses of 6-OHDA into the medial forebrain bundle of the same mouse over 15-49 days also provided us with the opportunity to study various stages of dopamine loss while allowing for the full engagement of potential compensatory mechanisms that may occur during chronic progressive dopamine degeneration (Willard et al., 2015). More recently, a similar strategy has been developed for rats, with daily intraventricular administration of 6-OHDA over 6-32 days (Quiroga-Varela et al., 2017). Repeated systemic injections of the MPTP in rodents has been less successful, however this treatment in non-human primates has been used to study the development of motor and non-motor symptoms (Fox and Brotchie, 2010). Another promising model involves daily intraperitoneal injections of the pesticide rotenone in rats. This resulted in ~50% loss of striatal dopamine and was accompanied by postural and rearing deficits after 6-10 days. This model is highly reproducible and, unlike 6-OHDA and MPTP models,

results in the presence of  $\alpha$ -synuclein aggregates (Cannon et al., 2009). The time course of this model is still very rapid but may be a promising tool for testing neuroprotective interventions.

As mentioned in Chapter 1, most current genetic models of PD typically do not undergo significant dopamine neurodegeneration and lack motor deficits, thereby limiting their usefulness in the study of disease progression. One promising genetic model was developed by selectively inactivating a mitochondrial transcription factor in dopamine neurons. These ‘MitoPark’ mice show adult onset neurodegeneration and progressive behavioral deficits over the course of 30 weeks and are responsive to L-DOPA treatments (Ekstrand and Galter, 2009). However, this model fails to display  $\alpha$ -synuclein pathology and involves the manipulation of a gene that has not been implicated in the human disease (Beal, 2010; Ekstrand and Galter, 2009; Ekstrand et al., 2007).

#### **4.1.2 Fusion models**

PD is likely the result of a combination of various environmental and genetic factors. One interesting new avenue of modeling PD in animals involves the ‘fusion’ of different existing models to simulate the synergy between environmental insult and genetic risk factors that may be responsible for the human condition (Manning-Boğ and Langston, 2007). Given that transgenic models fail to replicate dopamine neurodegeneration, researchers have explored the effects of exposing transgenic models to neurotoxins. In these studies, mice over-expressing  $\alpha$ -synuclein are administered systemic doses of MPTP and the degree to which dopamine degeneration is achieved is analyzed. One study showed no difference in the degree of degeneration between transgenic animals and littermate controls in two different lines of  $\alpha$ -synuclein over-expressing

mice (Rathke-Hartlieb et al., 2001). However, three additional studies in mice over-expressing either wild-type or mutant versions of the human  $\alpha$ -synuclein protein, reported increased sensitivity to MPTP (Nieto et al., 2006; Richfield et al., 2002; Song et al., 2004). These results have been further supported by studies done in transgenic mouse lines where  $\alpha$ -synuclein expression is deficient and animals were either partially or fully resistant to the degenerative effects of MPTP (Dauer et al., 2002; Drolet et al., 2004; Klivenyi et al., 2006; Schlüter et al., 2003). Further investigations of the interaction between genetic mutations and susceptibility to environmental toxins may unveil new targets for neuroprotective strategies.

An intriguing new study induces neurodegeneration in a transgenic  $\alpha$ -synuclein mouse through the manipulation of endogenous dopamine levels. Researchers injected a mutant form of the catalytic enzyme tyrosine hydroxylase into the SNc of transgenic  $\alpha$ -synuclein mice to increase endogenous dopamine production. This led to a progressive degeneration of dopamine neurons 5 months post injection with a detectable decrease in ambulatory activity (Mor et al., 2017). These findings highlight the importance of investigating the interactions between dopamine and  $\alpha$ -synuclein and how they contribute to disease progression. Overall, we are continuing to learn more about PD disease progression, the vulnerability of dopamine neurons, and the important interactions between genetic and environmental risk factors through the creative repurposing of new and old animal models of PD.

## 4.2 PHYSIOLOGICAL CORRELATES OF MOTOR DYSFUNCTION

While we have made great progress in understanding the pathophysiology present at the late stages of PD, very little is known about the process by which these circuits transition from a healthy to symptomatic state. In PD, motor symptoms typically do not present until dopamine levels have been reduced by 70-80%. Clinically, this means that patients who seek medical help at the onset of motor symptoms have likely been living with chronically low levels of dopamine for years. It has been proposed that this early, pre-symptomatic phase of PD, called the prodromal phase, is an ideal time to begin therapies (Olanow and Obeso, 2012). However, very little is known about the circuit changes occurring during these early stages of the disease, and when the pathophysiological changes associated with the late stages of the disease arise. Identifying the physiological changes that occur at the onset of motor deficits, or the physiological changes that are corrected when motor symptoms are alleviated, could help us identify which changes are most responsible for movement dysfunction and provide us with new targets for therapeutic strategies. These questions are of critical importance because intervening at earlier stages of the disease, before widespread circuit dysfunction has occurred, may allow us to slow or stop its progression.

We found that pathophysiology in the basal ganglia output followed a biphasic progression based on the relationship between a number of different physiological parameters during the transition from healthy to late-stage depletion. The following section will explore, in greater detail, the potential mechanisms through which basal ganglia output develops pathological activity patterns, how current treatments rescue basal ganglia output physiology,

and highlight other studies of the physiological changes accompanying the transition from asymptomatic to symptomatic.

#### **4.2.1 Influencers of basal ganglia output physiology**

In Chapter 3, we explored the question of when pathophysiology develops in the output nuclei of the basal ganglia and described a hierarchical series of changes that occur during the progression of dopamine loss resulting in two distinct physiological states: prodromal and end-stage. One question that remains is how pathophysiology in the output nuclei develops. Is this pathological activity simply imposed upon the output nuclei from upstream basal ganglia nuclei? If so, which nucleus exerts the most influence? Or do features develop due to changes intrinsic to the output nuclei? Determining the source of these pathological activity patterns may provide us with insight into how to intervene prior to symptom onset as well as additional therapeutic targets for recovering motor dysfunction.

The basal ganglia output nuclei (GPi/SNr) primarily receive input from the striatum via the direct pathway, GPe, and STN (Fig. 4.1). As mentioned in Chapter 1, chronic dopamine depletion significantly alters the activity patterns of neurons throughout the basal ganglia by increasing burst firing and synchrony (Bergman et al., 1994; Fillion and Tremblay, 1991; Galvan and Wichmann, 2008; Hutchison et al., 1994; Neumann et al., 2016; Raz et al., 2000; Singh et al., 2016; Wichmann and Soares, 2006). Given our current understanding of how basal ganglia circuitry is altered in parkinsonian conditions, it is likely that the STN plays the greatest role in influencing output nuclei activity (Fig 4.1 A). The STN has been hypothesized to play a key role in the generation and propagation of pathological synchrony due to its mutual excitatory-

inhibitory connections to the GPe (Bevan et al., 2002). Studies have also implicated STN as a potential propagator of burst firing in the basal ganglia. Recordings from STN neurons in *ex vivo* brain slices of dopamine depleted animals showed the generation of large bursts of excitatory postsynaptic currents in response to a single stimulation of its afferents in the internal capsule. These bursts reverberated several times in the absence of additional stimulation and this bursting activity was propagated to GPe neurons (Ammari et al., 2011). This phenomena can be attributed to recurrent excitation resulting from STN neurons innervation of neighboring STN neurons and has been shown to also drive burst spike in SNr neurons (Ammari et al., 2010; Shen and Johnson, 2006). In dopamine depleted animals, lesions of the STN led to more regular firing patterns in SNr neurons (Burbaud et al., 1995; Murer et al., 1997). Additionally it has been shown that therapeutic STN deep brain stimulation reduces bursting in the GPi and SNr (Hahn et al., 2008; Maltête et al., 2007). These results suggest that STN may play a role in the development of synchrony and burst firing in the output nuclei of the basal ganglia under conditions of dopamine depletion.

The output nuclei are also influenced by inhibitory projections from the striatum via the direct pathway and the GPe (Fig. 4.1 B, C). Increased synchrony and bursting has been observed in the striatum (Raz et al., 2001; Singh et al., 2016). In particular, blockade of dopamine D1-type receptors typically associated with neurons projecting directly to output nuclei have been shown to increase synchrony within the striatum (Burkhardt et al., 2009). Convergent synchronous inhibitory inputs from the striatum onto tonically active output nuclei neurons could result in synchronized pausing and subsequent rebound bursting activity. However, in a dopamine depleted state, the excitability of striatal neurons projecting through the direct pathway to cortical stimulation becomes diminished (Mallet et al., 2006). This suggests that influence of the direct

pathway is likely not the primary influencer of output activity. Striatal neurons that project to the GPe through the indirect pathway display enhanced excitability to cortical drive in dopamine depleted conditions, suggesting that they play a larger role in shaping downstream activity (Mallet et al., 2006). Given the increased coupling of STN-GPe activity in dopamine depleted states (Fan et al., 2012), it is possible that bursting and synchrony in basal ganglia output may be enhanced by inhibitory GPe inputs. It has been shown that therapeutic GPe deep brain stimulation reduces bursting in the GPi (Vitek et al., 2012), although GPe deep brain stimulation likely also impacts STN firing patterns, making it difficult to ascertain the influence of the GPe inputs alone.

A final possible source of pathological activity in output nuclei neurons are intrinsic changes related to the loss of dopamine signaling (Fig. 4.1 D). Recordings from SNr neurons in isolated brain slices from dopamine depleted rats or under acute dopamine blockade displayed increased bursting behavior (Aceves et al., 2011), possibly due to an upregulation of rebound HCN3-mediated currents (Meurers et al., 2009). Additionally in humans, it has been shown that effective GPi-DBS also reduced GPi burst firing (Cleary et al., 2013), although this was not found in MPTP-treated monkeys (McCairn and Turner, 2009). These results suggest that intrinsic changes in SNr neurons may be partially responsible for the increased burst firing present in dopamine depleted conditions, although it is more likely that synchronous excitatory (STN) and inhibitory (striatum and GPe) inputs have a greater control over shaping firing patterns in an intact network.

To determine which of these sources plays the greatest role in shaping activity patterns in the basal ganglia output, future experiments should attempt imposing distinct activity patterns through optogenetic activation or inhibition while recording in both the influencing nucleus and

the output nucleus in dopamine depleted conditions. If imposed patterns are reflected downstream in output nuclei, further investigation of these synapses in *ex vivo* brain slices may help identify plasticity that facilitates transfer of pathological activity within the basal ganglia.

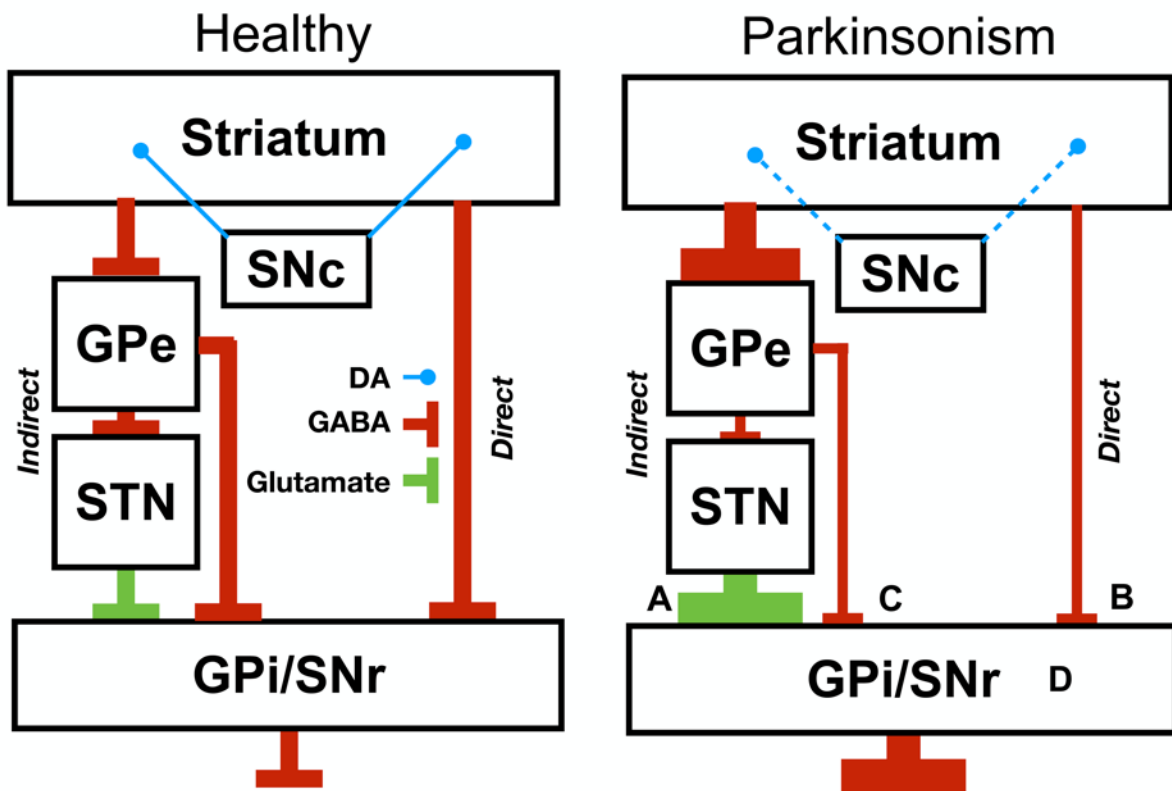


**Figure 4.1. Propagation of pathophysiology in the basal ganglia in Parkinsonian conditions.** Weight of green (excitatory) and red (inhibitory) lines indicate the presumed activity of each connection. (A) The influence of the subthalamic nucleus (STN) on the activity in the output nuclei. (B) The influence of the striatum on the activity in the output nuclei. (C) The influence of the globus pallidus externa (GPe) on the activity in the output nuclei. (D) Intrinsic changes influence on the activity in the output nuclei. SNc, substantia nigra pars compacta; GPI, globus pallidus interna; SNr, substantia nigra pars reticulata.

#### 4.2.2 Current treatments and their effect on physiology

Currently, the main treatment goal for patients with PD is minimizing debilitating motor symptoms. Drug treatment with L-DOPA and surgical intervention with DBS remain the gold standards in improving motor function (Fasano et al., 2012; Nagatsua and Sawadab, 2009).

While these treatments have been in practice for many decades, their respective mechanisms of action are still not fully understood (Obeso et al., 2017). Investigation into which pathological features these treatments restore may help us pinpoint those most responsible for motor dysfunction and aid in the design of more targeted treatments with fewer side effects and complications.

One of the first studies looking at the effects of L-DOPA on basal ganglia physiology was in MPTP-treated monkeys. Following MPTP treatment, they reported a predicted decrease in firing rate in the GPe and increase in firing rate in the GPi. In the GPe there was a slight increase in burst firing, while in the GPi there was a considerable increase in burst firing. Administration of L-DOPA normalized firing rate in the GPe and reduced firing rate in the GPi below that seen in controls. However, L-DOPA had no effect on the burst firing in GPe and only slightly decreased burst firing in the GPi (Boraud et al., 1998). Another study in MPTP-treated monkeys reported that L-DOPA reduced firing rates in the SNr but did not have any effect on burst firing (Gilmour et al., 2011). In humans, recordings performed through deep brain stimulation electrode implanted in patients revealed that L-DOPA administration prevented abnormal fluctuations in  $\beta$  oscillations in the STN and GPi during movement preparation, execution, and recovery (Priori et al., 2002). These results suggest that L-DOPA administration

is effective at restoring firing rate and may play a role in normalizing oscillatory activity but is ineffective at restoring normal firing patterns.

Early treatments for PD included surgical ablation of basal ganglia targets including the STN and GPi. Following the development and use of DBS to treat tremor, groups began pioneering the use of high-frequency stimulation as an alternative to irreversible lesions (Obeso et al., 2017). It was originally thought that high-frequency stimulation through DBS worked by inhibiting the target brain area, producing a similar effect as a lesion (Bergman et al., 1990; Limousin et al., 1995; Siegfried and Lippitz, 1994). However, studies of the effects of DBS on basal ganglia physiology have revealed that it has a far more complex impact on neural activity. Results from GPi-stimulation in humans showed changes in both firing rate and firing pattern, with a net decrease in overall activity in the GPi. DBS also entrained neuronal firing in complex patterns thereby disrupting pathological firing patterns (Cleary et al., 2013). Other reports of therapeutically effective DBS have shown paradoxical increases in the firing rate of GPi neurons, suggesting that firing rate changes may not be the primary therapeutic mechanism of DBS (Hahn et al., 2008; Hashimoto et al., 2003). Far more consistent, are reports detailing reductions in pathological firing patterns and reduced oscillatory and synchronous activity (Hahn et al., 2008; Hashimoto et al., 2003; McConnell et al., 2012).

While we are still in the process of understanding the mechanisms through which L-DOPA and DBS mediate their respective therapeutic effects, it is becoming clear that there is no one pathophysiological feature that must be manipulated to relieve motor dysfunction in PD. This is consistent with our findings from Chapter 3 that no one parameter could predict motor deficits, however interactions between various parameters and synchrony seemed to correlate

with motor dysfunction. These results suggest that there are various mechanisms through which motor function can be restored.

### **4.2.3 Prodromal pathophysiology in Parkinson's disease**

Clinical studies have provided supporting evidence for the existence of a prodromal period of PD, where patients experience a variety of nonmotor symptoms prior to the onset of classic motor symptoms (Pont-Sunyer et al., 2015; Schrag et al., 2015). In fact, it has been shown in a number of population studies that olfactory dysfunction, constipation, depression, and REM sleep disturbances are associated with a greater risk for developing PD in otherwise healthy subjects (Berg et al., 2015; Postuma et al., 2012, 2015; Ross et al., 2008; Savica et al., 2009; Shiba et al., 2000). However, many of these symptoms are also associated with a number of other disorders as well as normal ageing and therefore are largely unhelpful as diagnostic criteria. Due in large part to our inability to identify patients with PD prior to the development of overt motor symptoms, studies of prodromal pathophysiology in PD are largely limited to animal models. Additionally, the most commonly used animal models employ a neurotoxin to mimic the late stages of the disease and bypass the intermediary prodromal phases.

The few studies detailing physiological changes during the progression of dopamine loss mainly utilize the non-human primate MPTP model that involves systemic daily low-dose injection with behavioral assessment to delineate the transition to symptomatic PD. While this model has several advantages, such as being able to track physiology in an individual animal over time, there are a number of limitations as well. These studies involve very few animals with a high degree of variability between animals. Post-hoc analysis can reveal the total extent of

dopamine loss at the end of treatment, but it is unclear what level of dopamine is depleted following each dose in a given animal. While toxin doses are spread out to more gradually deplete dopamine, clinical symptoms still onset quite rapidly after only 15-20 days which is still an incredibly short amount of time in the lifespan of a monkey. Additionally, only subsets of individual physiological parameters are measured and the relationship between parameters is rarely explored.

One of the first studies to explore the gradual modification of physiology in the basal ganglia was in 1999 by Bezard and colleagues. They performed multiunit recordings in the STN, GPe, and GPi of two MPTP-treated monkeys over the course of 25 days. They found that mean firing rates of the STN and GPi became elevated two days prior to the onset of clinical symptoms, while firing rates in the GPe remained stable throughout the entire protocol (Bezard et al., 1999). In 2007, Leblois et al reported no changes in GPi firing rates over the course of MPTP dopamine depletion. They did observe an increase in burst firing patterns, synchrony, and oscillations but not until after the appearance of motor symptoms (Leblois et al., 2007). A more recent study attempted to correlate physiological parameters in the GPe and GPi of individual animals to their respective degree of motor deficits throughout progressive MPTP-treatment. While they did report changes in firing rate, burst firing, and oscillatory activity, their relationship to the severity of motor deficits was inconsistent and varied significantly across the three animals included in the study (Muralidharan et al., 2016).

Currently, there is sparse information available regarding electrophysiological changes in prodromal PD. The inconsistent and highly variable results from these studies highlight the need for developing a standard set of measurable physiological parameters and studying the relationship between them, rather than looking at any one parameter in isolation. The pathology

and symptoms seen in patients with idiopathic PD is heterogenous and likely reflects a complex interplay of pathological activity developing across a vast network of brain areas. Therefore, it is unsurprising that studies looking at individual parameters across a small set of animals reveal a high degree of variability. Rather than attempting to identify a single culprit responsible for the onset of motor deficits, future studies should focus on distinguishing an overall physiological state associated with motor dysfunction and design ways to disrupt or prevent it.

### **4.3 FINAL REMARKS**

In conclusion, the progression of pathophysiology in PD is complex. PD is an extremely heterogeneous disorder with a highly variable and wide-range of clinical features and disease progression. Isolating the underlying mechanisms that will provide the most therapeutic benefits for patients will require extensive study of many existing animal models of PD as well as the development of new and better models. Our first contribution was the development of a novel dopamine depletion paradigm that better recapitulates the progressive degeneration of dopamine. This paradigm provides an opportunity to study the various stages of dopamine loss including mechanisms of plasticity that may only be employed when dopamine loss occurs gradually. This model will be used in future studies to unveil the multifaceted reorganization that occurs during dopamine degeneration as well as test the most beneficial times to begin various therapies.

Our second contribution focused on exploring the onset and progression of dysfunction in the basal ganglia during the course of progressive dopamine loss. This study provides the first evidence for a biphasic transition from healthy physiology to severe pathophysiology in the SNr. These results suggest that the transition prodromal to symptomatic PD involves a complex array

of behavioral and physiological changes that warrant further investigation. Our data identify interactions between neural synchrony and rate and pattern changes as a potential predictor of motor symptom onset. Moving forward, mapping this trajectory in individual animals as well as in other brain areas at rest and during periods of movement will provide great benefit to understanding the underlying mechanisms of disease progression and identifying new ways to intervene and treat PD.

## APPENDIX A

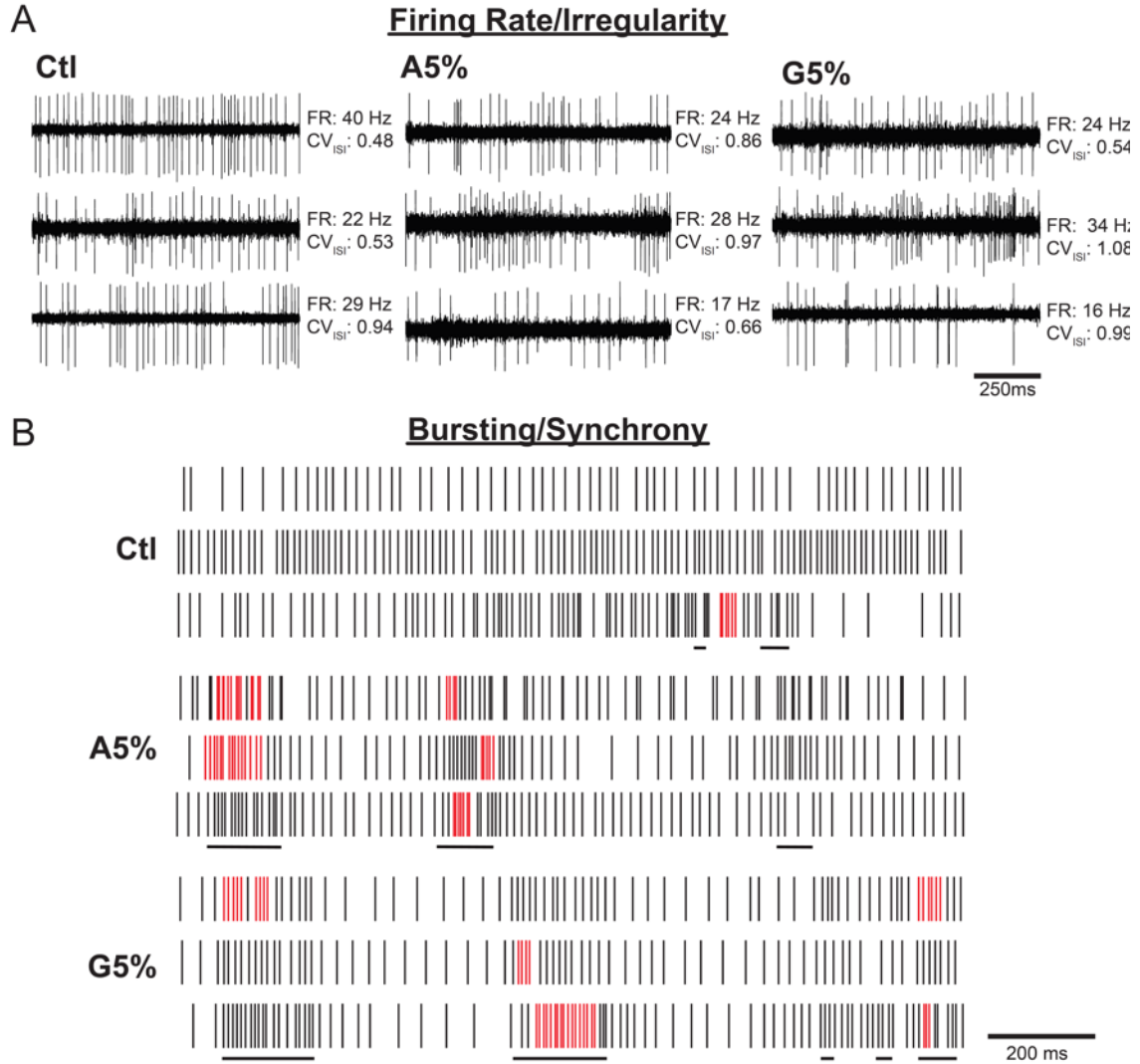


**Figure A1. SNr pathophysiology in bilateral 6-OHDA dopamine depletions.** (A) Three single-unit example traces from Ctl, Acute, and Gradual conditions showing firing rate and irregularity in firing pattern. (B) Three single-unit example rasters from Ctl, Acute, and Gradual conditions showing bursts identified from the Poisson Surprise Burst analysis in red (see Methods, bursts had to contain > 4 spikes) and bouts of high synchrony between simultaneously recorded units in black.

## BIBLIOGRAPHY

- Aceves, J. de J., Rueda-Orozco, P.E., Hernández, R., Plata, V., Ibañez-Sandoval, O., Galarraga, E., and Vargas, J. (2011). Dopaminergic Presynaptic Modulation of Nigral Afferents: Its Role in the Generation of Recurrent Bursting in Substantia Nigra Pars Reticulata Neurons. *Front. Syst. Neurosci.* 5.
- Albin, R.L., Young, A.B., and Penney, J.B. (1989). The functional anatomy of basal ganglia disorders. *Trends Neurosci.* 12, 366–375.
- Alexander, G.E., and Crutcher, M.D. (1990). Functional architecture of basal ganglia circuits: neural substrates of parallel processing. *Trends Neurosci.* 13, 266–271.
- Alexander, G.E., DeLong, M.R., and Strick, P.L. (1986). Parallel Organization of Functionally Segregated Circuits Linking Basal Ganglia and Cortex. *Annu. Rev. Neurosci.* 9, 357–381.
- Alexander, G.E., Crutcher, M.D., and DeLong, M.R. (1990). Basal ganglia-thalamocortical circuits: parallel substrates for motor, oculomotor, “prefrontal” and “limbic” functions. *Prog. Brain Res.* 85, 119–146.
- Ammari, R., Lopez, C., Bioulac, B., Garcia, L., and Hammond, C. (2010). Subthalamic nucleus evokes similar long lasting glutamatergic excitations in pallidal, entopeduncular and nigral neurons in the basal ganglia slice. *Neuroscience* 166, 808–818.
- Ammari, R., Bioulac, B., Garcia, L., and Hammond, C. (2011). The Subthalamic Nucleus becomes a Generator of Bursts in the Dopamine-Depleted State. Its High Frequency Stimulation Dramatically Weakens Transmission to the Globus Pallidus. *Front. Syst. Neurosci.* 5.
- Aziz, T.Z., Peggs, D., Agarwal, E., Sambrook, M.A., and Crossman, A.R. (1992). Subthalamic nucleotomy alleviates parkinsonism in the 1-methyl-4-phenyl-1,2,3,6-tetrahydropyridine (MPTP)-exposed primate. *Br. J. Neurosurg.* 6, 575–582.
- Balcioglu, A., Zhang, K., and Tarazi, F.I. (2003). Dopamine depletion abolishes apomorphine- and amphetamine-induced increases in extracellular serotonin levels in the striatum of conscious rats: A microdialysis study. *Neuroscience* 119, 1045–1053.
- Beal, M.F. (2010). Parkinson’s disease: A model dilemma. *Nature* 466, S8–S10.
- Beilina, A., and Cookson, M.R. (2015). Genes associated with Parkinson’s disease: Regulation of autophagy and beyond. *J. Neurochem.* 139, 1–17.
- Benabid, A.L., Pollak, P., Gross, C., Hoffmann, D., Benazzouz, A., Gao, D.M., Laurent, A., Gentil, M., and Perret, J. (1994). Acute and long-term effects of subthalamic nucleus stimulation in Parkinson’s disease. *Stereotact. Funct. Neurosurg.* 62, 76–84.
- Berg, D., Postuma, R.B., Adler, C.H., Bloem, B.R., Chan, P., Dubois, B., Gasser, T., Goetz, C.G., Halliday, G., Joseph, L., et al. (2015). MDS research criteria for prodromal Parkinson’s disease. *Mov. Disord.* 30, 1600–1611.
- Bergman, H., Wichmann, T., and DeLong, M.R. (1990). Reversal of experimental parkinsonism by lesions of the subthalamic nucleus. *Science* (80-. ). 249, 1436–1438.
- Bergman, H., Wichmann, T., Karmon, B., and DeLong, M.R. (1994). The primate

- subthalamic nucleus. II. Neuronal activity in the MPTP model of parkinsonism. *J. Neurophysiol.* 72, 507–520.
- Bernheimer, H., Birkmayer, W., Hornykiewicz, O., Jellinger, K., and Seitelberger, F. (1973). Brain dopamine and the syndromes of Parkinson and Huntington Clinical, morphological and neurochemical correlations. *J. Neurol. Sci.* 20, 415–455.
- Betarbet, R., Sherer, T.B., Timothy Greenamyre, J., and Greenamyre, J.T. (2002). Animal models of Parkinson’s disease. *Bioessays* 24, 308–318.
- Bevan, M.D., Magill, P.J., Terman, D., Bolam, J.P., and Wilson, C.J. (2002). Move to the rhythm: Oscillations in the subthalamic nucleus-external globus pallidus network. *Trends Neurosci.* 25, 525–531.
- Bezard, E., and Gross, C.E. (1998). Compensatory mechanisms in experimental and human parkinsonism: Towards a dynamic approach. *Prog. Neurobiol.* 55, 93–116.
- Bezard, E., Dovero, S., Bioulac, B., and Gross, C.E. (1997a). Kinetics of nigral degeneration in a chronic model of MPTP-treated mice. *Neurosci. Lett.* 234, 47–50.
- Bezard, E., Boraud, T., Bioulac, B., and Gross, C.E. (1997b). Compensatory effects of glutamatergic inputs to the substantia nigra pars compacta in experimental Parkinsonism. *Neuroscience* 81, 399–404.
- Bezard, E., Boraud, T., Bioulac, B., and Gross, C.E. (1999). Involvement of the subthalamic nucleus in glutamatergic compensatory mechanisms. *Eur. J. Neurosci.* 11, 2167–2170.
- Bezard, E., Gross, C.E., and Brotchie, J.M. (2003). Presymptomatic compensation in Parkinson’s disease is not dopamine-mediated. *Trends Neurosci.* 26, 215–221.
- Bezard, E., Gross, C.E., Parkinsonism, H., Bezard, E., Porras, G., Blesa, J., and Obeso, J.A. (2010). Compensatory mechanisms in Experimental and Compensatory Mechanisms in Experimental and Human Parkinsonism : Potential for New Therapies. *Prog. Neurobiol.* 55, 93–116.
- Björklund, A., and Dunnett, S.B. (2007). Dopamine neuron systems in the brain: an update. *Trends Neurosci.* 30, 194–202.
- Blesa, J., Juri, C., Collantes, M., Peñuelas, I., Prieto, E., Iglesias, E., Martí-Climent, J., Arbizu, J., Zubieta, J.L., Rodríguez-Oroz, M.C., et al. (2010). Progression of dopaminergic depletion in a model of MPTP-induced Parkinsonism in non-human primates. An 18F-DOPA and 11C-DTBZ PET study. *Neurobiol. Dis.* 38, 456–463.
- Blesa, J., Phani, S., Jackson-Lewis, V., and Przedborski, S. (2012). Classic and new animal models of Parkinson’s disease. *J. Biomed. Biotechnol.* 2012.
- Blume, S.R., Cass, D.K., and Tseng, K.Y. (2009). Stepping test in mice: A reliable approach in determining forelimb akinesia in MPTP-induced Parkinsonism. *Exp. Neurol.* 219, 208–211.
- Bolam, J.P., Hanley, J.J., Booth, P.A.C., and Bevan, M.D. (2000). Synaptic organisation of the basal ganglia. *J. Anat.* 196, 527–542.
- Bonito-Oliva, A., Masini, D., and Fisone, G. (2014). A mouse model of non-motor symptoms in Parkinson’s disease: focus on pharmacological interventions targeting affective dysfunctions. *Front. Behav. Neurosci.* 8.
- Boraud, T., Bezard, E., Guehl, D., Bioulac, B., and Gross, C. (1998). Effects of L-DOPA on neuronal activity of the globus pallidus externalis (GPe) and globus pallidus internalis (GPi) in the MPTP-treated monkey. *Brain Res.* 787, 157–160.

- Bostan, A.C., and Strick, P.L. (2010). The cerebellum and basal ganglia are interconnected. *Neuropsychol. Rev.* *20*, 261–270.
- Bostan, A.C., Dum, R.P., and Strick, P.L. (2010). The basal ganglia communicate with the cerebellum. *Proc. Natl. Acad. Sci.* *107*, 8452–8456.
- Bové, J., Prou, D., Perier, C., and Przedborski, S. (2005). Toxin-induced models of Parkinson's disease. *NeuroRx* *2*, 484–494.
- Breese, G., Baumeister, A.A., McCown, Thomas, J., Emerick, Susan, G., Frye, Gerald, D., Crotty, K., and Mueller, Robert, A. (1984). Behavioral differences between neonatal and adult 6-hydroxydopamine-treated rats to dopamine agonists: relevance to neurological symptoms in clinical syndromes with reduced brain dopamine. *J. Pharmacol. Exp. Ther.* *231*, 343–354.
- Brooks, D.J. (1999). Functional imaging of Parkinson's disease: is it possible to detect brain areas for specific symptoms? *J. Neural Transm. Suppl.* *56*, 139–153.
- Brooks, S.P., and Dunnett, S.B. (2009). Tests to assess motor phenotype in mice: A user's guide. *Nat. Rev. Neurosci.* *10*, 519–529.
- Brotchie, J., and Fitzer-Attas, C. (2009). Mechanisms compensating for dopamine loss in early Parkinson disease. *Neurology* *72*.
- Burbaud, P., Gross, C., Benazzouz, A., Coussemaq, M., and Bioulac, B. (1995). Reduction of apomorphine-induced rotational behaviour by subthalamic lesion in 6-OHDA lesioned rats is associated with a normalization of firing rate and discharge pattern of pars reticulata neurons. *Exp. Brain Res.* *105*, 48–58.
- Burkhardt, J.M., Jin, X., and Costa, R.M. (2009). Dissociable effects of dopamine on neuronal firing rate and synchrony in the dorsal striatum. *Front. Integr. Neurosci.* *3*.
- Campos, F.L., Carvalho, M.M., Cristovão, A.C., Je, G., Baltazar, G., Salgado, A.J., Kim, Y.-S., and Sousa, N. (2013). Rodent models of Parkinson's disease: beyond the motor symptomatology. *Front. Behav. Neurosci.* *7*, 75.
- Cannon, J.R., Tapias, V., Na, H.M., Honick, A.S., Drolet, R.E., and Greenamyre, J.T. (2009). A highly reproducible rotenone model of Parkinson's disease. *Neurobiol. Dis.* *34*, 279–290.
- Carlsson, A., Lindqvist, M., and Magnusson, T. (1957). 3,4-Dihydroxyphenylalanine and 5-hydroxytryptophan as reserpine antagonists [16]. *Nature* *180*, 1200.
- Carta, M., Lindgren, H.S., Lundblad, M., Stancampiano, R., Fadda, F., and Cenci, M.A. (2006). Role of striatal L-DOPA in the production of dyskinesia in 6-hydroxydopamine lesioned rats. *J. Neurochem.* *96*, 1718–1727.
- Cenci, M., and Lindgren, H. (2007). Advances in understanding l-DOPA-induced dyskinesia. *Curr. Opin. Neurobiol.* *17*, 665–671.
- Chesselet, M.-F., and Richter, F. (2011). Modelling of Parkinson's disease in mice. *Lancet Neurol.* *10*, 1108–1118.
- Chesselet, M.-F., Fleming, S., Mortazavi, F., and Meurers, B. (2008). Strengths and limitations of genetic mouse models of Parkinson's disease. *Parkinsonism Relat. Disord.* *14*, S84–S87.
- Chu, H.Y., McIver, E.L., Kovaleski, R.F., Atherton, J.F., and Bevan, M.D. (2017). Loss of Hyperdirect Pathway Cortico-Subthalamic Inputs Following Degeneration of Midbrain Dopamine Neurons. *Neuron* *95*, 1306–1318.e5.
- Cleary, D.R., Raslan, A.M., Rubin, J.E., Bahgat, D., Viswanathan, A., Heinricher, M.M.,

- and Burchiel, K.J. (2013). Deep brain stimulation entrains local neuronal firing in human globus pallidus internus. *J. Neurophysiol.* *109*, 978–987.
- Commins, D.L., Shaughnessy, R.A., Axt, K.J., Vosmer, G., and Seiden, L.S. (1989). Variability among brain regions in the specificity of 6-hydroxydopamine (6-OHDA)-induced lesions. *J. Neural Transm.* *77*, 197–210.
- Credle, J.J., George, J.L., Wills, J., Duka, V., Shah, K., Lee, Y.C., Rodriguez, O., Simkins, T., Winter, M., Moechars, D., et al. (2015). GSK-3 $\beta$  dysregulation contributes to parkinson's-like pathophysiology with associated region-specific phosphorylation and accumulation of tau and  $\alpha$ -synuclein. *Cell Death Differ.* *22*, 838–851.
- Damier, P., Hirsch, E.C., Agid, Y., and Graybiel, A.M. (1999). The substantia nigra of the human brain II. Patterns of loss of dopamine-containing neurons in Parkinson's disease. *Brain* *122*, 1437–1448.
- Date, I., Felten, D.L., and Felten, S.Y. (1990). Long-term effect of MPTP in the mouse brain in relation to aging: neurochemical and immunocytochemical analysis. *Brain Res.* *519*, 266–276.
- Dauer, W., and Przedborski, S. (2003). Parkinson's Disease: Mechanisms and Models. *Neuron* *39*, 889–909.
- Dauer, W., Kholodilov, N., Vila, M., Trillat, A.-C., Goodchild, R., Larsen, K.E., Staal, R., Tieu, K., Schmitz, Y., Yuan, C.A., et al. (2002). Resistance of alpha-synuclein null mice to the parkinsonian neurotoxin MPTP. *Proc. Natl. Acad. Sci.* *99*, 14524–14529.
- Dawson, T., Ko, H., and Dawson, V. (2010). Genetic Animal Models of Parkinson's Disease. *Neuron* *66*, 646–661.
- Day, M., Wang, Z., Ding, J., An, X., Ingham, C.A., Shering, A.F., Wokosin, D., Ilijic, E., Sun, Z., Sampson, A.R., et al. (2006). Selective elimination of glutamatergic synapses on striatopallidal neurons in Parkinson disease models. *Nat. Neurosci.* *9*, 251–259.
- Debaere, F., Swinnen, S.P., Beatse, E., Sunaert, S., Van Hecke, P., and Duysens, J. (2001). Brain areas involved in interlimb coordination: a distributed network. *Neuroimage* *14*, 947–958.
- Decressac, M., Mattsson, B., and Bjorklund, A. (2012a). Comparison of the behavioural and histological characteristics of the 6-OHDA and alpha-synuclein rat models of Parkinson's disease. *Exp Neurol* *235*, 306–315.
- Decressac, M., Mattsson, B., Lundblad, M., Weikop, P., and Björklund, A. (2012b). Progressive neurodegenerative and behavioural changes induced by AAV-mediated overexpression of  $\alpha$ -synuclein in midbrain dopamine neurons. *Neurobiol. Dis.* *45*, 939–953.
- Dehay, B., and Fernagut, P.-O. (2016). Alpha-synuclein-based models of Parkinson's disease. *Rev. Neurol. (Paris)*. *172*, 371–378.
- Delaville, C., Navailles, S., and Benazzouz, A. (2012). Effects of noradrenaline and serotonin depletions on the neuronal activity of globus pallidus and substantia nigra pars reticulata in experimental parkinsonism. *Neuroscience* *202*, 424–433.
- DeLong, M.R. (1983). The neurophysiologic basis of abnormal movements in basal ganglia disorders. *Neurobehav Toxicol Teratol* *5*, 611–616.
- DeLong, M.R. (1990). Primate models of movement disorders of basal ganglia origin.

- Trends Neurosci. *13*, 281–285.
- DeLong, M.R., and Wichmann, T. (2007). Circuits and circuit disorders of the basal ganglia. *Arch. Neurol.* *64*, 20–24.
- Desplats, P., Lee, H.J., Bae, E.J., Patrick, C., Rockenstein, E., Crews, L., Spencer, B., Masliah, E., and Lee, S.J. (2009). Inclusion formation and neuronal cell death through neuron-to-neuron transmission of  $\alpha$ -synuclein. *Proc. Natl. Acad. Sci.* *106*, 13010–13015.
- Deumens, R., Blokland, A., and Prickaerts, J. (2002). Modeling Parkinson's disease in rats: An evaluation of 6-OHDA lesions of the nigrostriatal pathway. *Exp. Neurol.* *175*, 303–317.
- Dickson, D.W., Braak, H., Duda, J.E., Duyckaerts, C., Gasser, T., Halliday, G.M., Hardy, J., Leverenz, J.B., Del Tredici, K., Wszolek, Z.K., et al. (2009). Neuropathological assessment of Parkinson's disease: refining the diagnostic criteria. *Lancet Neurol.* *8*, 1150–1157.
- Drago, J., Gerfen, C.R., Lachowicz, J.E., Steiner, H., Hollon, T.R., Love, P.E., Ooi, G.T., Grinberg, A., Lee, E.J., and Huang, S.P. (1994). Altered striatal function in a mutant mouse lacking D1A dopamine receptors. *Proc. Natl. Acad. Sci. U. S. A.* *91*, 12564–12568.
- Drolet, R.E., Behrouz, B., Lookingland, K.J., and Goudreau, J.L. (2004). Mice lacking  $\alpha$ -synuclein have an attenuated loss of striatal dopamine following prolonged chronic MPTP administration. *Neurotoxicology* *25*, 761–769.
- Duty, S., and Jenner, P. (2011). Animal models of Parkinson's disease: A source of novel treatments and clues to the cause of the disease. *Br. J. Pharmacol.* *164*, 1357–1391.
- Ekstrand, M.I., and Galter, D. (2009). The MitoPark Mouse - An animal model of Parkinson's disease with impaired respiratory chain function in dopamine neurons. *Park. Relat. Disord.* *15*, S185–S188.
- Ekstrand, M.I., Terzioglu, M., Galter, D., Zhu, S., Hofstetter, C., Lindqvist, E., Thams, S., Bergstrand, A., Hansson, F.S., Trifunovic, A., et al. (2007). Progressive parkinsonism in mice with respiratory-chain-deficient dopamine neurons. *Proc. Natl. Acad. Sci.* *104*, 1325–1330.
- Escande, M. V., Taravini, I.R.E., Zold, C.L., Belforte, J.E., and Murer, M.G. (2016). Loss of Homeostasis in the Direct Pathway in a Mouse Model of Asymptomatic Parkinson's Disease. *J. Neurosci.* *36*, 5686–5698.
- Fahn, S. (2003). Description of Parkinson's Disease as a Clinical Syndrome. *Ann. N. Y. Acad. Sci.* *991*, 1–14.
- Fahn, S. (2015). The medical treatment of Parkinson disease from James Parkinson to George Cotzias. *Mov. Disord.* *30*, 4–18.
- Fan, K.Y., Baufreton, J., Surmeier, D.J., Chan, C.S., and Bevan, M.D. (2012). Proliferation of External Globus Pallidus-Subthalamic Nucleus Synapses following Degeneration of Midbrain Dopamine Neurons. *J. Neurosci.* *32*, 13718–13728.
- Fasano, A., Daniele, A., and Albanese, A. (2012). Treatment of motor and non-motor features of Parkinson's disease with deep brain stimulation. *Lancet Neurol.* *11*, 429–442.
- Fearnley, J.M., and Lees, A.J. (1991). Ageing and parkinson's disease: Substantia nigra

- regional selectivity. *Brain* 114, 2283–2301.
- Fernagut, P.O., Chalon, S., Diguet, E., Guilloteau, D., Tison, F., and Jaber, M. (2003). Motor behaviour deficits and their histopathological and functional correlates in the nigrostriatal system of dopamine transporter knockout mice. *Neuroscience* 116, 1123–1130.
- Ferro, M.M., Bellissimo, M.I., Anselmo-Franci, J.A., Angellucci, M.E.M., Canteras, N.S., and Da Cunha, C. (2005). Comparison of bilaterally 6-OHDA- and MPTP-lesioned rats as models of the early phase of Parkinson’s disease: Histological, neurochemical, motor and memory alterations. *J. Neurosci. Methods* 148, 78–87.
- Fieblinger, T., Graves, S.M., Sebel, L.E., Alcacer, C., Plotkin, J.L., Gertler, T.S., Chan, C.S., Heiman, M., Greengard, P., Cenci, M.A., et al. (2014). Cell type-specific plasticity of striatal projection neurons in parkinsonism and L-DOPA-induced dyskinesia. *Nat. Commun.* 5.
- Filion, M., and Tremblay, L. (1991). Abnormal spontaneous activity of globus pallidus neurons in monkeys with MPTP-induced parkinsonism. *Brain Res.* 547, 142–151.
- Fleming, S.M., Salcedo, J., Fernagut, P.-O.P.O., Rockenstein, E., Masliah, E., Levine, M.S.M.S., and Chesselet, M.F.M.-F. (2004). Early and Progressive Sensorimotor Anomalies in Mice Overexpressing Wild-Type Human Alpha-Synuclein. *J. Neurosci.* 24, 9434–9440.
- Fleming, S.M., Delville, Y., and Schallert, T. (2005). An intermittent, controlled-rate, slow progressive degeneration model of Parkinson’s disease: Antiparkinson effects of Sinemet and protective effects of methylphenidate. *Behav. Brain Res.* 156, 201–213.
- Fleming, S.M., Salcedo, J., Hutson, C.B., Rockenstein, E., Masliah, E., Levine, M.S., and Chesselet, M.F. (2006). Behavioral effects of dopaminergic agonists in transgenic mice overexpressing human wildtype alpha-synuclein. *Neuroscience* 142, 1245–1253.
- Fox, S.H., and Brotchie, J.M. (2010). The MPTP-lesioned non-human primate models of Parkinson’s disease. Past, present, and future. *Prog. Brain Res.* 184, 133–157.
- Francardo, V. (2018). Modeling Parkinson’s disease and treatment complications in rodents: Potentials and pitfalls of the current options. *Behav. Brain Res.*
- Frechilla, D., Cobreros, A., Saldise, L., Moratalla, R., Insausti, R., Luquin, M.R., and Del Ro, J. (2001). Serotonin 5-HT(1A) receptor expression is selectively enhanced in the striosomal compartment of chronic Parkinsonian monkeys. *Synapse* 39, 288–296.
- Fuller, H.R., Hurtado, M.L., Wishart, T.M., and Gates, M.A. (2014). The rat striatum responds to nigro-striatal degeneration via the increased expression of proteins associated with growth and regeneration of neuronal circuitry. *Proteome Sci.* 12.
- Galvan, A., and Wichmann, T. (2007). GABAergic circuits in the basal ganglia and movement disorders. *Prog. Brain Res.* 160, 287–312.
- Galvan, A., and Wichmann, T. (2008). Pathophysiology of Parkinsonism. *Clin. Neurophysiol.* 119, 1459–1474.
- Gelb, D.J., Oliver, E., and Gilman, S. (1999). Diagnostic criteria for Parkinson disease. *Arch. Neurol.* 56, 33–39.
- Gerfen, C.R., and Surmeier, D.J. (2011). Modulation of Striatal Projection Systems by Dopamine. *Annu. Rev. Neurosci.* 34, 441–466.

- Gibb, W.R.G., and Lees, A.J. (1988). The relevance of the Lewy body to the pathogenesis of idiopathic Parkinson's disease. *J. Neurol. Neurosurg. Psychiatry* *51*, 745–752.
- Gilmour, T.P., Lieu, C.A., Nolt, M.J., Piallat, B., Deogaonkar, M., and Subramanian, T. (2011). The effects of chronic levodopa treatments on the neuronal firing properties of the subthalamic nucleus and substantia nigra reticulata in hemiparkinsonian rhesus monkeys. *Exp. Neurol.* *228*, 53–58.
- Giráldez-Pérez, R., Antolín-Vallespín, M., Muñoz, M., and Sánchez-Capelo, A. (2014). Models of alpha-synuclein aggregation in Parkinson's disease. *Acta Neuropathol. Commun.* *2*, 176.
- Gittis, A.H., Hang, G.B., LaDow, E.S., Shoenfeld, L.R., Atallah, B. V., Finkbeiner, S., and Kreitzer, A.C. (2011). Rapid target-specific remodeling of fast-spiking inhibitory circuits after loss of dopamine. *Neuron* *71*, 858–868.
- Goldberg, N.R.S., Haack, A.K., Lim, N.S., Janson, O.K., and Meshul, C.K. (2011). Dopaminergic and behavioral correlates of progressive lesioning of the nigrostriatal pathway with 1-methyl-4-phenyl-1,2,3,6-tetrahydropyridine. *Neuroscience* *180*, 256–271.
- Goldberg, N.R.S., Fields, V., Pflibsen, L., Salvatore, M.F., and Meshul, C.K. (2012). Social enrichment attenuates nigrostriatal lesioning and reverses motor impairment in a progressive 1-methyl-2-phenyl-1,2,3,6-tetrahydropyridine (MPTP) mouse model of Parkinson's disease. *Neurobiol. Dis.* *45*, 1051–1067.
- Graybiel, A.M., Aosaki, T., Flaherty, A.W., and Kimura, M. (1994). The basal ganglia and adaptive motor control. *Science* (80-. ). *265*, 1826–1831.
- Greenamyre, J.T., Betarbet, R., and Sherer, T.B. (2003). The rotenone model of Parkinson's disease: genes, environment and mitochondria. *Parkinsonism Relat. Disord.* *9*, 59–64.
- Guridi, J., and Alegre, M. (2017). Oscillatory activity in the basal ganglia and deep brain stimulation. *Mov. Disord.* *32*, 64–69.
- Guridi, J., Herrero, M.T., Luquin, R., Guillen, J., and Obeso, J.A. (1994). Subthalamotomy improves MPTP-Induced parkinsonism in monkeys. *Stereotact. Funct. Neurosurg.* *62*, 98–102.
- Hahn, P.J., Russo, G.S., Hashimoto, T., Miocinovic, S., Xu, W., McIntyre, C.C., and Vitek, J.L. (2008). Pallidal burst activity during therapeutic deep brain stimulation. *Exp. Neurol.* *211*, 243–251.
- Hammond, C., Bergman, H., and Brown, P. (2007). Pathological synchronization in Parkinson's disease: networks, models and treatments. *Trends Neurosci.* *30*, 357–364.
- Hashimoto, T., Elder, C.M., Okun, M.S., Patrick, S.K., and Vitek, J.L. (2003). Stimulation of the subthalamic nucleus changes the firing pattern of pallidal neurons. *J. Neurosci.* *23*, 1916–1923.
- Hazrati, L.N., and Parent, A. (1991). Projection from the external pallidum to the reticular thalamic nucleus in the squirrel monkey. *Brain Res.* *550*, 142–146.
- Heimer, G., Bar-Gad, I., Goldberg, J.A., and Bergman, H. (2002). Dopamine replacement therapy reverses abnormal synchronization of pallidal neurons in the 1-methyl-4-phenyl-1,2,3,6-tetrahydropyridine primate model of parkinsonism. *J. Neurosci.* *22*, 7850–7855.

- Hickey, M.A., Kosmalska, A., Enayati, J., Cohen, R., Zeitlin, S., Levine, M.S., and Chesselet, M.F. (2008). Extensive early motor and non-motor behavioral deficits are followed by striatal neuronal loss in knock-in Huntington's disease mice. *Neuroscience* 157, 280–295.
- Hilker, R., Schweitzer, K., Coburger, S., Ghaemi, M., Weisenbach, S., Jacobs, A.H., Rudolf, J., Herholz, K., and Heiss, W.D. (2005). Nonlinear progression of Parkinson disease as determined by serial positron emission tomographic imaging of striatal fluorodopa F 18 activity. *Arch. Neurol.* 62, 378–382.
- Hisahara, S., and Shimohama, S. (2010). Toxin-induced and genetic animal models of Parkinson's disease. *Parkinsons. Dis.* 2011, 951709.
- Hoehn, M.M., and Yahr, M.D. (1967). Parkinsonism : onset, progression, and mortality. *Neurology* 17, 427–442.
- Huang, C., Tang, C., Feigin, A., Lesser, M., Ma, Y., Pourfar, M., Dhawan, V., and Eidelberg, D. (2007). Changes in network activity with the progression of Parkinson's disease. *Brain* 130, 1834–1846.
- Hughes, A.J., Daniel, S.E., Kilford, L., and Lees, A.J. (1992). Accuracy of clinical diagnosis of idiopathic Parkinson's disease: A clinico-pathological study of 100 cases. *J. Neurol. Neurosurg. Psychiatry* 55, 181–184.
- Hutchison, W.D., Lozano, A.M., Davis, K.D., Saint-Cyr, J.A., Lang, A.E., and Dostrovsky, J.O. (1994). Differential neuronal activity in segments of globus pallidus in parkinson's disease patients. *Neuroreport* 5, 1533–1537.
- Iancu, R., Mohapel, P., Brundin, P., and Paul, G. (2005). Behavioral characterization of a unilateral 6-OHDA-lesion model of Parkinson's disease in mice. *Behav. Brain Res.* 162, 1–10.
- Iderberg, H., Francardo, V., and Pioli, E.Y. (2012). Animal models of l-DOPA–induced dyskinesia: an update on the current options. *Neuroscience* 211, 13–27.
- Jackson-Lewis, V., and Przedborski, S. (2007). Protocol for the MPTP mouse model of Parkinson's disease. *Nat. Protoc.* 2, 141–151.
- Jackson, A., and Crossman, A.R. (1981a). Subthalamic nucleus efferent projection to the cerebral cortex. *Neuroscience* 6.
- Jackson, A., and Crossman, A.R. (1981b). Subthalamic projection to nucleus tegmenti pedunculopontinus in the rat. *Neurosci. Lett.* 22, 17–22.
- Jeon, B.S., Jackson-Lewis, V., and Burke, R.E. (1995). 6-Hydroxydopamine lesion of the rat substantia nigra: time course and morphology of cell death. *Neurodegeneration* 4, 131–137.
- Jicha, G. a, and Salamone, J.D. (1991). Vacuous jaw movements and feeding deficits in rats with ventrolateral striatal dopamine depletion: possible relation to parkinsonian symptoms. *J. Neurosci.* 11, 3822–3829.
- Johannessen, J.N., Chiueh, C.C., Burns, R.S., and Markey, S.P. (1985). IV. Differences in the metabolism of MPTP in the rodent and primate parallel differences in sensitivity to its neurotoxic effects. *Life Sci.* 36, 219–224.
- Jwair, S., Coulon, P., and Ruigrok, T.J.H. (2017). Disynaptic Subthalamic Input to the Posterior Cerebellum in Rat. *Front. Neuroanat.* 11.
- Karstaedt, P.J., Kerasidis, H., Pincus, J.H., Meloni, R., Graham, J., and Gale, K. (1994). Unilateral destruction of dopamine pathways increases ipsilateral striatal serotonin turnover in rats. *Exp. Neurol.* 126, 25–30.

- Kelly, R.M., and Strick, P.L. (2004). Macro-architecture of basal ganglia loops with the cerebral cortex: use of rabies virus to reveal multisynaptic circuits. *Prog. Brain Res.* *143*, 449–459.
- Kirik, D., Rosenblad, C., and Björklund, A. (1998). Characterization of behavioral and neurodegenerative changes following partial lesions of the nigrostriatal dopamine system induced by intrastriatal 6-hydroxydopamine in the rat. *Exp. Neurol.* *152*, 259–277.
- Kita, H., and Kitai, S. (1987). Efferent projections of the subthalamic nucleus in the rat: light and electron microscopic analysis with the PHA-L method. *J. Comp. Neurol.* *260*, 435–452.
- Klivenyi, P., Siwek, D., Gardian, G., Yang, L., Starkov, A., Cleren, C., Ferrante, R.J., Kowall, N.W., Abeliovich, A., and Beal, M.F. (2006). Mice lacking alpha-synuclein are resistant to mitochondrial toxins. *Neurobiol. Dis.* *21*, 541–548.
- Kordower, J.H., Chu, Y., Hauser, R.A., Freeman, T.B., and Olanow, C.W. (2008). Lewy body-like pathology in long-term embryonic nigral transplants in Parkinson's disease. *Nat. Med.* *14*, 504–506.
- Kravitz, A. V., Freeze, B.S., Parker, P.R.L., Kay, K., Thwin, M.T., Deisseroth, K., and Kreitzer, A.C. (2010). Regulation of parkinsonian motor behaviours by optogenetic control of basal ganglia circuitry. *Nature* *466*, 622–626.
- Kreiner, G. (2015). Compensatory mechanisms in genetic models of neurodegeneration: are the mice better than humans? *Front. Cell. Neurosci.* *9*, 1–6.
- Kreitzer, A.C., and Malenka, R.C. (2007). Endocannabinoid-mediated rescue of striatal LTD and motor deficits in Parkinson's disease models. *Nature* *445*, 643–647.
- Kühn, A.A., Trottenberg, T., Kivi, A., Kupsch, A., Schneider, G.-H., and Brown, P. (2005). The relationship between local field potential and neuronal discharge in the subthalamic nucleus of patients with Parkinson's disease. *Spec. Issue Neuronal Oscil. Mov. Disord.* *194*, 212–220.
- Kumaran, R., and Cookson, M.R. (2015). Pathways to Parkinsonism Redux: Convergent pathobiological mechanisms in genetics of Parkinson's disease. *Hum. Mol. Genet.* *24*, R32–R44.
- Laitinen, L. V, Bergenheim, A.T., and Hariz, M.I. (1992). Leksell's posteroventral pallidotomy in the treatment of Parkinson's disease. *J Neurosurg* *76*, 53–61.
- Langston, J., Ballard, P., Tetrud, J., and Irwin, I. (1983). Chronic Parkinsonism in humans due to a product of meperidine-analog synthesis. *Science (80- )*. *219*, 979–980.
- de Lau, L.M.L., Breteler, M.M.B., Greenamyre, J., Hastings, T., Litvan, I., Bhatia, K., Burn, D., al., et, Rijk, M. de, Rocca, W., et al. (2006). Epidemiology of Parkinson's disease. *Lancet. Neurol.* *5*, 525–535.
- Lavoie, B., Smith, Y., and Parent, A. (1989). Dopaminergic innervation of the basal ganglia in the squirrel monkey as revealed by tyrosine hydroxylase immunohistochemistry. *J. Comp. Neurol.* *289*, 36–52.
- Leblois, A., Meissner, W., Bioulac, B., Gross, C.E., Hansel, D., and Boraud, T. (2007). Late emergence of synchronized oscillatory activity in the pallidum during progressive parkinsonism. *Eur. J. Neurosci.* *26*, 1701–1713.
- Lees, A.J., Tolosa, E., and Olanow, C.W. (2015). Four pioneers of L-dopa treatment: Arvid Carlsson, Oleh Hornykiewicz, George Cotzias, and Melvin Yahr. *Mov.*

- Disord. 30, 19–36.
- Limousin, P., Pollak, P., Benazzouz, a, Hoffmann, D., Le Bas, J.F., Broussolle, E., Perret, J.E., and Benabid, a L. (1995). Effect of parkinsonian signs and symptoms of bilateral subthalamic nucleus stimulation. *Lancet* 345, 91–95.
- Lindgren, H.S., Lelos, M.J., and Dunnett, S.B. (2012). Do alpha-synuclein vector injections provide a better model of Parkinson’s disease than the classic 6-hydroxydopamine model? *Exp. Neurol.* 237, 36–42.
- Little, S., and Brown, P. (2014). Focusing brain therapeutic interventions in space and time for Parkinson’s disease. *Curr. Biol.* 24, R898–R909.
- Lobb, C.J., and Jaeger, D. (2015a). Bursting activity of substantia nigra pars reticulata neurons in mouse parkinsonism in awake and anesthetized states. *Neurobiol. Dis.* 75, 177–185.
- Lobb, C.J., and Jaeger, D. (2015b). Bursting activity of substantia nigra pars reticulata neurons in mouse parkinsonism in awake and anesthetized states. *Neurobiol. Dis.* 75, 177–185.
- Lobb, C.J., Zaheer, A.K., Smith, Y., and Jaeger, D. (2013). In vivo electrophysiology of nigral and thalamic neurons in alpha-synuclein-overexpressing mice highlights differences from toxin-based models of parkinsonism. *J. Neurophysiol.* 110, 2792–2805.
- Luk, K.C., Kehm, V., Carroll, J., Zhang, B., Brien, P.O., Trojanowski, J.Q., and Lee, V.M. (2012). Pathological Alpha-Synuclein Transmission Initiates Parkinson-like Neurodegeneration in Nontransgenic Mice. *Science* (80-. ). 338, 949–954.
- Lundblad, M., Decressac, M., Mattsson, B., and Bjorklund, A. (2012). Impaired neurotransmission caused by overexpression of alpha-synuclein in nigral dopamine neurons. *Proc. Natl. Acad. Sci.* 109, 3213–3219.
- MacLeod, N.K., Ryman, A., and Arbutnott, G.W. (1990). Electrophysiological properties of nigrothalamic neurons after 6-hydroxydopamine lesions in the rat. *Neuroscience* 38, 447–456.
- Mallet, N., Ballion, B., Le Moine, C., and Gonon, F. (2006). Cortical Inputs and GABA Interneurons Imbalance Projection Neurons in the Striatum of Parkinsonian Rats. *J. Neurosci.* 26, 3875–3884.
- Mallet, N., Pogosyan, A., Marton, L.F., Bolam, J.P., Brown, P., and Magill, P.J. (2008). Parkinsonian Beta Oscillations in the External Globus Pallidus and Their Relationship with Subthalamic Nucleus Activity. *J. Neurosci.* 28, 14245–14258.
- Maltête, D., Jodoin, N., Karachi, C., Houeto, J.L., Navarro, S., Cornu, P., Agid, Y., and Welter, M.L. (2007). Subthalamic stimulation and neuronal activity in the substantia nigra in Parkinson’s disease. *J. Neurophysiol.* 97, 4017–4022.
- Maneuf, Y.P., Mitchell, I.J., Crossman, A.R., and Brotchiel, J.M. (1994). On the role of enkephalin cotransmission in the GABAergic striatal efferents to the globus pallidus. *Exp. Neurol.* 125, 65–71.
- Manning-Bog, A.B., and Langston, J.W. (2007). Model fusion: The next phase in developing animal models for Parkinson’s disease. *Neurotox. Res.* 11, 219–240.
- Mao, X., Ou, M.T., Karuppagounder, S.S., Kam, T.I., Yin, X., Xiong, Y., Ge, P., Umanah, G.E., Brahmachari, S., Shin, J.H., et al. (2016). Pathological  $\alpha$ -synuclein transmission initiated by binding lymphocyte-activation gene 3. *Science* (80-. ). 353.

- Marsden, C.D., and Obeso, J.A. (1994). The functions of the basal ganglia and the paradox of stereotaxic surgery in parkinson's disease. *Brain* *117*, 877–897.
- Mastro, K.J., Bouchard, R.S., Holt, H.A.K., and Gittis, A.H. (2014). Transgenic Mouse Lines Subdivide External Segment of the Globus Pallidus (GPe) Neurons and Reveal Distinct GPe Output Pathways. *J. Neurosci.* *34*, 2087–2099.
- Mastro, K.J., Zitelli, K.T., Willard, A.M., Leblanc, K.H., Kravitz, A.V., and Gittis, A.H. (2017). Cell-specific pallidal intervention induces long-lasting motor recovery in dopamine-depleted mice. *Nat. Neurosci.* *20*.
- Matsuura, K., Kabuto, H., Makino, H., and Ogawa, N. (1997). Pole test is a useful method for evaluating the mouse movement disorder caused by striatal dopamine depletion. *J. Neurosci. Methods* *73*, 45–48.
- McCairn, K.W., and Turner, R.S. (2009). Deep Brain Stimulation of the Globus Pallidus Internus in the Parkinsonian Primate: Local Entrainment and Suppression of Low-Frequency Oscillations. *J. Neurophysiol.* *101*, 1941–1960.
- McConnell, G.C., So, R.Q., Hilliard, J.D., Lopomo, P., and Grill, W.M. (2012). Effective Deep Brain Stimulation Suppresses Low-Frequency Network Oscillations in the Basal Ganglia by Regularizing Neural Firing Patterns. *J. Neurosci.* *32*, 15657–15668.
- McNaught, K.S.P., Perl, D.P., Brownell, A.L., and Olanow, C.W. (2004). Systemic exposure to proteasome inhibitors causes a progressive model of Parkinson's disease. *Ann. Neurol.* *56*, 149–162.
- Meredith, G.E., and Kang, U.J. (2006). Behavioral models of Parkinson's disease in rodents: a new look at an old problem. *Mov Disord* *21*, 1595–1606.
- Meredith, G.E., and Rademacher, D.J. (2011). MPTP mouse models of Parkinson's disease: An update. *J. Parkinsons. Dis.* *1*, 19–33.
- Meredith, G.E., Totterdell, S., Petroske, E., Santa Cruz, K., Callison, R.C., and Lau, Y.S. (2002). Lysosomal malfunction accompanies alpha-synuclein aggregation in a progressive mouse model of Parkinson's disease. *Brain Res.* *956*, 156–165.
- Meredith, G.E., Sonsalla, P.K., and Chesselet, M.-F. (2008a). Animal models of Parkinson's disease progression. *Acta Neuropathol.* *115*, 385–398.
- Meredith, G.E., Sonsalla, P.K., and Chesselet, M.-F. (2008b). Animal models of Parkinson's disease progression. *Acta Neuropathol.* *115*, 385–398.
- Meurers, B.H., Dziejczapolski, G., Bittner, A., Shi, T., Kamme, F., and Shults, C.W. (2009). Dopamine depletion induced up-regulation of HCN3 enhances rebound excitability of basal ganglia output neurons. *Neurobiol. Dis.* *34*, 178–188.
- Middleton, F.A., and Strick, P.L. (2000). Basal ganglia and cerebellar loops: Motor and cognitive circuits. In *Brain Research Reviews*, pp. 236–250.
- Miller, D.B., Ali, S.F., O'Callaghan, J.P., and Laws, S.C. (1998). The impact of gender and estrogen on striatal dopaminergic neurotoxicity. In *Annals of the New York Academy of Sciences*, pp. 153–165.
- Mink, J.W. (1996). The basal ganglia: Focused selection and inhibition of competing motor programs. *Prog. Neurobiol.* *50*, 381–425.
- Mitsumoto, Y., Watanabe, A., Mori, A., and Koga, N. (1998). Spontaneous regeneration of nigrostriatal dopaminergic neurons in MPTP-treated C57BL/6 mice. *Biochem. Biophys. Res. Commun.* *248*, 660–663.
- Mor, D.E., Tsika, E., Mazzulli, J.R., Gould, N.S., Kim, H., Daniels, M.J., Doshi, S.,

- Gupta, P., Grossman, J.L., Tan, V.X., et al. (2017). Dopamine induces soluble  $\alpha$ -synuclein oligomers and nigrostriatal degeneration. *Nat. Neurosci.* *20*, 1560–1568.
- Morrish, P.K., Sawle, G. V., and Brooks, D.J. (1996). An [18F]dopa-PET and clinical study of the rate of progression in Parkinson's disease. *Brain* *119* ( Pt 2), 585–591.
- Morrish, P.K., Rakshi, J.S., Bailey, D.L., Sawle, G. V., and Brooks, D.J. (1998). Measuring the rate of progression and estimating the preclinical period of Parkinson's disease with [18F] dopa PET. *J. Neurol. Neurosurg. Psychiatry* *64*, 314–319.
- Mullin, S., and Schapira, A. (2015). The genetics of Parkinson's disease. *Br. Med. Bull.* 1–14.
- Muralidharan, A., Jensen, A.L., Connolly, A., Hendrix, C.M., Johnson, M.D., Baker, K.B., and Vitek, J.L. (2016). Physiological changes in the pallidum in a progressive model of Parkinson's disease: Are oscillations enough? *Exp. Neurol.* *279*, 187–196.
- Murer, M.G., Riquelme, L.A., Tseng, K.Y., and Pazo, J.H. (1997). Substantia nigra pars reticulata single unit activity in normal and 60HDA-lesioned rats: Effects of intra-striatal apomorphine and subthalamic lesions. *Synapse* *27*, 278–293.
- Nagatsua, T., and Sawadab, M. (2009). L-dopa therapy for Parkinson's disease: past, present, and future. *Parkinsonism Relat. Disord.* *15 Suppl 1*, S3-8.
- Nelson, A.B., and Kreitzer, A.C. (2014). Reassessing Models of Basal Ganglia Function and Dysfunction. *Annu. Rev. Neurosci.* *37*, 117–135.
- Neumann, W.-J., Degen, K., Schneider, G.-H., Brücke, C., Huebl, J., Brown, P., and Kühn, A.A. (2016). Subthalamic synchronized oscillatory activity correlates with motor impairment in patients with Parkinson's disease. *Mov. Disord.* *31*, 1748–1751.
- Nieto, M., Gil-Bea, F.J., Dalfó, E., Cuadrado, M., Cabodevilla, F., Sánchez, B., Catena, S., Sesma, T., Ribé, E., Ferrer, I., et al. (2006). Increased sensitivity to MPTP in human alpha-synuclein A30P transgenic mice. *Neurobiol. Aging* *27*, 848–856.
- Obeso, J.A., Olanow, C.W., and Nutt, J.G. (2000). Levodopa motor complications in Parkinson's disease. *Trends Neurosci.* *23*.
- Obeso, J.A., Stamelou, M., Goetz, C.G., Poewe, W., Lang, A.E., Weintraub, D., Burn, D., Halliday, G.M., Bezard, E., Przedborski, S., et al. (2017). Past, present, and future of Parkinson's disease: A special essay on the 200th Anniversary of the Shaking Palsy. *Mov. Disord.* *32*, 1264–1310.
- Odekerken, V.J.J., Boel, J.A., Schmand, B.A., De Haan, R.J., Figuee, M., Van Den Munckhof, P., Schuurman, P.R., and De Bie, R.M.A. (2016). GPi vs STN deep brain stimulation for Parkinson disease: Three-year follow-up. *Neurology* *86*, 755–761.
- Ogawa, N., Hirose, Y., Ohara, S., Ono, T., and Watanabe, Y. (1985). A simple quantitative bradykinesia test in MPTP-treated mice. *Res Commun Chem Pathol Pharmacol* *50*, 435–441.
- Oh, S.W., Harris, J.A., Ng, L., Winslow, B., Cain, N., Mihalas, S., Wang, Q., Lau, C., Kuan, L., Henry, A.M., et al. (2014). A mesoscale connectome of the mouse brain. *Nature* *508*, 207–214.
- Olanow, C., and Tatton, W. (1999). Etiology and pathogenesis of Parkinson's disease.

- Annu. Rev. Neurosci. 27, 583–603, v.
- Olanow, C.W., and Obeso, J.A. (2012). The significance of defining preclinical or prodromal Parkinson's disease. *Mov. Disord.* 27, 666–669.
- Pan, H.S., and Walters, J.R. (1988). Unilateral lesion of the nigrostriatal pathway decreases the firing rate and alters the firing pattern of globus pallidus neurons in the rat. *Synapse* 2, 650–656.
- Parkinson, J. (2002). An essay on the shaking palsy [reprint of monograph published by Sherwood, Neely, and Jones, London, 1817]. *J. Neuropsychiatry Clin. Neurosci.* 14, 223–236.
- Penney, J.B., and Young, A.B. (1983). Speculations on the Functional Anatomy of Basal Ganglia Disorders. *Annu. Rev. Neurosci.* 6, 73–94.
- Poewe, W., Antonini, A., Zijlmans, J.C., Burkhard, P.R., and Vingerhoets, F. (2010). Levodopa in the treatment of Parkinson's disease: an old drug still going strong. *Clin. Interv. Aging* 5, 229–238.
- Polymeropoulos, M.H., Lavedan, C., Leroy, E., Ide, S.E., Dehejia, A., Dutra, A., Pike, B., Root, H., Rubenstein, J., Boyer, R., et al. (1997). Mutation in the  $\alpha$ -Synuclein Gene Identified in Families with Parkinson's Disease Mutation in the  $\alpha$ -Synuclein Gene Identified in Families with Parkinson's Disease. *Science* (80-. ). 276, 2045–2047.
- Pont-Sunyer, C., Hotter, A., Gaig, C., Seppi, K., Compta, Y., Katzenschlager, R., Mas, N., Hofeneder, D., Brücke, T., Bayés, A., et al. (2015). The Onset of Nonmotor Symptoms in Parkinson's disease (The ONSET PDStudy). *Mov. Disord.* 30, 229–237.
- Postuma, R.B., Lang, A.E., Gagnon, J.F., Pelletier, A., and Montplaisir, J.Y. (2012). How does parkinsonism start? Prodromal parkinsonism motor changes in idiopathic REM sleep behaviour disorder. *Brain* 135, 1860–1870.
- Postuma, R.B., Iranzo, A., Hogl, B., Arnulf, I., Ferini-Strambi, L., Manni, R., Miyamoto, T., Oertel, W., Dauvilliers, Y., Ju, Y. El, et al. (2015). Risk factors for neurodegeneration in idiopathic rapid eye movement sleep behavior disorder: A multicenter study. *Ann. Neurol.* 77, 830–839.
- Potashkin, J.A., Blume, S.R., and Runkle, N.K. (2010). Limitations of animal models of Parkinson's disease. *Parkinsons. Dis.* 2011, 658083.
- Priori, A., Foffani, G., Pesenti, A., Bianchi, A., Chiesa, V., Baselli, G., Caputo, E., Tamma, F., Rampini, P., Egidi, M., et al. (2002). Movement-related modulation of neural activity in human basal ganglia and its L-DOPA dependency: Recordings from deep brain stimulation electrodes in patients with Parkinson's disease. *Neurol. Sci.* 23.
- Przedborski, S., Leviver, M., Jiang, H., Ferreira, M., Jackson-Lewis, V., Donaldson, D., and Togasaki, D.M. (1995). Dose-dependent lesions of the dopaminergic nigrostriatal pathway induced by intrastriatal injection of 6-hydroxydopamine. *Neuroscience* 67, 631–647.
- Przedborski, S., Jackson-Lewis, V., Naini, A.B., Jakowec, M., Petzinger, G., Miller, R., and Akram, M. (2001). The parkinsonian toxin 1-methyl-4-phenyl-1,2,3,6-tetrahydropyridine (MPTP): A technical review of its utility and safety. *J. Neurochem.* 76, 1265–1274.
- Qiu, M.-H., Chen, M.C., Huang, Z.-L., and Lu, J. (2014). Neuronal activity (c-Fos)

- delineating interactions of the cerebral cortex and basal ganglia. *Front. Neuroanat.* 8.
- Quiroga-Varela, A., Aguilar, E., Iglesias, E., Obeso, J.A., and Marin, C. (2017). Short- and long-term effects induced by repeated 6-OHDA intraventricular administration: A new progressive and bilateral rodent model of Parkinson's disease. *Neuroscience* 361, 144–156.
- Ramnani, N., Toni, I., Passingham, R.E., and Haggard, P. (2001). The cerebellum and parietal cortex play a specific role in coordination: A pet study. *Neuroimage* 14, 899–911.
- Rascol, O., Sabatini, U., Fabre, N., Brefel, C., Loubinoux, I., Celsis, P., Senard, J.M., Montastruc, J.L., and Chollet, F. (1997). The ipsilateral cerebellar hemisphere is overactive during hand movements in akinetic parkinsonian patients. *Brain* 120, 103–110.
- Rathke-Hartlieb, S., Kahle, P.J., Neumann, M., Ozmen, L., Haid, S., Okochi, M., Haass, C., and Schulz, J.B. (2001). Sensitivity to MPTP is not increased in Parkinson's disease-associated mutant alpha-synuclein transgenic mice. *J. Neurochem.* 77, 1181–1184.
- Raz, A., Vaadia, E., and Bergman, H. (2000). Firing patterns and correlations of spontaneous discharge of pallidal neurons in the normal and the tremulous 1-methyl-4-phenyl-1,2,3,6-tetrahydropyridine vervet model of parkinsonism. *J. Neurosci.* 20, 8559–8571.
- Raz, A., Frechter-Mazar, V., Feingold, A., Abeles, M., Vaadia, E., and Bergman, H. (2001). Activity of pallidal and striatal tonically active neurons is correlated in MPTP-treated monkeys but not in normal monkeys. *J. Neurosci.* 21, RC128.
- Richfield, E.K., Thiruchelvam, M.J., Cory-Slechta, D. a, Wuertzer, C., Gainetdinov, R.R., Caron, M.G., Di Monte, D. a, and Federoff, H.J. (2002). Behavioral and neurochemical effects of wild-type and mutated human alpha-synuclein in transgenic mice. *Exp. Neurol.* 175, 35–48.
- Rico, A.J., Barroso-Chinea, P., Conte-Perales, L., Roda, E., Gómez-Bautista, V., Gendive, M., Obeso, J.A., and Lanciego, J.L. (2010). A direct projection from the subthalamic nucleus to the ventral thalamus in monkeys. *Neurobiol. Dis.* 39, 381–392.
- Riederer, P., and Wuketich, S. (1976). Time course of nigrostriatal degeneration in parkinson's disease - A detailed study of influential factors in human brain amine analysis. *J. Neural Transm.* 38, 277–301.
- Rohlf, A., Nikkhah, G., Rosenthal, C., and Rundfeldt, C. (1997). Hemispheric asymmetries in spontaneous firing characteristics of substantia nigra pars reticulata neurons following a unilateral 6-hydroxydopamine lesion of the rat nigrostriatal pathway. *Brain Res.* 761, 352–356.
- Rommelfanger, K.S., and Weinshenker, D. (2007). Norepinephrine: The redheaded stepchild of Parkinson's disease. *Biochem. Pharmacol.* 74, 177–190.
- Rosin, J.M., McAllister, B.B., Dyck, R.H., Percival, C.J., Kurrasch, D.M., and Cobb, J. (2015). Mice lacking the transcription factor SHOX2 display impaired cerebellar development and deficits in motor coordination. *Dev. Biol.* 399, 54–67.
- Ross, G.W., Petrovitch, H., Abbott, R.D., Tanner, C.M., Popper, J., Masaki, K., Launer, L., and White, L.R. (2008). Association of olfactory dysfunction with risk for

- future Parkinson's disease. *Ann. Neurol.* *63*, 167–173.
- Rylander, D., Parent, M., O-Sullivan, S.S., Dovero, S., Lees, A.J., Bezard, E., Descarries, L., and Cenci, M.A. (2010). Maladaptive plasticity of serotonin axon terminals in levodopa-induced dyskinesia. *Ann. Neurol.* *68*, 619–628.
- Sauer, H., and Oertel, W.H. (1994). Progressive degeneration of nigrostriatal dopamine neurons following intrastriatal terminal lesions with 6-hydroxydopamine: A combined retrograde tracing and immunocytochemical study in the rat. *Neuroscience* *59*, 401–415.
- Savica, R., Carlin, J.M., Grossardt, B.R., Bower, J.H., Ahlskog, J.E., Maraganore, D.M., Bharucha, A.E., and Rocca, W.A. (2009). Medical records documentation of constipation preceding Parkinson disease: A case-control study. *Neurology* *73*, 1752–1758.
- Savica, R., Rocca, W.A., and Ahlskog, J.E. (2010). When does Parkinson disease start? *Arch. Neurol.* *67*, 798–801.
- Savitt, J.M., Dawson, V.L., and Dawson, T.M. (2006). Diagnosis and treatment of Parkinson disease: molecules to medicine. *J. Clin. Invest.* *116*, 1744–1754.
- Schapira, A.H. V, and Tolosa, E. (2010). Molecular and clinical prodrome of Parkinson disease: Implications for treatment. *Nat. Rev. Neurol.* *6*, 309–317.
- Schlüter, O.M., Fornai, F., Alessandri, M.G., Takamori, S., Geppert, M., Jahn, R., and Südhof, T.C. (2003). Role of  $\alpha$ -synuclein in 1-methyl-4-phenyl-1,2,3,6-tetrahydropyridine-induced Parkinsonism in mice. *Neuroscience* *118*, 985–1002.
- Schober, A. (2004). Classic toxin-induced animal models of Parkinson's disease: 6-OHDA and MPTP. *Cell Tissue Res.* *318*, 215–224.
- Schrag, A., Horsfall, L., Walters, K., Noyce, A., and Petersen, I. (2015). Prediagnostic presentations of Parkinson's disease in primary care: A case-control study. *Lancet Neurol.* *14*, 57–64.
- Schroll, H., Vitay, J., and Hamker, F.H. (2014). Dysfunctional and compensatory synaptic plasticity in Parkinson's disease. *Eur. J. Neurosci.* *39*, 688–702.
- Schwartz, R.K.W., and Huston, J.P. (1996a). The unilateral 6-hydroxydopamine lesion model in behavioral brain research. Analysis of functional deficits, recovery and treatments. *Prog. Neurobiol.* *50*, 275–331.
- Schwartz, R.K.W., and Huston, J.P. (1996b). Unilateral 6-hydroxydopamine lesions of meso-striatal dopamine neurons and their physiological sequelae. *Prog. Neurobiol.* *49*, 215–266.
- Schwartz, R.K.W., Sedelis, M., Hofele, K., Auburger, G.W., and Huston, J.P. (1999). Strain-dependent recovery of open-field behavior and striatal dopamine deficiency in the mouse MPTP model of Parkinson's disease. *Neurotox. Res.* *1*, 41–56.
- Sedelis, M., Hofele, K., Auburger, G.W., Morgan, S., Huston, J.P., and Schwartz, R.K.W. (2000). MPTP susceptibility in the mouse: Behavioral, neurochemical, and histological analysis of gender and strain differences. *Behav. Genet.* *30*, 171–182.
- Sedelis, M., Schwartz, R.K.W., and Huston, J.P. (2001). Behavioral phenotyping of the MPTP mouse model of Parkinson's disease. In *Behavioural Brain Research*, pp. 109–125.
- Seeger-Armbruster, S., and Von Arnim-Mayerhofer, A. (2013). Short- and long-term

- unilateral 6-hydroxydopamine lesions in rats show different changes in characteristics of spontaneous firing of substantia nigra pars reticulata neurons. *Exp. Brain Res.* 224, 15–24.
- Sgambato-Faure, V., and Cenci, M.A. (2012). Glutamatergic mechanisms in the dyskinesias induced by pharmacological dopamine replacement and deep brain stimulation for the treatment of Parkinson's disease. *Prog. Neurobiol.* 96, 69–86.
- Shen, K.Z., and Johnson, S.W. (2006). Subthalamic stimulation evokes complex EPSCs in the rat substantia nigra pars reticulata in vitro. *J. Physiol.* 573, 697–709.
- Shiba, M., Bower, J.H., Maraganore, D.M., McDonnell, S.K., Peterson, B.J., Ahlskog, J.E., Schaid, D.J., and Rocca, W. a (2000). Anxiety disorders and depressive disorders preceding Parkinson's disease: a case-control study. *Mov Disord* 15, 669–677.
- Siegfried, J., and Lippitz, B. (1994). Bilateral chronic electrostimulation of ventroposterolateral pallidum: A new therapeutic approach for alleviating all parkinsonian symptoms. *Neurosurgery* 35, 1126–1130.
- Simola, N., Morelli, M., and Carta, A.R. (2007). The 6-hydroxydopamine model of Parkinson's disease. *Neurotox. Res.* 11, 151–167.
- Singh, A., Mewes, K., Gross, R.E., DeLong, M.R., Obeso, J.A., and Papa, S.M. (2016). Human striatal recordings reveal abnormal discharge of projection neurons in Parkinson's disease. *Proc. Natl. Acad. Sci.* 113, 9629–9634.
- Smith, Y., Bevan, M.D., Shink, E., and Bolam, J.P. (1998). Microcircuitry of the direct and indirect pathways of the basal ganglia. *Neuroscience* 86, 353–387.
- Soares, J., Kliem, M.A., Betarbet, R., Greenamyre, J.T., Yamamoto, B., and Wichmann, T. (2004). Role of External Pallidal Segment in Primate Parkinsonism: Comparison of the Effects of 1-Methyl-4-Phenyl-1,2,3,6-Tetrahydropyridine-Induced Parkinsonism and Lesions of the External Pallidal Segment. *J. Neurosci.* 24, 6417–6426.
- Song, D.D., Shults, C.W., Sisk, A., Rockenstein, E., and Masliah, E. (2004). Enhanced substantia nigra mitochondrial pathology in human  $\alpha$ -synuclein transgenic mice after treatment with MPTP. *Exp. Neurol.* 186, 158–172.
- Spillantini, M.G., Schmidt, M.L., Lee, V.M.-Y., Trojanowski, J.Q., Jakes, R., and Goedert, M. (1997).  $\alpha$ -Synuclein in Lewy bodies. *Nature* 388, 839–840.
- Sutton, A.C., O'Connor, K.A., Pilitsis, J.G., and Shin, D.S. (2015). Stimulation of the subthalamic nucleus engages the cerebellum for motor function in parkinsonian rats. *Brain Struct. Funct.* 220, 3595–3609.
- Tan, Z.-G., Zhou, Q., Huang, T., and Jiang, Y. (2016). Efficacies of globus pallidus stimulation and subthalamic nucleus stimulation for advanced Parkinson's disease: a meta-analysis of randomized controlled trials. *Clin. Interv. Aging* 11, 777–786.
- Taverna, S., Ilijic, E., and Surmeier, D.J. (2008). Recurrent Collateral Connections of Striatal Medium Spiny Neurons Are Disrupted in Models of Parkinson's Disease. *J. Neurosci.* 28, 5504–5512.
- Terzioglu, M., and Galter, D. (2008). Parkinson's disease: Genetic versus toxin-induced rodent models. *FEBS J.* 275, 1384–1391.
- Thach, W.T., Goodkin, H.P., and Keating, J.G. (1992). The Cerebellum and the Adaptive Coordination of Movement. *Annu. Rev. Neurosci.* 15, 403–442.

- Thullier, F., Lalonde, R., Cousin, X., and Lestienne, F. (1997). Neurobehavioral evaluation of lurcher mutant mice during ontogeny. *Dev. Brain Res.* *100*, 22–28.
- Tolosa, E., Gaig, C., Santamaría, J., and Compta, Y. (2009). Diagnosis and the premotor phase of Parkinson disease. *Neurology* *72*.
- Truong, L., Allbutt, H., Kassiou, M., and Henderson, J.M. (2006). Developing a preclinical model of Parkinson's disease: a study of behaviour in rats with graded 6-OHDA lesions. *Behav. Brain Res.* *169*, 1–9.
- Tseng, K.Y., Kargieman, L., Gacio, S., Riquelme, L.A., and Murer, M.G. (2005). Consequences of partial and severe dopaminergic lesion on basal ganglia oscillatory activity and akinesia. *Eur. J. Neurosci.* *22*, 2579–2586.
- Ungerstedt, U. (1968). 6-hydroxy-dopamine induced degeneration of central monoamine neurons. *Eur. J. Pharmacol.* *5*, 107–110.
- Valadas, J.S., Vos, M., and Verstreken, P. (2015). Therapeutic strategies in Parkinson's disease: What we have learned from animal models. *Ann. N. Y. Acad. Sci.* *1338*, 16–37.
- Vitek, J.L., Zhang, J., Hashimoto, T., Russo, G.S., and Baker, K.B. (2012). External pallidal stimulation improves parkinsonian motor signs and modulates neuronal activity throughout the basal ganglia thalamic network. *Exp. Neurol.* *233*, 581–586.
- Volpicelli-Daley, L.A., Luk, K.C., Patel, T.P., Tanik, S.A., Riddle, D.M., Stieber, A., Meaney, D.F., Trojanowski, J.Q., and Lee, V.M.Y. (2011). Exogenous  $\alpha$ -Synuclein Fibrils Induce Lewy Body Pathology Leading to Synaptic Dysfunction and Neuron Death. *Neuron* *72*, 57–71.
- Volpicelli-Daley, L.A., Luk, K.C., and Lee, V.M.Y. (2014). Addition of exogenous  $\alpha$ -synuclein preformed fibrils to primary neuronal cultures to seed recruitment of endogenous  $\alpha$ -synuclein to Lewy body and Lewy neurite-like aggregates. *Nat. Protoc.* *9*, 2135–2146.
- Volpicelli-Daley, L.A., Kirik, D., Stoyka, L.E., Standaert, D.G., and Harms, A.S. (2016). How can rAAV- $\alpha$ -synuclein and the fibril  $\alpha$ -synuclein models advance our understanding of Parkinson's disease? *J. Neurochem.* 131–155.
- Wallace, M.L., Saunders, A., Huang, K.W., Philson, A.C., Goldman, M., Macosko, E.Z., McCarroll, S.A., and Sabatini, B.L. (2017). Genetically Distinct Parallel Pathways in the Entopeduncular Nucleus for Limbic and Sensorimotor Output of the Basal Ganglia. *Neuron* *94*, 138–152.e5.
- Wang, J.-W., Zhang, Y.-Q., Zhang, X.-H., Wang, Y.-P., Li, J.-P., and Li, Y.-J. (2016). Cognitive and Psychiatric Effects of STN versus GPi Deep Brain Stimulation in Parkinson's Disease: A Meta-Analysis of Randomized Controlled Trials. *PLoS One* *11*, e0156721.
- Wichmann, T., and DeLong, M.R. (2003). Pathophysiology of Parkinson's disease: the MPTP primate model of the human disorder. *Ann. N. Y. Acad. Sci.* *991*, 199–213.
- Wichmann, T., and DeLong, M.R. (2011). Deep-brain stimulation for basal ganglia disorders. *Basal Ganglia* *1*, 65–77.
- Wichmann, T., and Soares, J. (2006). Neuronal Firing Before and After Burst Discharges in the Monkey Basal Ganglia Is Predictably Patterned in the Normal State and Altered in Parkinsonism. *J. Neurophysiol.* *95*, 2120–2133.

- Wichmann, T., Bergman, H., and DeLong, M.R. (1994). The primate subthalamic nucleus. III. Changes in motor behavior and neuronal activity in the internal pallidum induced by subthalamic inactivation in the MPTP model of parkinsonism. *J. Neurophysiol.* *72*, 521–530.
- Wichmann, T., Bergman, H., Starr, P.A., Subramanian, T., Watts, R.L., and DeLong, M.R. (1999). Comparison of MPTP-induced changes in spontaneous neuronal discharge in the internal pallidal segment and in the substantia nigra pars reticulata in primates. *Exp. Brain Res.* *125*, 397–409.
- Wichmann, T., Kliem, M.A., and Soares, J. (2002). Slow oscillatory discharge in the primate basal ganglia. *J. Neurophysiol.* *87*, 1145–1148.
- Willard, A.M., Bouchard, R.S., and Gittis, A.H. (2015). Differential degradation of motor deficits during gradual dopamine depletion with 6-hydroxydopamine in mice. *Neuroscience* *301*, 254–267.
- Wu, T., and Hallett, M. (2005). A functional MRI study of automatic movements in patients with Parkinson’s disease. *Brain* *128*, 2250–2259.
- Wu, T., and Hallett, M. (2013). The cerebellum in Parkinson’s disease. *Brain* *136*, 696–709.
- Yu, H., Sternad, D., Corcos, D.M., and Vaillancourt, D.E. (2007). Role of hyperactive cerebellum and motor cortex in Parkinson’s disease. *Neuroimage* *35*, 222–233.
- Zaccai, J., Brayne, C., McKeith, I., Matthews, F., and Ince, P.G. (2008). Patterns and stages of  $\alpha$ -synucleinopathy: Relevance in a population-based cohort. *Neurology* *70*, 1042–1048.
- Zhou, F.-M.F.-W., Jin, Y., Matta, S.G., Xu, M., and Zhou, F.-M.F.-W. (2009). An Ultra-Short Dopamine Pathway Regulates Basal Ganglia Output. *J. Neurosci.* *29*, 10424–10435.
- Zhou, F.-W., Matta, S.G., and Zhou, F.-M. (2008). Constitutively Active TRPC3 Channels Regulate Basal Ganglia Output Neurons. *J. Neurosci.* *28*, 473–482.
- Zigmond, M.J., and Hastings, T.G. (1997). Neurochemical Responses to Lesions of Dopaminergic Neurons: Implications for Compensation and Neuropathology. *Adv. Pharmacol.* *42*, 788–792.
- Zigmond, M.J., Acheson, A.L., Stachowiak, M.K., and Strickerm, E.M. (1984). Neurochemical Compensation After Nigrostriatal Bundle Injury in an Animal Model of Preclinical Parkinsonism. *Arch. Neurol.* *41*, 856–861.
- Zigmond, M.J., Hastings, T.G., and Perez, R.G. (2002). Increased dopamine turnover after partial loss of dopaminergic neurons: Compensation or toxicity? *Park. Relat. Disord.* *8*, 389–393.